University of Alberta

Density-Functional Theory Study of Methylcyclohexane Selective Ring Opening over ZrO_2

by

Alex Abraham 

A thesis submitted to the Faculty of Graduate Studies and Research in partial fulfillment of the requirements for the degree of Master of Science

in

Chemical Engineering

Department of Chemical & Materials Engineering

Edmonton, Alberta
Spring, 2006

Your file Votre référence
ISBN: 0-494-13778-9
Our file Notre référence
ISBN: 0-494-13778-9

Abstract

Modeling studies utilizing the density-functional theory (DFT) were performed to study the mechanism and energetics of methylcyclohexane (MCH) selective ring opening over ZrO_2 surfaces (cubic polymorph). Both classical bifunctional and Haag-Dessau reaction mechanisms were studied. It was determined that the classical bifunctional mechanism quoted in the literature did not occur over $ZrO_2(111)$, and required modification. As a comparison, additional calculations were performed over modified ZrO_2 and Al_2O_3 surfaces. The results indicate that there exists an optimum acidity which yields the most favorable energetics for the ring opening of MCH. The energetics and mechanism of multiring aromatic ring opening, i.e. decalin and tetralin, were also studied over ZrO_2. In all cases, ZrO_2 demonstrated very favorable reaction energetics and the (111) surface was found to be the most active crystallographic orientation. It was also observed that ZrO_2 offers very favorable energetics for the dissociation of H_2O to H^+ and OH^- and H_2 to H^+ and H^-.

Table of Contents

Chapter 4 Results

Chapter 5 Discussion

Chapter 6 Conclusion

List of Tables

List of Figures

List of Nomenclature

ACP-Alkyl Cyclo Pentane

ASAT- Aromatic Saturation

CH- Cyclo Hexane

DFT-Density Functional Theory

DN- Double Numerical

DNP- Double Numerical plus Polarization

ECP- Effective Core Potential

ECP- Ethyl Cyclo Pentane

GGA-General Gradient Approximation

HDN- Hydrodenitrogenation

HDS- Hydrodesulphurization

HX- Hexane

LCO- Light Cycle Oil

LDA-Local Density Approximation

LST- Linear Synchronous Transit

MCHE-Methyl Cyclohexene

MCH-Methylcyclohexane

MCP- Methyl Cyclo Pentane

MHXDE-Methyl Hexadiene

MP- Methyl Pentane

PCP- Pentyl Cyclo Pentane

PDMCPE- Protonated Dimethyl Cyclopentene

PMCHE-Protonated Methyl Cyclohexene

PMHXDE-Protonated Methyl Hexadiene

PW91-Perdew and Wang 91

QST-Quadratic Synchronous Transit

ROP- Ring Opening Product

SCF-Self Consistent Field

SRO- Selective Ring Opening

Chapter 1 Introduction

1.1 Reduction of Aromatics in Petroleum Distillates

The diminishing supplies of light crude oil is increasing pressure on the modern petroleum refining industry to process more and heavier feed feedstocks and convert them into lighter and more valuable products [1]. In addition, increasingly stringent environmental regulations throughout the global community require the reduction of aromatics and sulfur content in gasoline, as well as diesel fuels [2]. The excess aromatic by-products obtained from large scale petrochemical products were being conventionally used as high octane additives for gasoline. However, since aromatics, especially benzene, are known to be carcinogenic refineries have been legally obliged [2] to decrease the percentage of aromatics in gasoline [3]. This, in turn, is increasing research efforts for the development of novel catalysts and catalytic processes that transform aromatics and low value fractions in to high value fuels [1]. While catalyst technology is well established in the areas of hydrotreatment (HDS and HDN), additional insight into the mechanisms of selective ring opening is needed to increase the selectivity and conversion of aromatics in to desirable products. The need for novel selective ring opening catalysts and processes is all the more important for the Canadian petroleum industry as the utilization of aromatic-rich bitumen from oil sands will continue to increase over the next several years and decades.

1.2 Current Technologies

The current technologies for the production of low-aromatic diesel fuels are based on catalysts for hydrogenation and ring opening. There are several proven technologies available which operate as single or double stage processes. The single stage process using traditional catalysts like Co/Mo, Ni/Mo, Ni/W on high surface area alumina are limited by thermodynamic equilibrium conditions at high temperature. The noble metal catalysts used in the two stage process overcome the thermodynamic equilibrium constraint by hydrogenation at lower temperature, but these catalysts are easily poisoned by sulfur and/or nitrogen present in the feed stream [7]. Zeolite supported Pd/Pt catalysts are considered the most important industrial catalysts for aromatic hydrogenation, but

these highly acidic materials have the inherent disadvantage of accelerating coke deposition due to undesired cracking [7].

1.3 Selective Ring Opening and New Catalyst Development

Selective ring opening (SRO) of ring structured compounds will help meet the dual goal of reducing the aromatics content of the petroleum feedstocks and increasing the cetane value of the diesel fuels. In SRO, aromatic rings are selectively opened to yield straight chain hydrocarbons or hydrocarbons with minimum branching. In hydrocracking, SRO also reduces the undesired production of gases, and thus significantly reduces the consumption of hydrogen and increases the yield of desired fractions. Aromatics have lower cetane number and selectively converting them into straight chain compounds increases their cetane value. SRO can take place over monofunctional or bifunctional catalysts. Over bifunctional catalysts, six membered rings are contracted to five membered rings using the acidic function of the catalyst and then the ring is opened over the metal function of the catalyst [8], whereas over monofunctional catalysts, the reaction process via a non-classical Haag-Dessau mechanism where alkanes are directly protonated to non-classical carbonium ions in the transition state [9].

Aromatics conversion (ring opening) itself has been studied extensively over zeolite catalysts without the reporting of any significant selectivity towards more favorable ring opened products [6]. Treatment of diesel over a bimetallic Pt-Pd catalyst supported over mesoporous aluminosilicate resulted in a cetane improvement of 8 points [7]; however, this cetane improvement does not meet the requirement for future diesel fuel cetane specifications. Maity et al.[10] reported that they do not foresee any improvement of conventional catalysts for cetane improvement, but rather they argue for the development of a new catalyst support and fine tuning of dispersed active metals on the catalyst support. In this context, they indicate ZrO_2 has been attracting the attention of researchers as a catalyst and catalyst support due to a high thermal stability, hardness, and specific mass. Bhaskar et al.[11] also advocates zirconia as a novel catalyst and catalyst support, similarly citing high thermal stability, chemical inertness, acidity, and reducibility as supporting reasons. Indeed, zirconia as a catalyst support has been

employed in many industrially important reactions such as hydroprocessing, oxidation of alcohols, synthesis of alcohols, and methanation reactions [11].

1.4 Objective of This Study

The objective of this study is to develop a fundamental understanding of selective ring opening reaction networks and energetics, including hydrodecyclization of naphthenic compounds, over zirconia and other metal oxides. This purely modeling study utilizes density-functional theory (DFT) and is focused on both classical bifunctional and non-classical ring opening mechanisms. A literature review of ring opening and catalyst development research is provided in Chapter 2. The DFT calculations in this study were performed using Material Studio DMol^3 from Accelrys. A detailed description of DFT is available in Chapter 3. The complete characterization of zirconia is performed and the results are compared with available experimental observations. Characterization of the surface, as well as the bulk, was performed before and after modifier element incorporation. The probe molecules used to study classical and non-classical ring opening mechanisms on the different geometrical planes of zirconia include both mono and multiring aromatics. In addition, the reactions were studied on other catalyst surfaces to understand the role of acidity on the energetics and mechanism of these reactions. Zirconia was also studied for its ability to facilitate hydrogen and water dissociation, since the formation of hydrogen ions (protons) and hydroxyl groups on the surface is very important for ring opening reactions. The results of these calculations are given in Chapter 4. The results from the calculations are analyzed, discussed, and compared to previously reported experimental observations in Chapter 5, and the conclusions are summarized in Chapter 6.

Chapter 2 Literature Review

2.1 Aromatics Reduction in Transportation Fuels

The tightening transportation fuel specifications require the development of more active and selective catalysts for the hydrotreatment of crude oil fractions. The diminishing supply of light crude oil has further driven the need to upgrade heavy oil and vacuum residues to middle and light distillates. Two key issues that are addressed in heavy oil upgrading are the removal of heteroatoms, and cetane improvement of the gas oil fractions. Technology is, generally speaking, mature for heteroatom removal. However, despite considerable research there has been little progress regarding cetane improvement.

Diesel fuel is defined as a petroleum fraction with hydrocarbons having individual boiling points in the range of 210 - 340 °C [1]. One of the most desirable properties of diesel fuel is the cetane number. The cetane number of a fuel is defined as the volume percent of n-hexadecane in a blend of n-hexadecane and 1-methylnaphthalene that gives the same ignition delay period as the test sample [46]. Future diesel fuel specifications will include a substantial reduction in aromatics and polyaromatics to produce a diesel fuel with lower density and higher cetane number [22]. For example, the 2005 European Union cetane specification for diesel fuel is a cetane number of 58 [41].

The new specifications for diesel fuel are expected to generate a surplus of aromatics. One of the major sources of aromatics is pyrolysis gasoline, a byproduct from steam cracking of naphtha for the production of ethane and propane [4]. Increasing attention is, therefore, being given to the development of catalysts and catalytic processes that effectively transform low value oil fractions to high quality fuel fractions [1]. Aromatics have poor compression ignition properties, and thus, a low cetane number. A net increase in cetane number can be obtained by decreasing aromatic concentration in the diesel fuels through hydrogenation processes. However, for high aromatics diesel fractions such as light cycle oil (LCO) produced in catalytic cracking units, the simple saturation of aromatics is not enough to reach the required cetane due to the relatively low cetane values of the resulting napthenes. Moreover, the higher density of napthenes gives lower volumetric yield compared to the alkanes of the same carbon number. In these cases, an additional increase of cetane can be achieved by coupling the

hydrogenation of polyaromatics with the selective opening of naphthenic rings [22]. Despite the moderately high cetane number of naphthenes, the direct use of naphthenes in fuels is also problematic as they may be reconverted to aromatics in internal combustion engines and give rise to soot in the exhaust [9]. Although aromatics have been traditionally used as octane boosters in gasoline, aromatics, especially benzene, are known to be carcinogenic [9], and consequently there is additional pressure on refineries by way of legislation to reduce the aromatics content in gasoline.

Thus, there is a compulsion for removing aromatics from gasoline and diesel, but there is a greater incentive for removal of aromatics by selective ring opening. Selective conversion of aromatics even without any statutory requirement is strategically important for Canada. While Canada has abundant resources of bitumen derived from oil sands, the highly aromatic straight run gas oil fractions of the bitumen is not a good candidate for diesel fuels. The economic impact of an efficient upgrading is substantial.

2.2 Current Refining Practices

Distillate fuels typically contain paraffins, naphthenes, and aromatics. Paraffins are the most desirable components for fuel quality parameters such as cetane, specific gravity and emissions, followed by naphthenes and then aromatics. The least desirable are multi-ring aromatic compounds. While there are a variety of licensed refinery processes to produce distillate fuels, they are typically limited in their capability to produce high quality and/or yields of distillate fuels [47].

A well established refinery process for producing distillate fuels is hydrocracking. Hydrocracking catalysts are typically bifunctional catalysts composed of a hydrogenation function (metals) and an acidic function (e.g. zeolites). These catalysts are effective for aromatic hydrogenation and reducing the number of ring structures, but also result in extensive cracking to lower boiling products, including low value gases which reduces the overall boiling range and limits the volume of final distillate product. An analysis of the paraffin distillate boiling range in the feed and product shows that there is no appreciable paraffin generation. The apparent increase in distillate boiling range paraffins is due to the concentration of paraffins in a reduced volume of distillate product [47].

Other than fuels, there is an increasing demand for paraffinic-class low toxicity biodegradable solvents. In this context, there is a need to reduce the cyclic compound content of solvent blends. This also calls for conversion of aromatics/naphthenes to paraffins, or in other words selective ring opening (SRO). An ideal selective ring opening process would result in endocyclic ring bond cleavage to produce molecules having an equivalent number of carbon atoms and one less ring than the original molecule with no reduction in molecular weight [47]. Acidity, which is the function primarily responsible for ring opening in commercial hydrocracking catalysts, also catalyzes hydroisomerization of the resulting napthenes and paraffins. For every increase in the number of methyl branches, there is a concomitant loss of 18-20 units in cetane number. In this context, the acidity of the catalyst needs to be optimized for yield and conversion [47].

2.3 Acid Catalysts for Ring Opening

Metal oxides are an important part of catalyst systems for ring opening, and are used both as catalysts and catalyst supports. Many of these materials contain Lewis and Brønsted acidity making them favorable for catalysis involving electron and proton transfer. According to the concepts independently proposed by J.M. Brønsted and T.M. Lowry in 1923, an acid is any hydrogen-containing species able to release a proton. This definition does not exclusively imply water as the reaction medium. In the same year, 1923, G.N. Lewis proposed a different approach. In his view an acid is any species that because of the presence of an incomplete electronic grouping can accept an electron pair to give rise to a dative or coordination bond [48].

Metal oxide catalysts are compounds of oxygen with one or more metal or semimetal elements. *True* metal oxides are composed of a metal and oxygen and are, therefore, characterized by an ionic bond. When pure, they are most commonly crystalline materials. The ideal surface of a metal oxide crystal is composed of crystal faces held together by corner and edges. The coordination of ions at the ideal surface is incomplete with respect to the coordination in the bulk; they lack the coordination from one side. Atoms at corners or edges are even more incomplete with respect to coordination. The surface undergoes reconstruction in order to decrease the free energy

of the atoms exposed at the surface, but coordinative unsaturation will remain. These ions can act as acids and bases, respectively, according to the Lewis definition [48]. The reversible interaction of water (present in the environment) with such surfaces is in part dissociative and the coordinatively unsaturated cations and anions can, in part, convert into surface hydroxyl-groups. These groups are potentially Brønsted acids, although they mostly behave as basic -OH groups [48].

Ring opening has previously been studied using metal oxides, including Al_2O_3, SiO_2 and zeolites [49]. From the ensuing literature review, it can be seen that zeolites are widely used in research on ring opening. Zeolites are widely used as catalysts in present day fluid catalytic cracking units (FCCU) and hydrocrackers [50]. Although zeolites are essentially metal oxides (i.e. alumino silicates), their structure is quiet different from other metal oxides. They are aluminosilicate framework structures made from corner sharing of SiO_4 and AlO_4 tetrahedra with small pores (1-20 Å) throughout the solid [42]. When compared with other solid acids, zeolites possess certain characteristics which make them unique materials. These characteristics include high surface area, control over the number and strength of acid sites, higher adsorption capacity, and media solvent effects. Also, the ability to control the pore size dimensions result in shape selective effects and preactivation of the molecules inside the pores by strong dielectric fields and molecular confinement [6]. Practically every type of zeolite has been studied for ring opening reactions. It was observed that medium pore size zeolites like ZSM-5 can be good catalysts for steam cracker feed (C_{2+}n-alkanes) preparation, and large pore zeolites like USY and Beta zeolite are suitable for ring opening though at a lower yield and selectivity [28, 17, 22].

2.4. Ring Opening Mechanisms

The proposed reaction mechanisms for catalytic ring opening fall broadly into two categories; a classical bifunctional mechanism which involves isomerization followed by ring opening, and the Haag-Dessau mechanism. The previously proposed ring opening pathways for different probe molecules were reported to essentially follow one of these mechanisms. The mechanisms are discussed briefly in the following literature review.

Weitkamp et al. [3] describes the ring opening pathway of cycloalkanes as follows; "On bifunctional catalysts, methylcyclohexane is dehydrogenated on metallic sites, and the resulting cycloalkenes are protonated to carbenium ions on acidic sites. Usually, skeletal isomerization into highly branched isomers occurs first, whereupon classical β-scission can proceed. Finally, the diene formed is hydrogenated on a metal site. On monofunctional acidic catalysts, two different mechanisms can be operative: On the one hand, beta-scission of classical carbenium ions is possible, but the latter can only form through a bimolecular hydride transfer. On the other hand, methylcyclohexane can be directly protonated forming a nonclassical carbonium ion with a three-center, two-electron bond in the transition state (Haag - Dessau cracking)" [3].

McVicker et al. [2] suggests three pathways for the ring opening. Free radical conversion is discussed as one possible reaction pathway, and is proposed to be initiated by either pyrolysis at high temperatures or by the addition of radical initiators formed via thermal decomposition of reactive compounds. Naphthenoaromatics, such as tetralin, are found to be quite reactive, and radical type ring opening to butyl benzene has been reported. Dehydrogenation of tetralin to naphthalene as well as secondary cracking and dealkylation of butyl benzene, are important competing reactions which severely limit the yield of ring-opening products. Because radical cracking of product alkanes is a fast reaction mechanism which is 5 to 50 times faster than those of naphthenes of the same carbon number, maintaining high ring-opening yields, especially at high conversion levels, is a difficult task [2].

A second possible ring-opening route proposed, which is similar to what is proposed by Weitkamp et al. [3] is via acid-catalyzed carbocation cleavage of ring C–C bonds. Naphthenic molecules are activated either by direct formation of a cationic species by a Lewis acid performing hydride abstraction or by protonation of an olefin intermediate formed by naphhthene dehydrogenation over a metal function. Ring opening and/or cracking may proceed by a β-scission mechanism. The rates of β-scission of exocyclic C–C bonds in alkyl group substituents with three or more carbon atoms are reported to be similar in magnitude to those of mono- and di-branched alkanes. However, the rates of β-scission of endocyclic naphthene ring C–C bonds are two to three orders of magnitude slower than cleaving of exocyclic bonds [51]. These differences in rates are

reportedly responsible for the very low selective ring opening yields over bifunctional hydrocracking catalysts, where an acidity function has predominance over a metal function resulting in excessive naphthene side-chain and product alkane cracking [52].

The third potential ring-opening pathway proposed by McVicker et al. [2] is via metal-catalyzed hydrogenolysis. With additional references from the literature, they have shown that the ring opening of methylcyclopentanes (MCP) to an isomeric mixture of C_6–alkanes can be accomplished with high selectivity over a number of supported Group VIII metals and metal alloys. Sinfelt et al.[27] give a detailed discussion about catalytic hydrogenolysis on metals. This work shows that the optimum chemisorption strength a surface should have for the optimum catalyst activity is an intermediate chemisorption strength; one which is not too strong or not too weak. In this perspective, Sinfelt et al. [27] rates group VIII metals as the ones with maximum catalytic activity.

2.5 Previous Research on Ring Opening Catalysts

Most of the previous research on ring opening catalysts has been preformed using zeolites with MCP as a probe molecule. MCP has been widely used as a probe molecule due to the many reaction pathways it can take on different catalysts. For example, MCP can undergo cracking resulting in molecules with less than 6 carbon atoms, and this mainly occurs at high temperatures or in the presence of Brønsted acidity. MCP can also undergo isomerization/ring enlargement resulting in cyclohexane and benzene as products. Additionally, MCP can undergo ring opening producing C_6 isomers. However, ring enlargement and ring opening are in competition [2]. Most of the commercial catalysts employed currently for ring opening are bifunctional catalysts with metals dispersed on acidic supports, mainly zeolites. Literature is rife with work regarding ring opening, especially with 5 membered rings and alkyl derivatives on platinum and platinum group metals as the metal and zeolites, alumina and silica, as acidic supports [9]. The following is a summary of the literature reviewed regarding ring opening reactions and catalysts.

2.5.1 MCP Ring Opening

MCP ring opening was first reported about 50 years ago [53], and since then MCP ring opening has been widely studied and reported over mono and bimetallic catalysts at variety of conditions. For example, the ring opening of MCP was reported using Ni/Al_2O_3 [56], Rh/Al_2O_3, Rh/SiO_2 [57,33, 58], Pd/SAPO-11 [59], Pt/mordenite, Pt/Y [60], Pt, $Pt\text{-}Re/Al_2O_3$ [61], Pt/SiO_2, Pt/Al_2O_3, Pt/KLT [62], $Pt\text{-}Ru/SiO_2$ [63], Rh/Y [64], Pd/Al_2O_3 [65], and $Rh\text{-}Ag/TiO_2$ [66]. The ring opening studies on the previous catalysts mainly concentrated on the catalyst metal function and on the effects of reaction conditions (temperature, pressure), catalyst support materials, and the size and location of metal aggregates on the selectivity of the catalyst [49]. Although MCP ring opening has been widely studied, researchers differ over the exact contribution of acid and metal sites in bifunctional catalysts. In 1955, Hansel [53] proposed that MCP ring opening can be achieved by the acid catalyst sites. Iijima et al. [37] were the first to show that this can take place on both metal as well as acid sites. Later, researchers at Mobil [38] showed that a Pt/Al_2O_3 bifunctional catalyst behaves like a monofunctional metal catalyst in the presence of propylamine (poisoned acid sites) and promotes the carbonium ion mechanism of ring opening when the metal function is poisoned by sulfur. Ponek et al. [40] studied the contribution of metal and acid sites of sulfur modified Pt/Al_2O_3, $Pt\text{-}Co/Al_2O_3$ and $Pt\text{-}Re/Al_2O_3$ for the selectivity of MCP conversion. They concluded that 2-methylpentane (2MP) and 3-methylpentane (3MP) formed exclusively on catalyst metal sites while cyclohexane (CH), benzene and hexane (HX) required the presence of both the metal and acid sites.

It has also reported that acid sites provided by zeolites seem to be predominantly involved, if not exclusively involved, in the ring opening reaction and Pt may be behaving like an inert [9]. The above view is supported by Roessner et al. [34] who did not find any significant activity and selectivity differences in the decyclization of cyclohexane performed in an H_2 atmosphere over monofunctional ZSM-5 and bifunctional Pt/H-ZSM-5 catalysts . However, this observation cannot be generalized for other Pt group metals as decyclization of MCP was found to be catalyzed by Rh loaded on non-acidic alumina [49]. Activity of Rh for ring opening is supported by the work of McCarthy et al. [35]. They studied the conversion of MCP over zeolite-Y supported

rhodium catalysts with a variety of proton concentrations. Ring opening of MCP to hexane isomers was found to be catalyzed by metal sites, but for ring enlargement of MCP to cyclohexane and benzene it was observed that metal sites and acid protons were required.

There are also differing views on the role of Pt in MCP ring opening. Avarez et al.[1] studied MCP ring opening on Pt supported on non acidic Pt/L zeolites and Pt/Mg(Al)O. They found that when the support is non-acidic and the reaction is conducted at low temperatures, the only reaction path that proceeds is ring opening. Gault et al. [54] noted that in metal catalyzed skeletal isomerization of hydrocarbons, essentially identical "initial" ratios of hexane isomers are formed from the ring opening of MCP and the isomerization of n-hexane (nC_6), 2-methylpentane (2MP) and 3-methylpentane (3MP) over Pt on non-acidic alumina. This observation led Gault and coworkers to propose that the isomerization of MCP and 3 acyclichexane involved a common 5 membered ring intermediate. Additional work done by Chow et al. [29] also supports the previous mechanism. They reported the conversion of MCP and acyclic hexanes over Pt/SiO_2 with an average Pt particle size less than 20 Å, and concluded that hexane isomerization via a 5 ring intermediate is best approximated by a sequential reaction (nC_6,2MP,3MP) to MCP to (nC_6,2MP,3MP), in which a quasi steady-state approximation is applicable. The 5 ring closure of hexane was found to be rate controlling in the overall reaction.

The above intermediate mechanism is supported by Galperin et al.[49] who studied MCP ring opening over platinum containing catalysts prepared on acidic and basic (neutral) supports at atmospheric pressure and 250 – 400 °C. They observed that equilibrium exists between cyclohexane and ring opening products with MCP as the intermediate. They also observed that on bifunctional catalysts with high acidity, the main reaction was isomerization of MCP to cyclohexane followed by the formation of aromatics, while catalysts prepared on basic supports catalyzed nonselective ring opening with the formation of methylpentanes and hexane. In the presence of potassium (acidic sites blocked), the bifunctional catalyst behaved like a monofunctional catalyst which converted the MCP through a nonselective ring opening mechanism to a mixture of C_6 paraffins.

It has been seen that, other than the function itself, the nature of the function (i.e. metallic, acidic) also strongly influences the ring opening of MCP, in addition to typical reaction operating conditions (pressure, temperature etc.). Galperin et al. [49] showed that activity and selectivity of mono and bifunctional catalysts containing Pt group metals were found to be rather sensitive to particle morphology and dispersion of the metal component in the conversion of MCP over Rh/Al_2O_3, to the acid/metal function balance in the hydroisomerization of n-paraffins over Pt/Beta, and the structural features of zeolites in the hydroisomerization of normal paraffins over Pt containing zeolites. Similar observations were made by Gault [26] in the case of MCP hydrogenolysis over Pt. It was observed that small particles promoted non-selective ring opening to n-hexane and methylpentanes, whereas large particles catalyzed selective ring opening to methylpentanes alone. McCarthy et al. [35] studied the conversion of MCP over zeolite Y supported rhodium catalysts, and observed that hydroconversion of cyclohexane and MCP over forms of wide pore zeolites resulted in the product spectrum significantly different from H-ZSM-5. This suggests that pore size is an important factor in using zeolites. Zhuang et al. [20] studied the kinetics of MCP ring opening on Euro Pt-1 (6.3 wt% Pt/SiO_2), and reported the products to be 2-methylpentane and n-hexane, and the ratio of 2MP/nHX increased with MCP pressure and decreased with H_2 pressure. The activity changed monotonically with increasing MCP pressure and exhibited a maximum with H_2 pressure. They proposed two parallel reactions, one forming n-HX and the other forming 2MP. Garin et al. [19] studied the catalytic transformation of 2-methylpentane and MCP over Co/NaY, Pt-Co/NaY, $Pt\text{-}Co/Al_2O_3$ and NaY catalysts. Co/NaY was found to be an excellent isomerization catalyst in contrast to Co/Al_2O_3, over which the main reaction observed was cracking. This was attributed to the difference in cobalt reducibility over the 2 surfaces.

From the above discussion, it is clear that while MCP ring opening has been widely studied, there is disagreement over the exact mechanism through which ring opening proceeds over a monofunctional or bifunctional catalyst. The above review clearly shows that ring opening can proceed over metal sites, acid sites or both together. It appears that it is not possible to propose a mechanism based on generic functionalities; rather the mechanism is specific to the type of acid or metal.

2.5.2 Cyclohexane and Methylcyclohexane Ring Opening

In contrast to MCP, the ring opening reaction of cyclohexane (CH) has not been as extensively studied. However, these limited studies do provide some information regarding the activity of pure transition state metals and transition group metals dispersed on acidic zeolites. It has been observed that unlike other Group VIII metals, Pt does not promote hydrogenolysis of cyclohexane, rather cyclohexane is dehydrogenated in to aromatic hydrocarbons. Cycloheptanes also undergo ring contraction and aromatization rather than hydrogenolysis [26]. As in the case of MCP conversion, it has been reported that metal dispersion and crystallite size has a significant effect in the case in the case of cyclohexane. Akhmedov et al. [36] studied the conversion of cyclohexane, cyclopentane and C5-C7 paraffins over bifunctional catalysts with Ru, Ru-Re, Ru-Rh and Ru-Ni as the metallic constituent on H-ZSM-5 zeolite where the metal was dispersed by metal vaporization. They observed that the product distribution was significantly different from that of conventional metal deposition by impregnation. In the case of catalysts prepared by the metal vapor method, 2MP, 3MP and nC6 were dominant compared to methane in the case of conventional catalyst. This was ascribed to highly dispersed metal particles on the zeolite support. This view of metal dispersion is also supported by the work of Sinfelt et al. [27], who observed that using Ru/SiO_2 catalysts, the conversion of CH to benzene (dehydrogenation) was favored at high metal dispersion, but the formation of short-chain paraffins (hydrogenolysis) dominated at low metal dispersion.

Onyestyák et al. [9] studied the conversion of cyclohexane over H-ZSM-5 catalysts in a hydrogen or nitrogen atmosphere at a pressure of 13 bar. This study showed that hydrodecyclization of cyclohexane over H-zeolites is a thermodynamically controlled process; both CH and MCP were present. Higher hydrogen partial pressures were required to shift the equilibrium of hydrogenation from aromatics to napthenes. They argue that decyclization of cyclohexane and MCP were probably not affected by Pt, but proceed on Brønsted acid sites with intermediate hexyl carbenium ions, which are converted to paraffins via either hydrogenation and release of hexanes from the surface or dimerization and subsequent cracking. As noted with MCP conversion, it is clear that metal dispersion and pore size of the support affect the product distribution from CH ring opening.

The ring opening of methylcyclohexane (MCH) has been studied over alumina supported Pt, Ir and Ru catalysts. McVicker et al. [2] reported that Pt/Al_2O_3 does not promote ring opening; however, it was observed that ring opening occurs on Ir and Ru catalysts, and the ring opening was essentially selective [14]. Dehydrogenation to toluene was the only reaction observed on Pt catalysts, regardless the particle size. This observation is in agreement with the view of Gault [26]. It has also been observed that deactivation by coking and aromatics formation can be suppressed by higher H_2 partial pressures during ring opening of MCH over H-ZSM-5. However, it was noted that too high hydrogen partial pressure would generate more undesirable branched alkanes than straight chain alkanes. This was ascribed to a blocking effect of the acidic sites by hydrogen. The reaction produced a good steam cracker feed stock (high percentage of C_{2+} -n alkanes) [44].

Sulfated zirconias were reported to be alternatives for the isomerization of napthenes. Francois et al. [7] studied conversion of MCH over a series of bifunctional catalysts prepared from sulfated zirconia deposited with Pt. They observed that the main reaction was the isomerization of alkyl cyclopentanes, the slow step of which was the acid catalyzed contraction of the ring. They proposed a classical bifunctional mechanism in the presence of Pt where the number of active Brønsted acid sites increased with hydrogen pressure. The main reaction, the isomerization of MCH to alkyl cyclopentanes (ACPs), has been shown to proceed through the skeletal isomerization of methyl cyclohexyl carbocation formed by the protonation of a cyclohexane intermediate, which is considered to be a facile reaction. They also concluded that the conversion of MCH is a good test to characterize the acidity of bifunctional catalysts.

2.5.3 Multi-ring Aromatics Ring Opening

The influence of the metal function in bifunctional Pt/USY catalysts for the combined hydrogenation and ring opening of tetralin was studied by Arribas et al.[17]. They observed that the key step in the reaction pathway leading to the formation of the desired ring opening products (ROPs) was isomerization (ring contraction) of the C6 naphthenic rings of decalin. It was reported that the presence of Pt in the bifunctional Pt/USY catalyst significantly increased the rate of isomerization and hence the formation

of ROP as compared to the monofunctional USY sample. They also reported that the formation of the high cetane ROP increased with increasing proximity between the Pt and acid sites, and with increasing the Pt loading (i.e. the metal/acid ratio) in the range of 0.25 – 4.0 wt. %. They concluded that the ring opening of naphthenes occurred exclusively on the Brønsted acid sites of the zeolite. The incorporation of a hydrogenolysis metal (Ir) to the bifunctional Pt/USY catalyst did not lead to a further increase in the formation of ROP and significantly reduced the sulfur tolerance of Pt. This was ascribed to a higher electron density on the Pt sites induced by Ir in bimetallic Pt–Ir particles. However, this work did not discuss how the support influenced this reaction. Ring opening of tetralin over Pt containing catalysts based on large pore Al-containing ITQ-21 zeolite was also studied by Arribas et al. [22]. This was found to be an excellent catalyst for complete saturation of the tetralin, but the ring opening yields were low.

The effect of catalyst pore structure on product distribution using decalin and tetralin probe molecules was studied by Corma et al. [28]. They used a set of zeolites with medium, large and extra large pore sizes as well as mesoporous MCM-41. The studies carried out at 723 K showed that the pore size and topology had a strong influence on diffusion and consequently activity and selectivity in reactions, such as ring opening, dealkylation, transalkylation, hydride transfer and coke formation. According to their findings, zeolites with medium pore sizes are adequate in combination with large pore zeolites to crack napthenes and aromatic-naphthenic rings of the type present in LCO to produce propane. Large pore zeolites showed good selectivity for naphthenic ring opening and appeared to be better suited for hydrotreating LCO.

Ring opening of indan was studied at 325 °C and atmospheric pressure over a bimetallic 2 wt. % $Pt_{25}Ir_{75}$/boehmite catalyst by Ulf Nylén et al. [4]. They compared the results with the catalytic performance of corresponding monometallic Pt and Ir/boehmite catalysts. The results indicated superior catalytic activity for the Ir and Pt-Ir catalysts, however, the product distribution varied widely, with hydrogenation and selective ring opening being the most prominent reactions at high pressure and atmospheric pressure conditions, respectively. At atmospheric pressure, all catalysts were slightly deactivated whereas at high pressure, the Pt-Ir catalyst showed a high operating stability with no deactivation. Pt alone did not show any intrinsic catalytic effect for this particular

reaction. They observed that incorporation of Pt tempered the cracking activity of Ir and changed the selectivity. It is worth noting that the behavior of Pt for selective ring opening is in accordance with what has been observed with other probe molecules.

Naphthalene ring opening was studied on mesoporous alumino silicates with Rh, Pt, Ir and Ru [31]. It was observed that rhodium, ruthenium and iridium showed higher selectivity towards hydrogenolysis and/or ring-opening products than the platinum-containing catalyst. As in the previous studies, it was observed that higher hydrogen partial pressures prevented deactivation. From all the previous work with multiring hydrocarbons, it is clear that a monofunctional catalyst is not effective for ring opening of multiring hydrocarbons. A classical bifunctional mechanism is suggested as the most probable ring opening pathway with Ru, Rh, Re and Ir as the most promising metals. Although there is general agreement that acidity needs to be optimized to achieve ring opening selectivity, there are no directions provided how this should be done.

2.6 Selective Ring Opening

In comparison to ring opening, much less work has been done to understand the mechanism of selective ring opening. The literature emphasizes the need to convert 6 membered rings to 5 membered rings to facilitate selective ring opening. Five membered rings are more easily ring opened than 6 membered rings. Ring-strain energies of approximately 1 and 7 kcal mol^{-1} respectively, for six- and five-membered rings provide the rational behind this experimental observation [2].

McVicker et al.[2] in their study of Pt, Ir, Ru and Rh supported on Al_2O_3 observed that for the Ir/Al_2O_3 system using MCP and PCP probe molecules, the ring opened product distribution was substantially different and was in agreement with a dicarbene mechanism (selective ring opening). For the hydrogenolysis of 6 membered ring napthenes, only Ir/Al_2O_3 exhibited a high selectivity (87%) for the direct opening of the 6 membered ring of MCH. Using bicyclic naphthenic molecules, McVicker et al. [2] also observed that the ease of converting two-ring naphthenes containing combinations of five- and six-membered rings over 0.9% Ir/Al_2O_3 is directly linked to the relative number of saturated five-membered rings in the molecule. Under the reaction conditions employed, perhydroindan containing one five-membered ring was more easily converted

to mixture of single-ring alkylcyclohexanes than decalin (which has only six-membered rings). In marked contrast, bicyclo[3,3,0]octane with two saturated five membered rings was selectively and completely (82% at 99% conversion) ring opened to C8–alkanes, whereas the conversion of decalin was only 4.4%. This again shows to the necessity of isomerising 6 membered rings to 5 membered rings before ring opening.

The need to further concentrate on this isomerization step is emphasized by McVicker et al. [2]. Highly branched isomerization is undesirable as more substituted carbons will retard ring opening for Ir based catalysts, and the ring opening product will be a highly branched alkane which has a lower cetane number. In the case of MCH conversion, high ethyl cyclo pentane (ECP) yield was observed by low to moderate acidic amorphous SiO_2/Al_2O_3, highly dealuminated USY and ECR-32 zeolites; however, this was at the expense of very low conversion. Lower ECP selectivities were exhibited by highly acidic materials like LZY-82 and zeolite beta.

The ability of Ir to selectively open ring structures was observed by Van Senden et al. [32] using Ir and Pt on Al_2O_3. They observed that the Ir/Al_2O_3 surface promotes selective ring opening of MCP. They also observed that the influence of particle size on product distribution is less pronounced in the case of Ir than Pt. This conclusion is supported by the work of Gault and coworkers who also observed similar selectivity with Ir [26,54]. Nylén et al. [4] also reported the ability of Ir to promote selective ring opening in their work with indan as the probe molecule. Additionally, rhodium was observed to promote selective ring opening of MCP. Techner et al. [33] studied hydrogenolytic ring opening of MCP over Rh/Al_2O_3 at high temperature. The catalyst showed selective ring opening for MCP with a variation in ring opening product distribution as a function of temperature and hydrogen pressure.

2.7 Zirconium Oxide and Zirconia Catalyst Systems

The above literature review shows that most of the published research on ring opening catalysts is based on solid acid supports such as zeolites, alumina, and silica. Despite considerable research using these metal oxides, there has been little progress developing an industrial selective ring opening catalyst. Therefore, there is a need to examine additional novel metal oxides for ring opening and selective ring opening

catalysts. Zirconium dioxide (ZrO_2) has attracted attention as a catalyst and catalyst support in recent years. Bhasker et al. [55] discusses the use of zirconia as a catalyst support, and notes that zirconia has several key attributes, including (1) it interacts strongly with the active phase, (2) it possesses high thermal stability and is more chemically inert than the classical supported oxides, (3) it is the only metal oxide which may possess all four chemical properties, namely acidity, basicity, reducing ability and oxidizing ability, and (4) it exhibits super-acidic properties when modified with small quantities of sulfate ions. Zirconia as a catalyst support has been employed in many industrially important reactions such as hydroprocessing, oxidation of alcohols, synthesis of methanol and higher alcohols, and methanation reactions. The surface properties of ZrO_2 and its interaction with deposited molybdenum were found to be favorable for hydrotreating reactions. The extreme hardness and high specific mass of zirconia is also considered an advantage for its potential use as catalyst support [23].

It is well accepted that zirconia assumes a monoclinic or *baddeleyite* unit cell containing four ZrO_2 molecules at ambient conditions. It transforms into a tetragonal form at about 1440 K, a cubic *fluorite* form around 2640 K, with a melting temperature of 2950 K. The addition of impurities like Ca^{2+}, Mg^{2+} or Y^{3+} improves substantially the thermo-mechanical properties of zirconia facilitating the production of materials with extremely high toughness, strength, and thermal shock resistance. It is known that these properties are closely related to the stabilizing effect. These anion deficient materials have important ceramic and superionic conduction properties, and are known collectively as cubic stabilized zirconias [24]. Previous work done by Kenney [45] suggested that incorporation of Mo^{6+} also has a stabilization effect on pure zirconia. The monoclinic phase of pure zirconia was confirmed, and it was observed that the phase transition to tetragonal phase occurred at 9.0 % Mo loading. The stabilized zirconia-molybdena catalyst (monofunctional) was tested for MCP ring opening. This catalyst demonstrated MCP conversion activity and the highest activity corresponded to the zirconia-molybdena catalyst with the highest acidity (Mo/Zr = 0.03), although the products were not analyzed.

2.8 Summary

1. There is a need to upgrade heavy oil fractions than is currently being performed to increase the cetane quality of diesel fuels. The driving forces are both statutory and economical.
2. The need for this betterment calls for catalysts with superior activity for selective ring opening. For the Canadian oil sands industry, the economics of selective ring opening are substantial.
3. When it comes to ring opening catalysts, essentially all ring opening catalysts are bifunctional in nature; a metallic function for hydrogenation/dehydrogenation and an acidic function for isomerization/ring opening.
4. While the ability of the metal for hydrogenation/dehydrogenation or the ability of the acid function for isomerization is not questioned, there are different conclusions regarding the ability of the metal to isomerize/ring open. It has been seen that this is variant with metal itself and the support used.
5. Thermodynamically, 5 membered ring structures are easier to open than 6 membered ring structures, thus, isomerization from 6 to 5 membered rings is very important in selective ring opening. The acidity function which is responsible for this isomerization also promotes cracking; therefore, the acidity need to be optimized.
6. Group VIII metals are the most active for ring opening. Among these metals, Ir was found to be the most suitable for selective ring opening.
7. Metal support interaction, metal dispersion and metal particle size play an important role in the activity and selectivity of the catalyst. While considerable work has been performed on ring opening, there very little done on selective ring opening.
8. Most of the ring opening studies were performed using zeolites, alumina and silica, and nearly all combinations of zeolites with different transition metals have been studied.
9. Zirconia shows promise as an emerging catalyst. Very little or no work has been done on zirconia systems towards selective ring opening.
10. Zirconia has unique properties which apparently can be exploited to make a good selective ring opening catalyst. The exploratory work with zirconia shows that zirconia has the potential to be explored further.

Chapter 3 Simulation Methods

3.1 Introduction

All of the calculations in this study were performed using DMol^3 in the Materials Studio® (version 2.2) molecular simulation software from Accelrys. DMol^3 is a unique density functional theory (DFT) quantum mechanical code that allows the user to perform variety of calculations in gases, surfaces, and solids [4].

3.2 Development of Density Functional Theory (DFT) - A Brief History

Density-functional theory is one of the most popular and successful quantum mechanical approaches currently used. It is routinely applied in physics and chemistry for calculating the binding energy of molecules and the band structure of solids. The application of DFT has also begun to appear in fields such as biology and mineralogy. The versatility of DFT is owed to its fundamental concepts and the flexibility one has in implementing them to study complex systems [1].

Density functional theory considers the particle density to be the fundamental variable to describe the state of a system in an external potential. The external potential itself may be static or time dependant, and the system may be composed of particles obeying classical or quantum mechanics [2]. The quantum mechanical behavior of electrons in solids can completely be described, only if the many-electron wave function for the system can be calculated. In principle, for a single electron moving in a potential $v(\mathbf{r})$ this may be obtained from the time-independent Schrodinger equation

$$\left[\frac{-h^2\nabla^2}{2m}+v(r)\right]\Psi(r)=\varepsilon\Psi(r) \quad \text{---------- (1)}$$

where Ψ represents the wave function of the particle. If there is more than one electron (many-body problem), the Schrodinger equation becomes

$$H\Psi=[T+U+V]\Psi=\left[\sum_i^N -\frac{h^2}{2m}\nabla_i^2+\sum_i^N V(r_i)+\sum_{i<j}^n U(r_i,r_i)\right]\Psi=E\Psi \text{ ----------(2)}$$

where H represents the Hamiltonian operator, N is the number of electrons, U is the operator for electron- electron interaction, T is the operator for the kinetic energy of electrons, and V is the operator for potential energy. The variables T and U are termed *universal operators* whereas V is system dependant, as it depends on the potential $v(\mathbf{r})$ of the system. The Schrodinger equation yields the quantized energies and form of the wavefunction from which other properties can be calculated [8]. However, the solution of Schrodinger equation is a computationally challenging problem. This has led to attempts for simpler solutions [1, 3, 7].

Historically, the density functional approach began with the idea that locally the behavior of a collection of particles (the electron cloud) could be approximately represented by that of the free electron gas of the same density at that point. The Thomas-Fermi model of 1920s was very successful in many ways and demonstrated the basics steps to obtain the density functional for the total energy [2]. In this approach, the energy of an atom was calculated by representing its kinetic energy as a functional of the electron density and combining it with the 1 expressions for the nuclear-electron interaction and electron-electron interactions [7]. The relation between the kinetic energy and electron density is given by the following equation.

$$T_{TF}[\rho] = C_F \int h^{\frac{2}{3}}(r) dr \; ; \quad C_F = \tfrac{3}{10}(3\pi^2)^{\frac{2}{3}} = 2.871 \text{----------} (3)$$

However, the accuracy of the results using this equation are not satisfactory because of the inaccurate treatment of the kinetic energy terms in the functional [3, 4, 7].

Hartree was one of the earlier people attempted to solve the problem [3]. He made assumption about the form of the many-electron wavefunction in an attempt to simplify the problem. In this approach, the many-electron wave function Ψ is approximated by the product of one-electron functions Φ for each of the N electrons (Equation 4).

$$\Psi(r_1, r_2, r_3 .... r_N) = \phi_1(r_1)\phi_2(r_2) .... \phi_N(r_N) \text{----------} (4)$$

In this equation, $\mathbf{r}_i$ are the positional coordinates and a spin coordinate for the i^{th} electron. These wavefunctions would take the form of simple plane waves in a uniform system. This assumption made it possible to proceed using the *variational* principle. The variational principle states that if we take some wave function Ψ (e.g., some approximate one) for a system and calculate the expectation value of energy E, this energy will be either higher, or equal to the ground state energy E_0 for this system.

$$E = \frac{\langle \Psi | H | \Psi \rangle}{\langle \Psi | \Psi \rangle} \geq E_0 = \frac{\langle \Psi_0 | H | \Psi_0 \rangle}{\langle \Psi_0 | \Psi_0 \rangle} \text{----------(5)}$$

The $E = E_0$ occurs only if Ψ is equivalent to Ψ_0, or else $E > E_0$ [9]. The approach assumed that electrons in the atom can be described independently, i.e., their movement is independent of each other and their interaction is not paired, but each electron interacts with some averaged field of other electrons. However, the fact is that electrons have to avoid each another (correlate their movements) since they repel each other as they are of the same charge. In other words, the Hartree approximation effectively ignored the Pauli exclusion principle. As a result, the Hartree approach failed to recognize the binding energies in solids, but it worked well for atoms. The function also did not have a proper symmetry for interchanging particle indices for fermions [3, 9].

Improvement to Hartree theory was made by Hartree-Fock [3]. In this model, the antisymmetric many-electron wavefunction is specially constructed out of single-electron wavefunction. The many-body Hamiltonian is used to model the interaction between the electrons and the nucleus.

$$H = \sum_i -\frac{1}{2}\nabla_i^2 + \sum_i \sum_a \frac{Z_a}{|r_i - d_a|} + \frac{1}{2}\sum_i \sum_{j \neq i} \frac{1}{|r_i - r_j|} + \frac{1}{2}\sum_a \sum_{b \neq a} \frac{Z_a Z_b}{|d_a - d_b|} \text{-------(6)}$$

The first term in the above equation is the sum of the kinetic energy operators for each electron in the system. The second term is the sum of the electron-nucleus coulombic attractions. The third term is the sum of the electron-electron coulombic repulsions, and the last term is the sum of the nucleus-nucleus coulombic repulsions, also known as the

nuclear repulsion energy. The reason behind the electron-electron repulsion was the inclusion of Paulis exclusion principle through the use of an antisymmetrised wavefunction [3, 7]. Although the Hartree-Fock approach effectively recognized binding energy in a neutral system through the contribution of exchange potential, the approach was actually inferior to the Hartree approach in calculating many other properties of the system. The reason was that Hartree-Fock approach ignored the electrostatic correlation of electrons which was somewhat balancing the exchange effect. Thus, the Hartree-Fock approach worked for systems where there were few electrons [3]. The ultimate failure of both Hartree and the Hartree-Fock models is ascribed to not having good enough approximate forms for the wavefunction to begin with [3].

3.3 Advancements in Density Functional Theory

Hohenberg and Kohn (1964) suggested that the real problem lied in dealing with the many-electron wavefunction as the fundamental variable in a variational approach. First, it needed $\sim 10^{23}$ parameters to be adequately described. Second, it had that additional complication of possessing a phase as well as a magnitude. So they chose the electron density as their fundamental variable. That is, they considered the electron density distribution which minimized the total energy defined the ground state of the system. They also showed that all other ground state properties of the system are functionals of the ground state electron density, so that once the ground state electron density is known all other ground state properties can be estimated, at least in principle [3].

In 1965, Kohn and Sham derived the Kohn-Sham equation where the potential experienced by the electrons is formally expressed as a functional of the electron density. The equation was effectively a single-particle equation which had Hartree potential and an exchange-correlation potential making up for electron-electron interaction potential, in addition to the contribution from the electron-ion interaction [3].

$$E[\rho] = T_s[\rho] + V_N[\rho] + J_{ee}[\rho] + E_{xc}[\rho] \quad \text{---------- (7)}$$

where E[ρ] is the total electronic energy, T_s [ρ] is the kinetic energy of non interacting electrons, V_N [ρ]describes the electron-nuclei interaction and J_{ee} [ρ] is the coulombic interaction (Hartree term) among the electrons. The last term is the exchange correlation energy functional E_{xc}[ρ]. The exact form of the exchange potential is not known which necessitates the use an approximate functional. Also, there are no methods to systematically improve this exchange correlation functional [3, 10]. In effect Kohn-Sham approach simplified the many-body problem of interacting electrons to a system of non-interacting electrons moving in an effective potential where the effective potential included the external potential and the coulomb interactions between electrons [6].

Since 1970s, DFT has been used for calculations in solid state physics. 1990s saw more refinements in the approximations used in the theory, which made it more acceptibile as an accurate method for calculations in quantum chemistry. Today both the fileds employs DFT as a leading tool for electronic structure calculations [6].

3.4 Limitations of DFT

The major limitation with DFT, with the exception of the free electron gas, is that the exact functionals for exchange and correlation are not known. However certain physical quantities can be calculated with high degree of accuracy using certain approximations.[6]. Also, as an energy minimum approach, its reliability is in question when dealing with the excited states of the system (i.e. states other than the ground state) [3].

3.5 DFT Parameters

Described below are some of the important parameters which need to be specified when performing DFT calculation in DMol^3. Parameters are described briefly with arguments for choosing their value or form in the present study.

The atomic basis set is the number and type of atomic orbitals used in the expansion of the molecular orbitals. DMol^3 uses numerical orbitals for the basis functions, with each function corresponding to an atomic orbital [4, 5]. Greater variational freedom is obtained by providing larger basis sets. Generation of an entire second set of functions results in doubling the basis set size and this is referred to as a

double-numerical (DN) basis set. In the present simulations, an atomic basis set of DN plus a polarization p-function for all hydrogen atoms (DNP). The DNP basis set includes one numerical function for each occupied atomic orbital and a second set of functions for valence atomic orbitals, plus a polarization *d* function on all atoms. This is the basis set with the highest accuracy, however, this comes with a high computational cost. This is deemed the most appropriate for systems involving hydrogen [4, 5].

The selected functional specifies the type of DFT exchange-correlation potential to be used in the calculation. The functionals available in $DMol^3$ are broadly classified into local-density approximation (LDA) types and generalized gradient approximation (GGA) types [4, 5]. Historically, the most important type of approximation used was LDA. For many decades, LDA has been applied in calculations of band structures and total energies in solid-state physics. In quantum chemistry it is much less popular, because it fails to provide results that are accurate enough to permit a quantitative discussion of the chemical bond in molecules [1]. In applications to molecules, it was found that the LDA tends to overbind producing high values of molecular binding energies. Also, weaker bonds, such as hydrogen bonds, are significantly overestimated using LDA. This has led to the development of a gradient corrected approximation. The use of gradient corrections has resulted in significant improvements in the energy changes when a molecule is formed from atoms or when a molecule is bonded to a surface. The LDA is exact for a perfect metal (which has a constant electron density) and becomes less accurate for systems with varying electron density [4].

Because the present study involved insulating solids (metal oxides), gases, surface adsorption, and the resultant energy changes a gradient corrected approximation (GGA) was deemed more appropriate and it was used in all calculations. However GGA is known to fail when weak interactions like van der waals interactions occur [1]. This was of little concern in the present study, as the primary interests were not examining the attributes of weak interactions. Of the many functionals available using GGA, the functional by Perdew and Wang (PW91) was chosen. PW91 is derived by considering low and high density regimes and by enforcing various summation rules. The system in this research encounters low and high density regimes, and thus PW91 was considered as the most appropriate [4, 5].

Convergence tolerance specifies the threshold used to determine convergence. The 'coarse' option was chosen as this would speed up computation time without significantly compromising accuracy. With this option, the simulation would converge if the energy (total) difference between two consecutive steps was less than 0.062 k.cal (1×10^{-4} Ha). This accuracy was considered to be acceptable considering the nature and objective of the work [5]. The corresponding values for energy change, maximum force, and maximum displacement between optimization cycles were 0.0001Ha, 0.02 Ha/Å, and 0.05 Å respectively. The charge allows the user to specify a net charge on the model system. For nearly all simulations, the charge was set as zero as the net charge of the system was zero [5]. In the simulation of reactions in the gas phase involving protons, a charge of +1 was used. The integration accuracy specifies the precision used in the numerical integration of the Hamiltonian. The 'medium' option uses about 1000 grid points for each atom in the calculation [5]. The 'coarse' option was chosen to speed up the calculation, as this was deemed sufficient. Self-consistent field (SCF) calculation specifies the threshold used to determine whether an SCF has converged. The convergence criterion for the SCF cycle was set at 0.0001 [5].

The k-point set defines the number of integration points that will be used to integrate the wavefunction in reciprocal space. The 'coarse' option was chosen which would give a k-point separation of 0.07 1/Å. This value was chosen for reasonable accuracy with acceptable computational time. The option of 'effective core potential' (ECP) was selected for all calculations. ECP does not account for all electrons explicitly, rather it replaces core electrons by a single effective potential reducing the computational cost. The 'all electron relativitistic' is the most accurate option available but comes at a higher computational cost. Though this could influence the value of the calculated total energies, the differences are expected to cancel when calculating heats of reaction, heats of adsorption, or other thermodynamic quantities. Real space cut-off specifies the finite range cutoff of the atomic basis set. Decreasing the cutoff reduces the computational time required for a calculation but introduces large approximations. The proposed range for a cut-off value is 3.175 Å – 15.0 Å, with a default cutoff value of 5.0 Å. However, a cutoff of 4.5 Å was chosen and used for all calculations [5]. In practical sense this means two atoms beyond these distances do not influence each other. Considering the fact that

the bond lengths involved in the present study ranged from 1.0 Å to 2.5 Å, the selected cutoff value of 4.5 Å was considered to be sufficient.

3.6 Simulation Procedures

The simulations performed in this work can be broadly classified in to three categories; (1) geometry optimization , (2) energy calculation, and (3) transition state search. Geometry optimization is performed to find out the optimum geometry of systems corresponding to the minimum energy. The system can be a molecule, unit cells (bulk phase), clean surfaces, or surfaces with adsorbed molecules. In this process, atoms are moved within the constraints of the parameters specified to reach at the geometry corresponding to the lowest energy of the system. The time taken for such a calculation can vary from one minute to several days, depending on the size of the system and computing hardware, with the required time increasing exponentially with the number of atoms involved. Energy calculations were performed to determine the total energy of the given system. The system can be an atom, a molecule, a unit cell, or a vacuum slab. In this process, atoms are not moved but the energy corresponding to the geometry of the given system is calculated from the first principles. This is often a quick calculation in the time scale of molecular simulation. The time taken for the energy calculation of a primitive unit cell is about an hour. Transition state search is performed exclusively to map the energetics of model reactions. To begin with, the optimized reactant and optimized product need to be determined and specified. Transition state search traces the reaction path between the reactant and the product, and is much more time consuming than geometry optimization. Depending on the size of the system, the calculation may require several hours to several days. A detailed discussion on how these tasks are performed is given in the following section.

3.6.1 Calculation of the Heat of Adsorption

The heat of adsorption of the adsorbate can be calculated from the energies of the optimized structures. The equation is as follows.

$$\Delta E = E_{\text{adsorbate on vaccslab}} - (E_{\text{vaccslab}} + E_{\text{adsorbate}}) \quad \text{---------- (8)}$$

If ammonia is the gas molecule used, the above calculation gives the heat of adsorption of NH_3, which in turn is a measure of the Lewis acidity of that surface at the point of adsorption. In a similar way, the Brønsted acidity of the surface also can be calculated by simulating the adsorption of ammonia on a surface hydroxyl group. The process of surface -OH formation can be written as follows;

$$\text{Vacuum Slab} + H_2O \longrightarrow \text{Vacuum Slab–OH} + 0.5\ H_2 \quad \text{---------- (9)}$$

With this equation, the heat of adsorption of the –OH groups on surface can be written as

$$\mathbf{\Delta E} = \mathbf{E}_{\text{vaccslab+-OH}} + \mathbf{E}_{\text{0.5 H2}} - (\mathbf{E}_{\text{vaccslab}} + \mathbf{E}_{\text{H2O}}) \quad \text{---------- (10)}$$

The heat of adsorption of NH_3 can be written as

$$\mathbf{\Delta E} = \mathbf{E}_{\text{(vaccslab +-OH+ NH3)}} - (\mathbf{E}_{\text{vaccslab+-OH}} + \mathbf{E}_{\text{NH3}}) \quad \text{---------- (11)}$$

This methodology was applied to determine the heat of adsorption for all probe molecules investigated in this study.

3.6.2 Transition State Search

The chemical reaction is represented by a path where the molecular coordinate space from the reactants into products is determined [12]. Chemical reactions proceed via a series of elementary reactions (elementary steps) [13]. Any chemical reaction can be viewed as a transition between one minimum (reactants) to another minimum (products) on the potential energy surface describing the energy of all the atoms in the system as a function of their coordinates. Every point along the minimum energy path has the property of being the lowest energy point in all degrees of freedom except for the one along the path. The highest energy point along the minimum energy path represents the classical barrier height for the transformation described by that path [14]. The term transition state is often used to describe the system at the top of the energy barrier and molecule(s) at this point is generally termed activated complex [13]. Transition state

theory supposes that the nature of the activated complex (TS) is such that it represents a population of molecules in equilibrium with one another, and also in equilibrium with the reactant(s). The activated complex can form products or deactivate back to the reactants. Higher the barrier, slower the reaction rate is [13]. Synchronous transit methods are used to find a transition state (TS) when reasonable structures for the reactants and products exist, but the location of the TS is unknown. The linear synchronous transit (LST) method performs a single interpolation to a maximum energy. The quadratic synchronous transit (QST) method alternates searches for an energy maximum with constrained minimizations in order to refine the transition state to a high degree [15]. The 'complete LST/QST method' available in DMol^3 is used for all the transition state searches in the present study. This method begins by performing an LST/Optimization calculation. The TS approximation obtained in that way is used to perform QST maximization. From that point, another conjugate gradient minimization is performed. The cycle is repeated until a stationary point is located or the number of allowed QST steps is exhausted. This is considerably more accurate than all the other methods.

Chapter 4 Results

4.1 DFT Calculations

The discussion in the previous chapter regarding the DFT calculations is summarized as follows. All of the calculations were performed using DMol^3 from Accelrys® (version 2.2). The double-numerical plus polarization functions (DNP) and Perdew–Wang generalized gradient approximation (GGA-PW91) were used in all calculations. The real space cutoff radius was 4.5 Å. Effective Core Potentials (ECP) were used to treat core electrons and a *k*-point set corresponding to a *k*-point separation of 0.07 Å^{-1} was chosen because of the large super cells used [1]. To determine the activation energy for a specific reaction path, a transition state that connects two immediate stable structures through a minimum energy path was identified by complete synchronous transit (LST) and quadratic synchronous transit (QST) search methods [1,2]. If a parameter used in the calculations differs from the above, it will be presented in the discussion for that particular simulation. All energies are reported in kcal mol^{-1} unless otherwise specified.

4.2 Structure and Properties of ZrO_2

As noted previously, it is well accepted that zirconia prefers a monoclinic or *baddeleyite* unit cell containing four ZrO_2 molecules at ambient conditions. ZrO_2 transforms into a tetragonal structure at about 1440 K, and a cubic *fluorite* structure around 2640 K with a melting temperature of 2950 K. The addition of impurities like CaO, MgO or Y_2O_3 substantially improves the thermo-mechanical properties of zirconia [4]. Additionally, previous experimental work has shown that MoO_3 also produces a similar zirconia stabilization effect [5]. The structures of monoclinic and cubic zirconia were available in the Materials Studio structural library (Fig. 4.1), and the crystal structures were compared with crystallographic data. The structures were further refined by performing geometry optimization. The total energy calculated for both the structures turned out to be similar, so the simulation was repeated with more stringent parameters and tolerances. All electron relativistic was chosen to represent the core electrons. The energy cutoff was increased to 5.5 Å. The integration accuracy, *k*-point set and SCF tolerance were set at 'fine'. The total energy of a unit cell of cubic zirconia containing

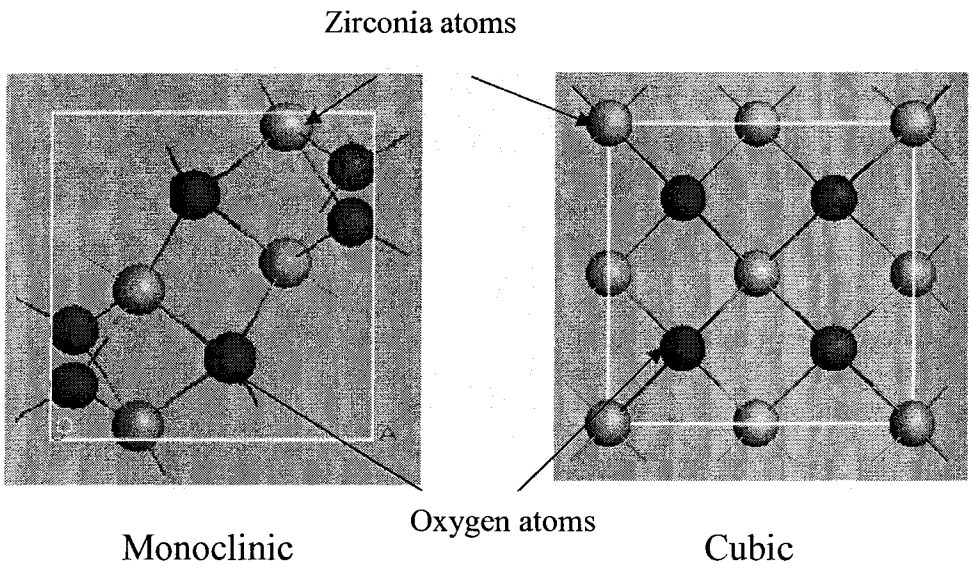

Fig. 4.1 Monoclinic and cubic phase structures of zirconia [11]

four ZrO_2 was calculated as -15,378.38 Ha (1 Ha = 627.51 kcal mol^{-1}) and that of the monoclinic cell was calculated as –15,378.39 Ha. The lattice parameters of cubic zirconia did not change with optimization; the lattice dimensions were a = b = c = 5.07Å and the angles were $\alpha = \beta = \gamma = 90°$. The optimized lattice dimensions of monoclinic zirconia were a = 5.14 Å, b = 5.20 Å and c = 5.31 Å and the angles were $\alpha = 90^0$, $\beta = 99.23^0$ and $\gamma = 90^0$. It should be noted during the optimization of the monoclinic structure, there was minor rearrangement of the bulk atoms. The total energy figure shows that monoclinic zirconia is more stable at ambient conditions.

4.2.1 Surface Energy of Cubic ZrO_2

Simulations were performed to determine which geometrical plane is more probable for cubic zirconia. The conclusion was based solely on the energetics, assuming that the lower energy surface will be the more probable. $DMol^3$ does not have a module to calculate the surface energy, but with the help of some assumptions geometry optimization could be used to find out the surface energy. It was assumed that in a slab of some appreciable thickness, regardless the surface orientation of the exposed plane, the bulk energy remains constant and only the surface energy changes according to orientation. This is a reasonable assumption as the surface orientation does not affect the bulk structure and the energy of the bulk phase is solely dependant on its structure. It was also assumed that there were no kinetic limitations for the surface to achieve the required orientation. With these assumptions, the total energy can be used to compare surface energy and the system with the least total energy can be considered to be the most probable

In this study, three stoichiometric vacuum slabs each containing four ZrO_2 from cubic zirconia were prepared with three different surface orientations , namely (100), (110) and (111) surface planes. As the unit cell under study was cubic, these three Miller indices represent all the lower indices involving 1 and 0 (for cubic system, (110) is the same as (101)). No atoms were constrained, thereby allowing every atom to move to minimize energy. The results are as follows.

Total energy of (100) vacuum slab containing four ZrO_2 = -790.99 Ha

Total energy of (110) vacuum slab containing four ZrO_2 = -791.19 Ha

Total energy of (111) vacuum slab containing four ZrO_2 = -790.99 Ha

Therefore, it can be concluded the (110) orientation is the most stable surface orientation, and would be the most prominent in a cubic zirconia system. The vacuum slabs with their calculated energies are shown in Fig.4.2

4.2.2 Activity of Different Planes of ZrO_2

The activity of an isomerization catalyst can be correlated to its inherent acidity. Strengths and types of acidity are discussed in the *Literature Review* (Chapter 2). Simulations were performed on different surface orientations using ammonia as the probe molecule of adsorption due to fact that ammonia is commonly used in experiments to quantify surface acidity.

Vacuum slabs of each surface orientation were cleaved out of the bulk cubic structure of zirconia, and each vacuum slab comprised of two layers of atoms. The bottom layer of the slab was constrained (fixed in its position) to speed up the calculation. This constraint is similar to actual materials, as the atoms on the surface will have more freedom for movement than the atoms in the bulk. Standard parameters were chosen and the geometry optimization of the pure vacuum slab was performed. One NH_3 molecule was docked on a Zr atom and the geometry optimization performed, and Lewis acidity was calculated from the relative energetics according to the calculation method discussed in the *Experimental* (Chapter 3). In a similar fashion, Brønsted acidity was also determined by adsorbing a hydroxyl group to surface Zr atom(s). Geometry optimization of this structure was performed, and once converged, a NH_3 molecule is docked above the H atom of the hydroxyl group. Geometry optimization of this structure is also performed, and from these results Brønsted acidity can be calculated. The systems involved in these calculations are shown in Fig.4.3.

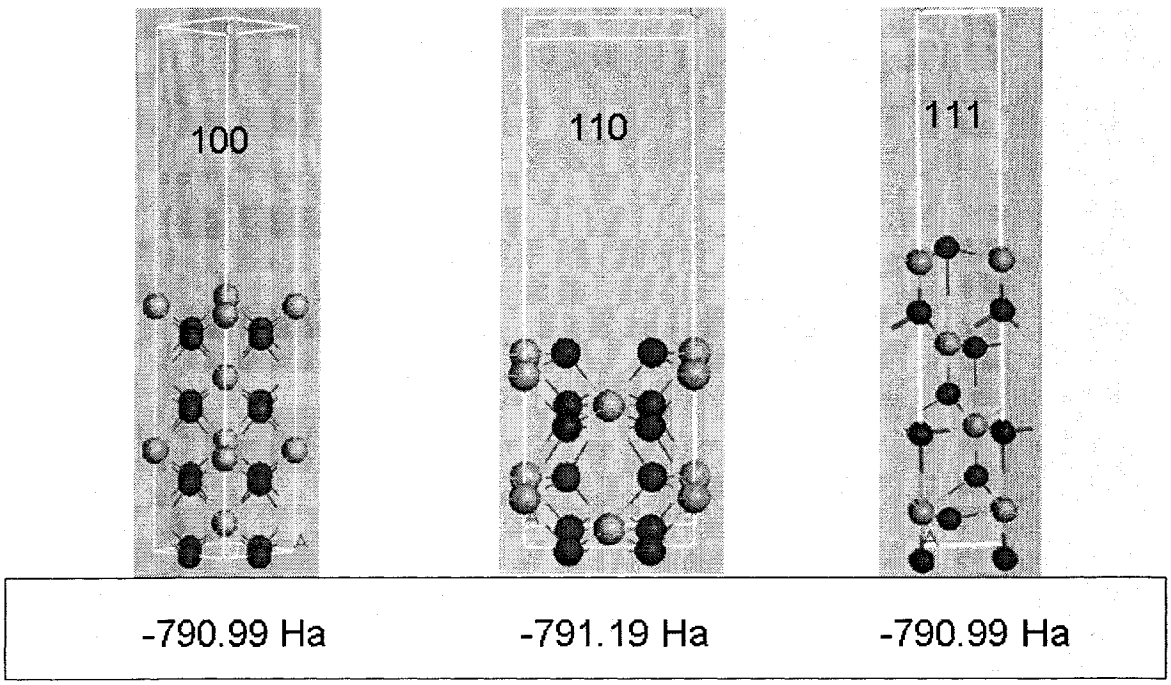

Fig. 4.2 Total energies (Hartrees) of stoichiometric slabs of cubic zirconia at different orientations [11]

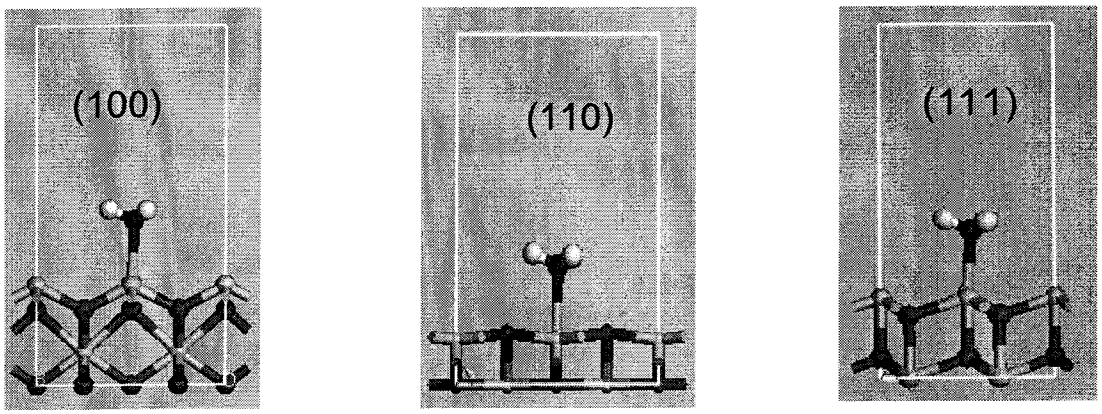

Fig. 4.3 (a) Optimized structures to calculate Lewis acidity [11]

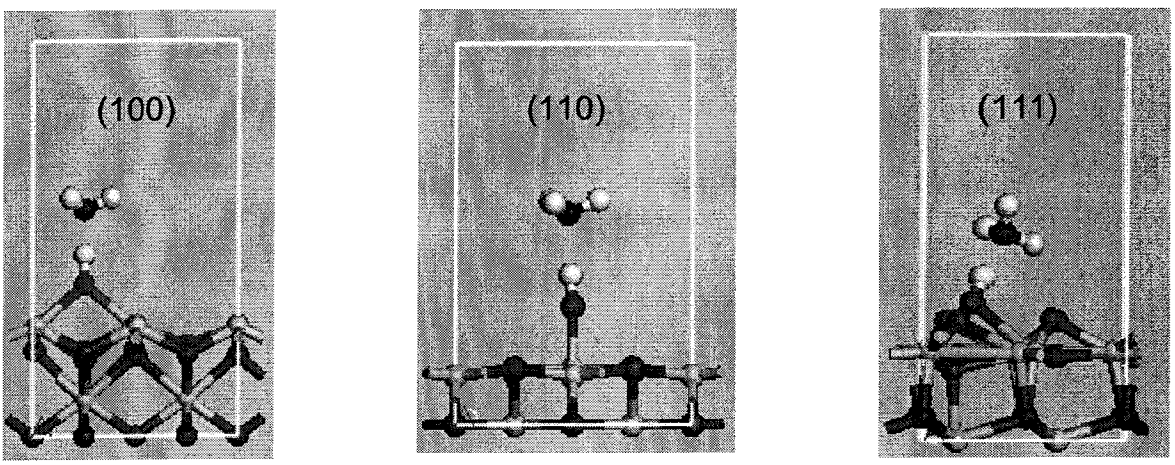

Fig. 4.3 (b) Optimized structures to calculate Brønsted acidity [11]

4.2.3 ZrO_2 Lewis and Brønsted Acidity

Lewis Acidity of ZrO_2 (111) surface

Total Energy (Vacuum Slab + NH_3) = -2015.01 Ha

Energy (Vacuum Slab) = -1958.40 Ha

Energy (NH_3) = - 56.56 Ha

Heat of adsorption = -2015.01–(-1958.40 + - 56.56)

= -0.04 Ha

Heat of adsorption = -29.0 kcal mol^{-1}

Brønsted Acidity of ZrO_2 (111) surface

Energy of vacuum slab = -1958.40 Ha

Energy of vacuum slab with –OH = -2034.56Ha

Energy of vacuum slab with –OH and NH_3 = -2091.14 Ha

Energy of H_2O = -76.44 Ha

Energy of H_2 = -1.17 Ha

Energy of NH_3 = - 56.56 Ha

Heat of adsorption of -OH = - 2034.56+ 0.5 * -1.17

- (-1958.40 +-76.44)

= -0.30 Ha

= -191.0 kcal mol^{-1}

Heat of adsorption of NH_3 = -2091.14 – (-2034.56+

-56.56)

= -0.02 Ha

= -12.5 kcal mol^{-1}

The results are summarized in Table 4.1

ΔH NH3 on surface, kcal mol^{-1}			ΔH -OH on surface, kcal mol^{-1}			ΔH NH3 on –OH on surface, kcal mol^{-1}		
(100)	**(110)**	**(111)**	**(100)**	**(110)**	**(111)**	**(100)**	**(110)**	**(111)**
-39.0	-21.3	-29.1	-69.2	-15.9	-191.0	-	-4.3	-12.5

Table 4.1 Lewis and Brønsted acidity of various surfaces of cubic zirconia

4.2.4 Modifier Element Incorporation into ZrO_2

Simulations were performed to determine the influence of modifier element incorporation on the properties of zirconia, specifically acidity. Modifier element incorporation was performed both in the bulk and surface.

4.2.4.1 Bulk Modifier Element Incorporation

Molybdenum incorporation was performed in the bulk structure to determine if it forms a stable structure, and also to see if Mo has any preferential location for Zr replacement. This simulation was done on both monoclinic and cubic zirconia. For monoclinic zirconia, Mo substitution was done at 3 locations (Fig. 4.4). The total energies of the unit cell with Mo substitution at different locations are 9322.50 eV, 9322.49 eV and 9322.49 eV. For cubic zirconia, Mo substitution was done at different locations for different concentrations (Fig.4.5). For a 7% concentration of Mo in the bulk, the energies were 8837.29 eV and 8837.18 eV for 2 different locations. For a 10 % concentration of Mo in the bulk, the energies were 8891.09 eV and 8891.09 eV for 2 different locations. For a 15 % concentration of Mo in the bulk, the energies were 8898.76 eV and 88898.76 eV for 2 different locations.

4.2.4.2 Surface Modifier Element Incorporation

One surface atom of Zr was replaced by the modifier element to study the effect on the surface properties. To maintain a uniform basis for comparison, the same vacuum slabs used to characterize pure zirconia were used. The bottom layer was constrained and the atoms in the top layers were free to move. The modifiers incorporated were Al, Mo, Si, Ti, W, B and Mg, and simulations were performed for both the (110) and (111) surfaces.

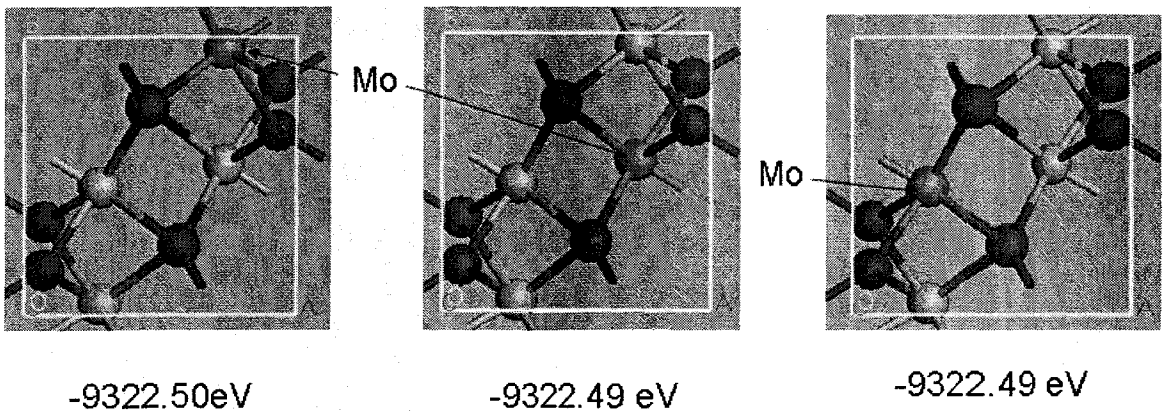

Fig 4.4 Energies of unit cells of monoclinic zirconia with Mo incorporation at different Locations [11].

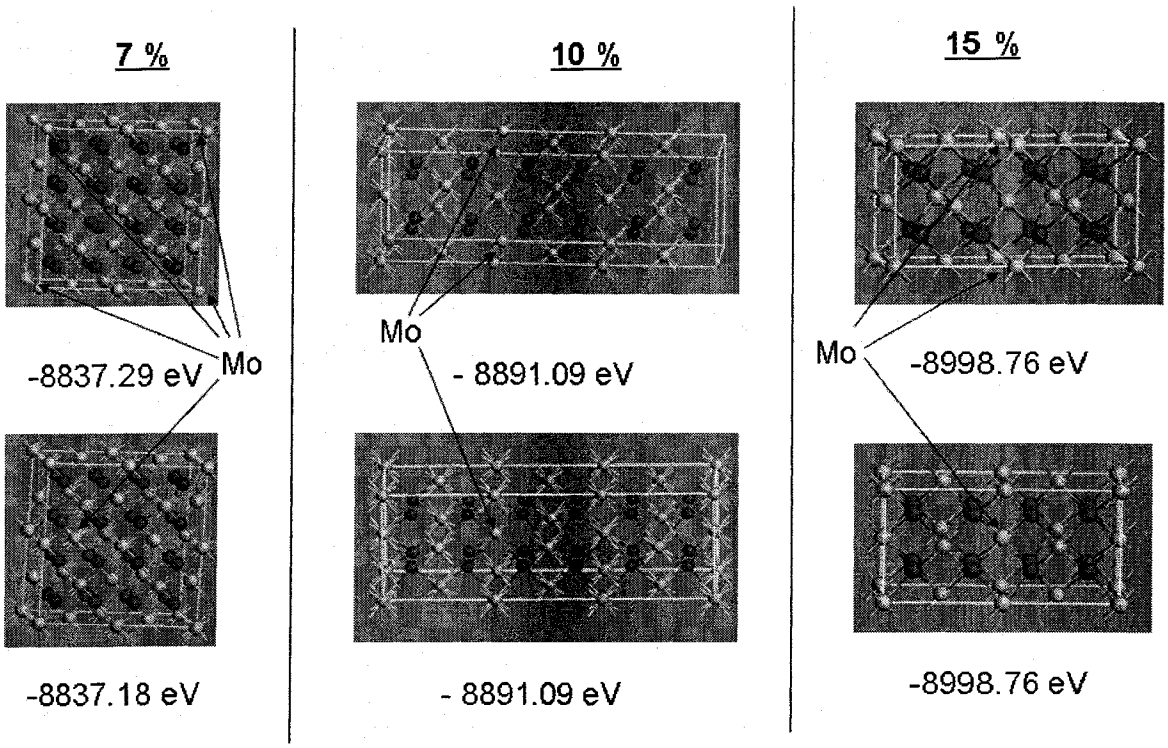

Fig 4.5 Energies of unit cells of monoclinic zirconia with Mo incorporation at different locations for different concentrations [11].

The simulation began with geometry optimization of the vacuum slab with a Zr atom on the surface replaced by the modifier. This corresponds to to a concentration of 15% of the modifier element on the surface. For convenience, a r atom at the centre of the slab was replaced by the respective modifier, and for the reference this position is termed location #1. The Zr atom next to this position is labeled location #2 and the Zr atom next to location # 2 is labeled location #3. This is graphically explained in Fig. 4.6. Once this optimization was completed, one NH_3 molecule was docked on this modifier atom and geometry optimization performed. From these results the Lewis acidity corresponding to the modifier atom in the zirconia matrix could be calculated. It was also of interest to understand the influence of the modifier on the activity of the neighboring Zr atoms. To measure this, the docking point of NH_3 molecule was changed to location #2 and the geometry optimization done. This was also repeated for location # 3. In a similar fashion, the Brønsted acidity was also calculated for the modifier element, and Zr in location #2 and #3.

4.2.5.2.1 Al as the Modifier

For the (110) surface, Al was observed to have a coordination number of 2 versus the coordination of 6 Zr has on the surface. The Lewis acidity was calculated as -22.8, -22.3 and -21.86 kcal mol^{-1} at locations 1, 2 and 3, respectively. The Brønsted acidity was not calculated as the hydroxyl groups had positive heat of adsorption values. For the (111) surface, Al had a coordination number of 4, the same as that of Zr. However, the neighboring oxygen atoms had lower coordination numbers, and thus making the surface less stable. The (111) surface exhibited both Lewis and Brønsted acidity. At locations 1 and 2, the oxygen of the hydroxyl group bonded with the Al and Zr atoms in bridging position. The Lewis acidity was calculated as -22.5, -25.0 and -27.0 kcal mol^{-1} for locations 1, 2 and 3, respectively. The Brønsted acidity was calculated as -12.5, -15.5 and -12.8 kcal mol^{-1}, respectively, for these locations.

4.2.5.2.2 Mo as the Modifier

For the (110) surface Mo retained the coordination number of 6 zirconium has on the surface. The Lewis acidity was calculated as -21.9, -22.0 and -21.63 kcal mol^{-1} at

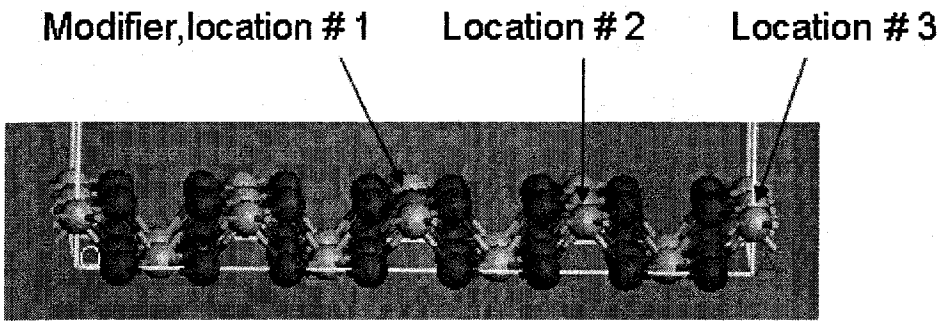

Fig.4.6 Different zirconia atoms chosen to study NH_3 adsorption [11]

locations 1, 2 and 3 respectively. The modified surface exhibited Brønsted acidity as well. The hydroxyl groups had a heat of adsorption of -22.0, -8.3 and -4.77 kcal mol^{-1} at locations 1, 2 and 3, respectively. The Brønsted acidity was weak and these were calculated as -4.2, -4.6 and -3.5 kcal mol^{-1}, respectively for these locations

For the (111) surface, Mo reduced the number of metal-oxygen bonds on the surface thus making the surface less stable. The Lewis acidity was calculated as -21.9, -22.5 and -27.5 kcal mol^{-1} at locations 1, 2 and 3, respectively. The hydroxyl groups were observed to be bonding in the bridging position for locations 2 and 3. Heat of adsorption of hydroxyl groups were calculated as -23.0,-39.2 and -73.5 kcal mol^{-1} at locations 1, 2 and 3, respectively. The Brønsted acidity was calculated as -8.9, -10.4 and -11.3 kcal mol^{-1}, respectively for these locations.

4.2.5.2.3 Ti as the Modifier

Ti retained the same coordination Zr has on surface. For the (110) surface it exhibited a Lewis acidity of -20.9, -22.2 and -22.8 kcal mol^{-1} at locations 1, 2 and 3, respectively. The heat of adsorption of hydroxyl groups was found to be positive, so further work was not done on Brønsted acidity.

For the (111) surface, Ti retained the original coordination number. Lewis acidity was calculated as -36.5,-27.7 and -22.4 kcal mol^{-1} at locations 1, 2 and 3, respectively. The hydroxyl groups were adsorbing in bridging position for all locations.. The heat of adsorption of hydroxyl groups were calculated as -33.8, -46.7 and -42.4 kcal mol^{-1} at locations 1, 2 and 3, respectively. The Brønsted acidity was calculated as -11.3, -11.2 and -11.7 kcal mol^{-1}, respectively for these locations.

4.2.5.2.4 Si as the Modifier

For the (110) surface, Si replaced Zr without reducing the number of bonds Zr had in the original matrix. The Lewis acidity calculated was -23.2,-23.5 and -22.2 kcal mol^{-1} at locations 1, 2 and 3, respectively. The hydrogen from the hydroxyl group on location 1 exhibited hydrogen bonding. The heat of adsorption for hydroxyl groups were -20.7, -12.5 and +13.2 kcal mol^{-1} at locations 1, 2 and 3, respectively. The Brønsted acidity was calculated as -5.8, -2.7 kcal mol^{-1} at locations 1 and 2, respectively.

For the (111) surface, Si reduced the number of metal-oxygen bonds on the surface thus making the surface less stable. The Lewis acidity was calculated as -28.5, -21.6 and -28.5 kcal mol^{-1} at locations 1, 2 and 3, respectively. Though NH_3 was bonding with Si, it was exhibiting hydrogen bonding with nearby oxygen. Heat of adsorption of hydroxyl groups were calculated as -64.9, -23.0 and -42.0 kcal mol^{-1} at locations 1, 2 and 3, respectively. The Brønsted acidity was calculated as -14.5, -13.8 and -24.2 kcal mol^{-1} , respectively for these locations.

4.2.5.2.5 W as the Modifier

For the (110) surface W retained the same coordination zirconium has on the surface. The Lewis acidity was calculated as -24.3, -22.4 and -22.4 kcal mol^{-1} at locations 1, 2 and 3, respectively. The hydroxyl groups had a heat of adsorption of -33.3, -17.4 and -14. kcal mol^{-1} at locations 1, 2 and 3, respectively. The Brønsted acidity was calculated as -4.7, -4.5 and -3.9 kcal mol^{-1} ,respectively for these locations.

For the (111) surface, W reduced the number of metal-oxygen bonds on the surface. The Lewis acidity was calculated as -22.8, -24.8 and -21.8 kcal mol^{-1} at locations 1, 2 and 3, respectively. Though there was appreciable heat of reaction of NH_3 with W, it did not make a bond with W. Heat of adsorption of hydroxyl groups were calculated as -26.3, -41.3 and -40.6 kcal mol^{-1} at locations 1, 2 and 3, respectively. The Brønsted acidity was calculated as -9.4, -14.2 and -10.7 kcal mol^{-1}, respectively for these locations.

4.2.5.6 Other Modifiers

Magnesium and Boron were tested as potential modifiers. It was observed that both the atoms were not bonding on both the (110) and (111) surfaces, so further studies were not performed.

The results are summarized in Tables 4.2- 4.5. For the sake of comparison, the values corresponding to pure zirconia are also included.

Modifier	Heat of Adsorption of NH3, kcal mol^{-1}		
	Location # 1	Location # 2	Location # 3
Zr	- 21.2	- 21.3	-21.3
Mo	-21.9	-22.0	-21.6
Al	- 22.8	- 22.3	- 21.9
Ti	-20.9	-22.2	-22.1
Si	-23.2	-23.5	-22.2
W	-24.3	-22.4	-22.4

Table 4.2 Lewis acidity on zirconia (110) surface with various modifiers

Modifier	Heat of Adsorption of NH3, kcal mol^{-1}		
	Location # 1	Location # 2	Location # 3
Zr	-28.9	-29.1	-29.0
Mo	-21.9	-22.5	-27.1
Al	-22.5	-25.0	-27.5
Ti	-36.5	-27.7	-22.5
Si	-28.5	-21.6	-28.5
W	-22.8	-24.8	-21.8

Table 4.3 Lewis acidity on zirconia (111) surface with various modifiers

Modifier	Heat of Adsorption of -OH Groups, kcal mol^{-1}			Heat of Adsorption of NH_3 kcal mol^{-1}		
	Loc. #1	Loc. #2	Loc. #3	Loc. #1	Loc. #2	Loc. #3
Zr	+15.9	+15.9	+16.1	-4.3	-4.4	-4.4
Mo	-22.0	-8.3	-4.8	-4.2	-4.6	-3.5
Al	+30.3	+19.7	+17.8	-NA-	-NA-	-NA-
Ti	+19.0	+15.7	+15.8	-NA-	-NA-	-NA-
Si	-20.7	-12.5	+13.2	-5.8	-2.7	-NA-
W	-33.3	-17.4	-14.6	-4.7	-4.5	-3.9

Table 4.4 Brønsted acidity on zirconia (110) surface with various modifiers

Modifier	Heat of Adsorption of -OH Groups, kcal mol^{-1}			Heat of Adsorption of NH_3 kcal mol^{-1}		
	Loc. #1	Loc. #2	Loc. #3	Loc. #1	Loc. #2	Loc. #3
Zr	-191.0	-191.0	-191.4	-11.1	-12.5	-
Mo	-23.0	-39.2	-73.5	-8.9	-10.4	-11.3
Al	-50.3	-47.4	-39.2	-12.5	-15.5	-12.8
Ti	-33.8	-46.7	-42.4	-11.3	-11.2	-11.7
Si	-64.9	-23.1	-42.1	-14.5	-13.8	-24.2
W	-26.3	-41.3	-40.6	-9.4	-14.2	-10.7

Table 4.5 Brønsted acidity on zirconia (111) surface with various modifiers

4.3. Ring Opening on ZrO_2 (111)

Both classical bifunctional and Haag-Dessau ring opening mechanisms were simulated to map out the energy surfaces [3]. For each step, the reactants and the products were geometrically optimized. To decrease computation time, the vacuum slab was constructed with only one layer of zirconia. This type of approach has been successfully employed in DFT calculations, and even local clusters of finite size have been shown to perform reasonably well for transition metal oxides and zeolites [6, 7]. The (111) surface was employed for all the calculations, since based on the acidity calculations, this surface was considered to be the most reactive surface. Atomic hydrogen attached to Zr atoms was taken as the source of proton (against hydrogen available from hydroxyl group). To compare the effect of acidity on the ring opening reactions, other metal oxides were also attempted. Metal oxides studied were bohemite, titania, molybdena and modified surfaces of zirconia with different modifier elements. Methylcyclohexane (MCH) was the principal probe molecule for studying the ring opening reaction. Probe molecules such as decalin and tetralin were also studied. For zirconia, ring opening was also studied with multiring aromatics using decalin and tetralin as probe molecules.

4.3.1 Hydrogen Adsorption on ZrO_2 (111)

As the bifunctional mechanism involved adsorption of hydrogen on to the surface, an attempt was made to simulate this adsorption. It was observed the ZrO_2(111) surface has the ability to dissociatively adsorb hydrogen. This adsorption had an activation energy of 1.2 kcal mol^{-1} and a reaction energy of -11.2 kcal mol^{-1}. It was also observed that the dissociated hydrogen atoms which are attached to a single Zr atom achieve a more stable state when one H atom moves to the neighboring Zr atom. This was achieved with a reaction energy of -14.3 kcal mol^{-1}. However, all the attempts to calculate the energy barrier for this change failed despite several attempts.

4.3.2 H_2O Adsorption on ZrO_2 (111)

In a similar fashion, water adsorption on ZrO_2(111) was also studied. Water adsorbed on the surface with a reaction energy of -19.1 kcal mol^{-1}. The simulation to

calculate the barrier for this adsorption step failed probably because this is a non-activated process. The adsorbed water dissociated with a reaction energy of -30.5 kcal mol^{-1} and an activation energy barrier of 7.5 kcal mol^{-1} with a resultant hydroxyl group attached to one Zr atom and a hydrogen atom attached to the neighboring Zr atom. This configuration was further stabilized by the hydroxyl group coordinating with three neighboring Zr atoms. This step had activation energy of 1.4 kcal mol^{-1} and a reaction energy of -22.2 kcal mol^{-1}.

4.3.3 Bifunctional Methylcyclohexane Ring Opening on ZrO_2 (111)

The first step for bifunctional MCH ring opening is the dehydrogenation of MCH, resulting in methyl cyclohexene (hereafter called MCHE). The second step is protonation of MCHE. The third step is the isomerization of protonated MCHE to protonated 1, 3 dimethyl cyclopentene (hereafter called PDMCPE). The fourth step is the ring opening of this to protonated 2-methyl-1,4-hexadiene (hereafter called PMHXDE). The fifth step is the deprotonation of to 2-methyl-1,4-hexadiene (hereafter called MHXDE). The sixth and last step is the hydrogenation of the previous intermediates to 2-methyl hexane. The first step (dehydrogenation over a metal) and the last step (hydrogenation over a metal) was omitted for two reasons;

(1) Transition state metals are known to perform hydrogenation and dehydrogenation reactions easily, and hydrogen is known to adsorb on metals dissociatively [8, 9, 10]. So this step is not considered to be a rate limiting one.

(2) Addition of the metal cluster to the surface significantly increases the computational cost.

The second step is the protonation reaction of MCHE. As the protonation reaction could proceed through one of the two common mechanisms (Langmuir-Hinshelwood and Eley-Rideal), both were attempted. The Langmuir-Hinshelwood mechanism resulted in an activation energy and heat of reaction of 57.0 kcal mol^{-1} and 26.0 kcal mol^{-1}, respectively whereas for the Eley-Rideal mechanism the values were 6.0 kcal mol^{-1} and -18.0 kcal mol^{-1}, respectively. In the Eley-Rideal mechanism, the reactants consisted of MCH in the gas phase and the proton attached to the catalyst surface and the product consisted of protonated MCHE on the surface. The results are graphically represented in the Fig 4.7.

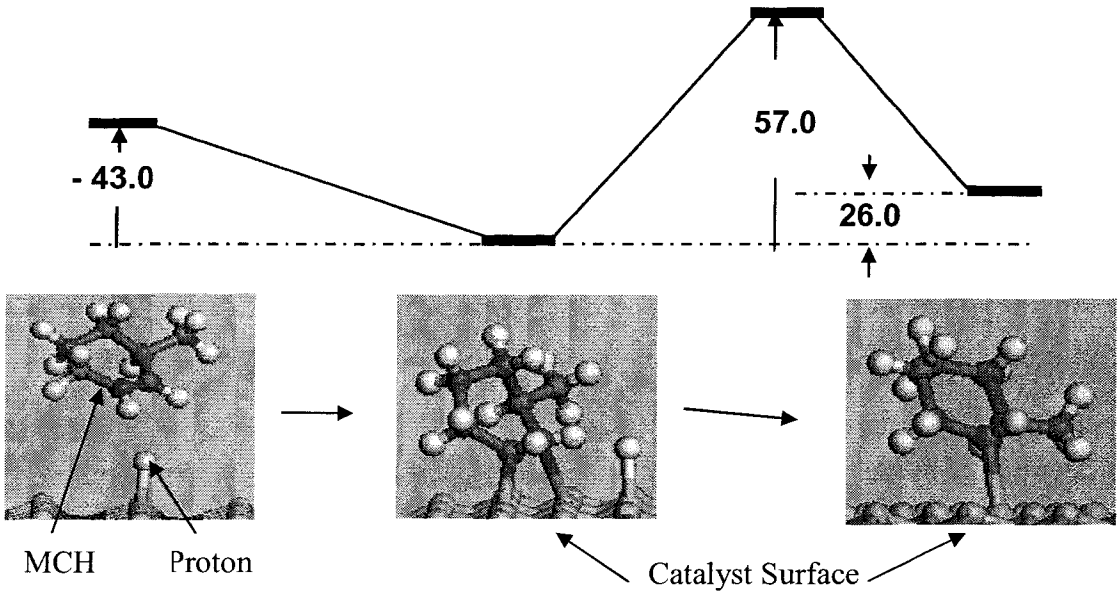

Fig. 4.7 (a) Energetics of Langmuir-Hinshelwood mechanism for protonation reaction [11]

Units: kcal mol^{-1}

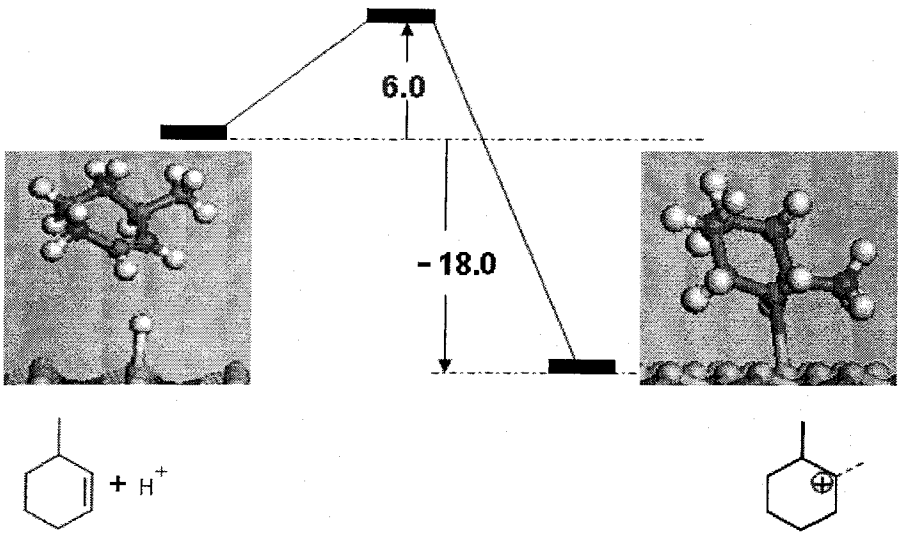

Units: kcal mol^{-1}

Fig. 4.7 (b) Energetics of Eley-Rideal mechanism for protonation reaction [11]

The third step, the isomerization of protonated MCHE to PDMCPE failed despite several attempts. The fourth step, ring opening PDMCPE was successfully completed. The activation energy of β scission of PDMCPE was 52.0 kcal mol^{-1} and the reaction energy was -20.0 kcal mol^{-1}. The fifth step (the deprotonation of PMHXDE) also failed despite several attempts. In this step, the geometry optimization of the deprotonated product was failing. Hydrogen was being abstracted from one of the carbon atoms. The simulation for the entire process is shown in Fig. 4.8. The failure of the two steps prompted revisiting the classical bifunctional mechanism proposed by Weitkamp et al. [3]. As the first step, the absolute values energies of the 3 possible isomers of the starting point (MCHE) were calculated. The results are shown in Fig.4.9. The results show that there is no appreciable difference between the energies of these isomers and so all are almost equally probable (provided the activation energies are of similar order for the dehydrogenation step). Thus, the classical bifunctional mechanism was tried with different starting points but reaching at the same ring opened product. The isomers of MCHE are named MCHE-1, MCHE-2 and MCHE-3 according to the position of the double bonds with respect to the methyl substituted carbon atom (α-carbon atom).

The first one to be attempted for ring opening was MCHE-1. While simulating for the protonation step, the Langmuir-Hinshelwood mechanism failed in spite of several attempts. However, the Eley-Rideal mechanism was successful and the gas phase protonation MCHE-1 at α-carbon had activation energy of 6.0 kcal mol^{-1} and a reaction energy of -18.0 kcal mol^{-1}. As the isomerization of protonated MCHE-1 to PDMCPE was seen to fail in the previous attempt, it was not tried again. To map the energetics, it was necessary to attempt a different isomerization product. In the original mechanism, the charge was attached to the α-carbon atom of the PDMCPE, so a different isomer with charge attached to the β-carbon was attempted. Again, this isomerization could proceed through two paths; one in which the 5,6 C-C bond was broken and another mechanism in which the 3,4 C-C bond was broken. These isomerizations were successfully simulated. The first case had activation energy of 18.0 kcal mol^{-1} and a reaction energy of 7.0 kcal mol^{-1}. The second case had activation energy of 40.0 kcal mol^{-1} and a reaction energy of 7.0 kcal mol^{-1}. The simulation of the β-scission step starting with these was successful. Several possible routes were attempted as this involved multiple bonding to

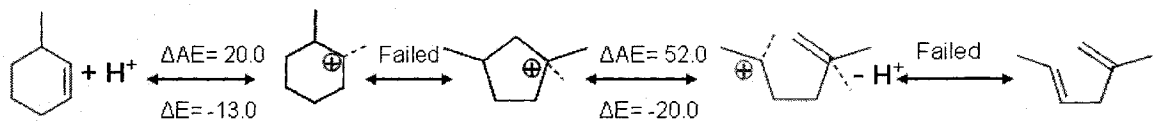

Fig.4.8 Energetics of the original ring opening mechanism described by Weitkamp et al. [3] simulated on ZrO_2 (111).The symbol '--------' represents the bonding to the surface.

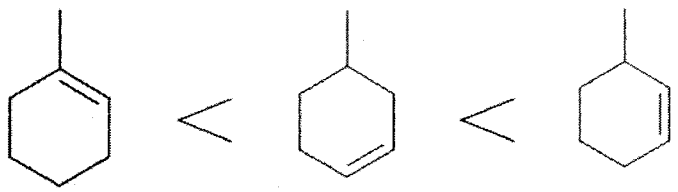

-171,900 kcal mol^{-1} -171,897 kcal mol^{-1} -171,896 kcal mol^{-1}

Fig.4.9 Energies of different isomers of mono olefinic MCH

the surface. Two mechanisms were successfully simulated; one resulting in the ring opened product having two bonds from carbon atoms to the catalyst surface and another involving one bond from a hydrogen atom and another bond from a carbon atom (Fig.4.10). For the sake of discussion, the first product is called PMHXDE-1 and the second one is called PMHXDE-2. The first mechanism had activation energy of 55.0 kcal mol^{-1} and a reaction energy of -29.0 kcal mol^{-1}. The second mechanism had activation energy of 49.0 kcal mol^{-1} and a reaction energy of -34.0 kcal mol^{-1}.

Deprotonation of PMHXDE-1 was successfully simulated through two mechanisms. Both the products (MHXDE) had two bonds to the surface, however they were from different carbon atoms (Fig.4.10). For the formation of the product with the terminal carbon atom having a surface bond, the activation energy was 21.0 kcal mol^{-1} and the reaction energy was -8.0 kcal mol^{-1}. For the other case, the activation energy was 22.0 kcal mol^{-1} and the reaction energy was -25.0 kcal mol^{-1}. Deprotonation of PMHXDE-2 was successfully simulated to yield MHXDE. The activation energy was 14.0 kcal mol^{-1} and the reaction energy was -20.0 kcal mol^{-1}. The entire sequence is given in Fig.4.10

The protonation of MCHE-1 with proton addition at a β carbon was also attempted (Fig. 4.11). The resultant activation energy was 25.0 kcal mol^{-1} and the reaction energy was -12.0 kcal mol^{-1}. The isomerization of this to PDMCPE was successful. This step had an activation energy of 52.0 kcal mol^{-1} and the reaction energy of 2.0 kcal mol^{-1}. β-scission of this product to PMHXDE proceeded with an activation energy of 52.0 kcal mol^{-1} and a reaction energy of -20.0 kcal mol^{-1}. However, the product from this fourth step was the same as that of the product from the fourth step of the original mechanism. So the failed deprotonation step was not attempted again.

The next attempt involved studying the ring opening of MCHE-2 (Fig. 4.12). Protonation of MCHE-2 was attempted at the β-carbon atom. This was successful and this reaction had activation energy of 6.0 kcal mol^{-1} and a reaction energy of -20.0 kcal mol^{-1}. The isomerization of the protonated MCHE-2 to PDMCPE could result in two isomers, one having the positive charge attached to α-carbon atom and the other having the positive charge to β-carbon atom. The isomerization of the protonated MCHE-2 to

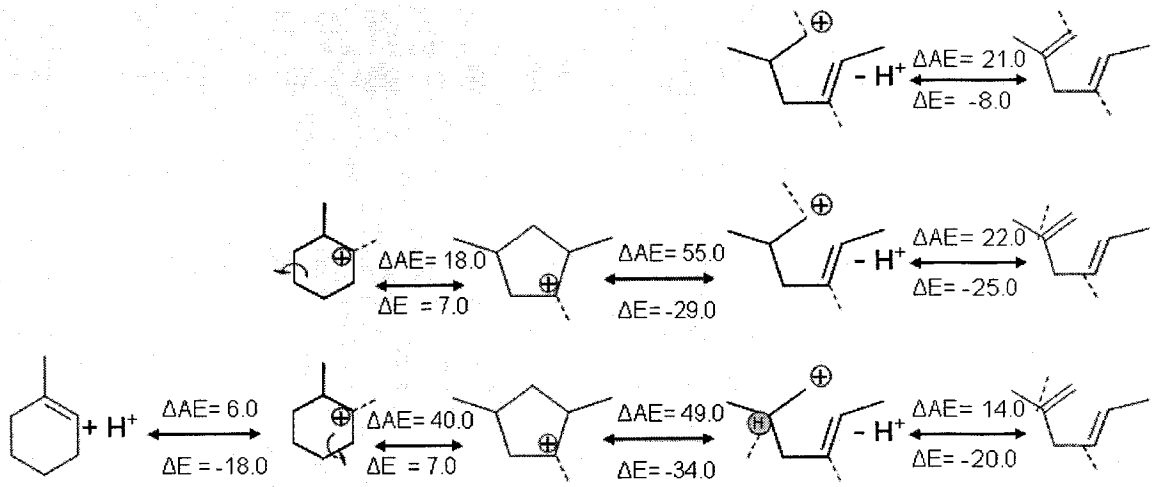

Fig.4.10 Energies of protonation of MCHE-1 at α-carbon atom on ZrO_2 (111)

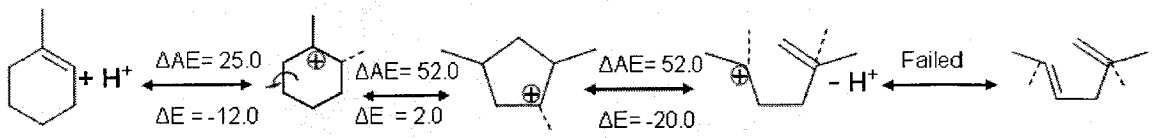

Fig.4.11 Energetics of ring opening starting with protonation of MCHE-1 at β carbon atom on ZrO_2 (111)

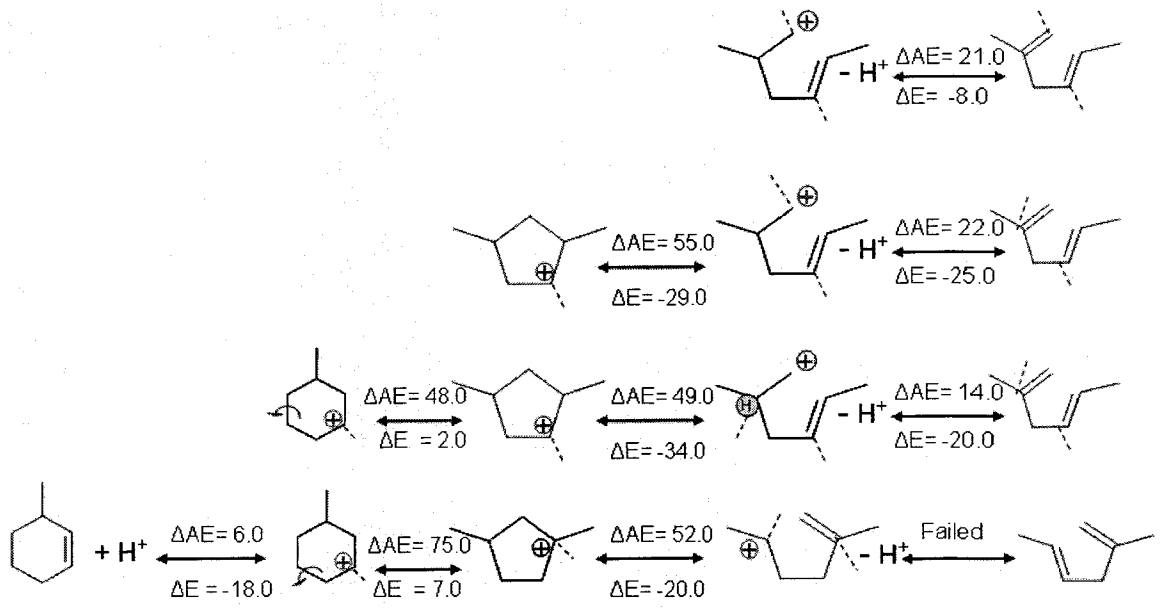

Fig.4.12 Energetics of ring opening starting with protonation of MCHE-2 at β-carbon atom on ZrO_2 (111)

PDMCPE resulted in a positive charge attached to a α-carbon had activation energy of 75 kcal mol^{-1} and a reaction energy of 7.0 kcal mol^{-1}. Ring opening of this failed before, so it was not attempted again. Isomerization to PDMCPE with the charge on the β-carbon atom had an activation energy of 48.0 kcal mol^{-1} and a reaction energy of 2.0 kcal mol^{-1}. The energetics of the ring opening of this PDMCPE is already known from previous simulations, so it was not attempted again.

The protonation of MCHE-2 with proton addition at γ-carbon atom was also attempted. This had an activation energy of 20.0 kcal mol^{-1} and a reaction energy of -13.0 kcal mol^{-1}. The entire energetic profile is given in Fig.4.13. The Langmuir-Hinshelwood mechanism was successful for the protonation of MCHE-2. As it is already presented in the discussion of the original proposed mechanism (Fig.4.7(a)), it will not be discussed again.

Ring opening with MCHE-3 was also simulated (Fig. 4.14). The protonation of MCHE-3 was successful through both Langmuir-Hinshelwood mechanism and Eley-Rideal mechanism. Protonation involving a Langmuir-Hinshelwood mechanism at the γ-carbon atom showed an activation energy of 62.0 kcal mol^{-1} and a reaction energy of 16.0 kcal mol^{-1}, whereas the Eley-Rideal mechanism showed an activation energy of 17.0 kcal mol^{-1} and a reaction energy of -19.0 kcal mol^{-1}. Isomerization of protonated MCHE produced PDMCPE with positive charge on the α-carbon atom (the only possible product). This reaction had an activation energy of 15.0 kcal mol^{-1} and a reaction energy of 7.0 kcal mol^{-1}. The ring opening of this is already known to fail, so not tried again. Protonation of MCHE-3 at the δ carbon atom was also attempted and was successful (Fig. 4.15). This step had activation energy of 6.0 kcal mol^{-1} and a reaction energy of -12.0 kcal mol^{-1}. As the reaction product of this step was already attempted before, it was not further worked on.

4.3.3.1 Protonation by Brønsted Acidity

Protonation reaction was attempted with different sources of a proton other than the one considered in the previous section (proton as the atomic hydrogen attached to the Zr atoms in the surface). A proton from hydroxyl group was attempted for protonation to

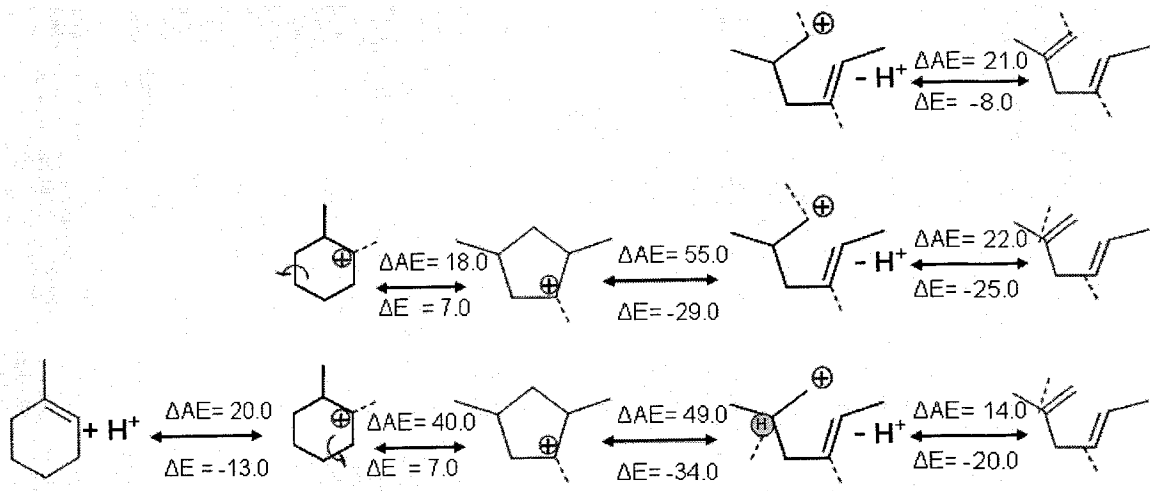

Fig.4.13 Energetics of ring opening on ZrO_2 (111) starting with protonation of MCHE-2 at β-carbon atom and the charge in the isomerized product on β-carbon atom.

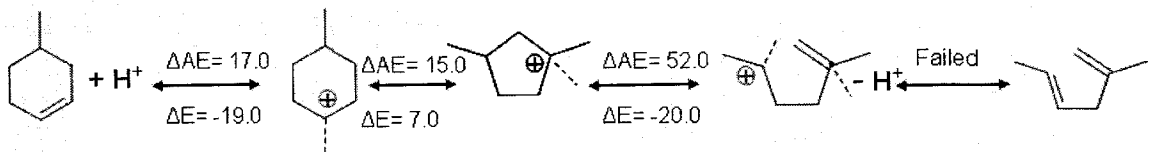

Fig.4.14 Energetics of ring opening of MCHE-2 with protonation at γ-carbon atom on ZrO_2 (111)

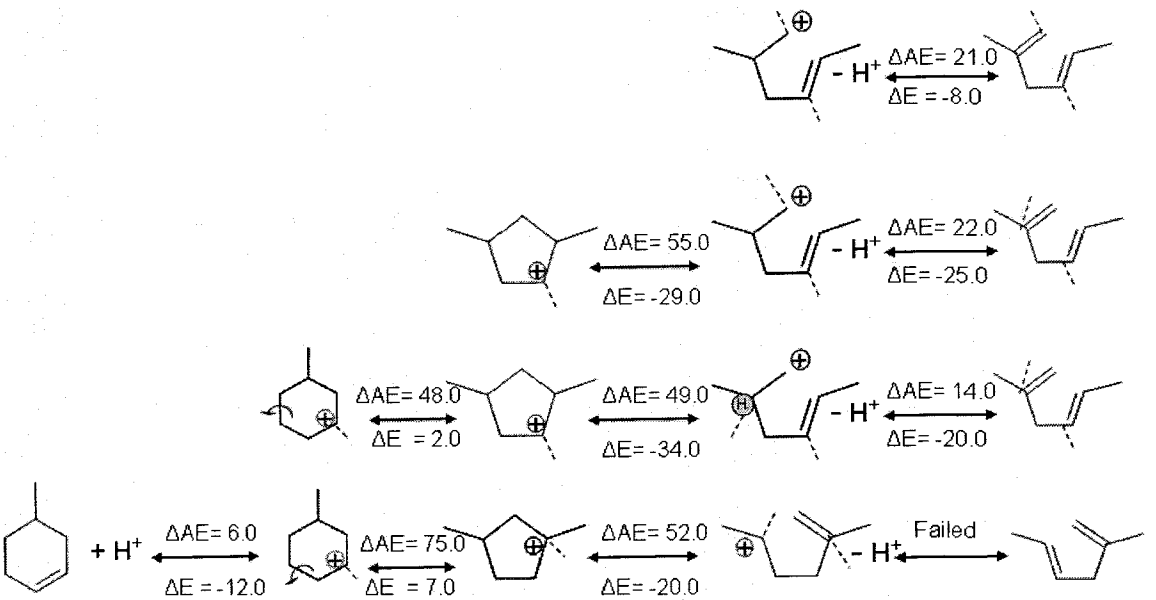

Fig.4.15 Energetics of protonation of MCHE-3 with protonation at γ-carbon atom

find out its energetics. Based on the previous study, hydroxyl group was coordinated to 3 Zr atoms on ZrO_2 (111).

Protonation of MCHE-2 was attempted with the proton from hydroxyl group (Eley-Rideal mechanism). The calculation failed several attempts, although it was ultimately successful at a particular adsorption location. The reaction had activation energy of 35.0 kcal $mol^{-1}$and a reaction energy of -41.0 kcal mol^{-1}. The high activation energy of this reaction compared to protonation from atomic hydrogen at the surface has prompted to attempt alternate mechanisms. A case was simulated where there hydrogen from the hydroxyl group was used for protonation but the oxygen left behind in this process was further hydrogenated by an atomic hydrogen from the surface. This simulation was successful; the reaction had activation energy of 7.0 kcal mol^{-1} and a reaction energy of -19.0 kcal mol^{-1}. The scheme is shown in Fig. 4.16

4.3.4 Bifunctional Decalin Ring Opening on ZrO_2 (111)

Ring opening of decalin was studied over ZrO_2(111). The mechanism attempted was the classical bifunctional mechanism used to model the ring opening of MCH. The proposed mechanism is given in Fig.4.17.

The first step is the dehydrogenation of decalin resulting in a mono olefinic species, dehydrodecalin. The second step, the protonation step involves proton addition to one of the carbon atoms holding the double bond resulting in protonated dehydrodecalin. The third step is the isomerization the above product to protonated olefinic methyl bicyclic nonane. The fourth step is the ring opening of this to protonated methyl propenyl cyclohexene. The fifth step is the deprotonation of this to methyl propenyl cyclohexene. The last step is to hydrogenate this to methyl propyl cyclohexane. To study the energetics of the ring opening decalin, all the steps were simulated step by step. As before, the dehydrogenation and hydrogenation steps were not studied for the same reason it was not attempted for MCH ring opening. For step 2, the protonation step, only Eley-Rideal mechanism was attempted, and protonation was attempted at α and β carbon atoms. Other carbon atoms were not attempted as they would result in the same products. All the standard parameters were used except for SCF convergence. SCF convergence was

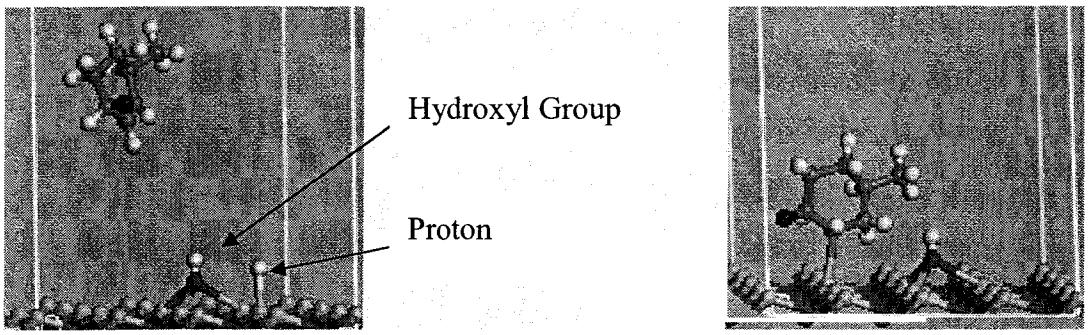

Fig.4.16 Protonation of MCHE-2 from hydroxyl group on ZrO_2 (111) [11]

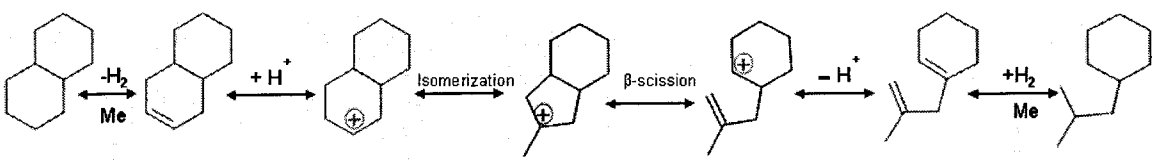

Fig. 4.17 Proposed classical bifunctional mechanism for the ring opening of decalin

relaxed to 0.0005 as it was seen that the simulations were failing on account of the original convergence value of 0.0001.

The energetics of the entire steps is shown in Fig 4.18. For the protonation of the α-carbon atom, the activation energy observed was 3.0 kcal mol^{-1} and the reaction energy observed was -28.0 kcal mol^{-1}. Isomerization of this process was simulated for 2 possible isomers of protonated olefinic methyl bicyclic nonane. One with the α –carbon atom forming the methyl group, one with the γ –carbon atom forming the methyl group. For the isomerization to protonated olefinic methyl bicyclic nonane where the α –carbon atom formed the methyl group, the reaction had an activation energy of 64.0 kcal mol^{-1} and a reaction energy of 16.0 kcal mol^{-1}. β-scission of this isomerization product to protonated methyl propenyl cyclohexene had an activation energy of 46.0 kcal mol^{-1} and a reaction energy of -22.0 kcal mol^{-1}. For the isomerization to protonated olefinic methyl bicyclic nonane where the γ –carbon atom formed the methyl group, the reaction had an activation energy of 26.0 kcal mol^{-1} and a reaction energy of 16.0 kcal mol^{-1}. β-scission of this isomerization product to protonated methyl propenyl cyclohexene had an activation energy of 31.0 kcal mol^{-1} and a reaction energy of -22.0 kcal mol^{-1}. Deprotonation of this to methyl propenyl cyclohexene was also performed successfully. This step had an activation energy of 15.0 kcal mol^{-1} and a reaction energy of -12.0 kcal mol^{-1}. Protonation of dehydrodecalin at β-carbon atom was also attempted successfully. This step had an activation energy of 5.0 kcal mol^{-1} and a reaction energy of 22.0 kcal mol^{-1}.

4.3.5 Bifunctional Tetralin Ring Opening on ZrO_2 (111)

Ring opening of tetralin was studied over ZrO_2(111). The mechanism attempted was the classical bifunctional mechanism used to model the ring opening of MCH. The proposed mechanism is given in Fig.4.19. As tetralin already has double bonds, there is no need for hydrogen abstraction for protonation. Protonation was done on the double bond on the primary ring which was sharing the secondary ring. This was done so to facilitate β-scission of one of the bonds in the secondary ring. For the simulation, standard parameters were used except for the SCF convergence of 0.0005 against the standard of 0.0001.

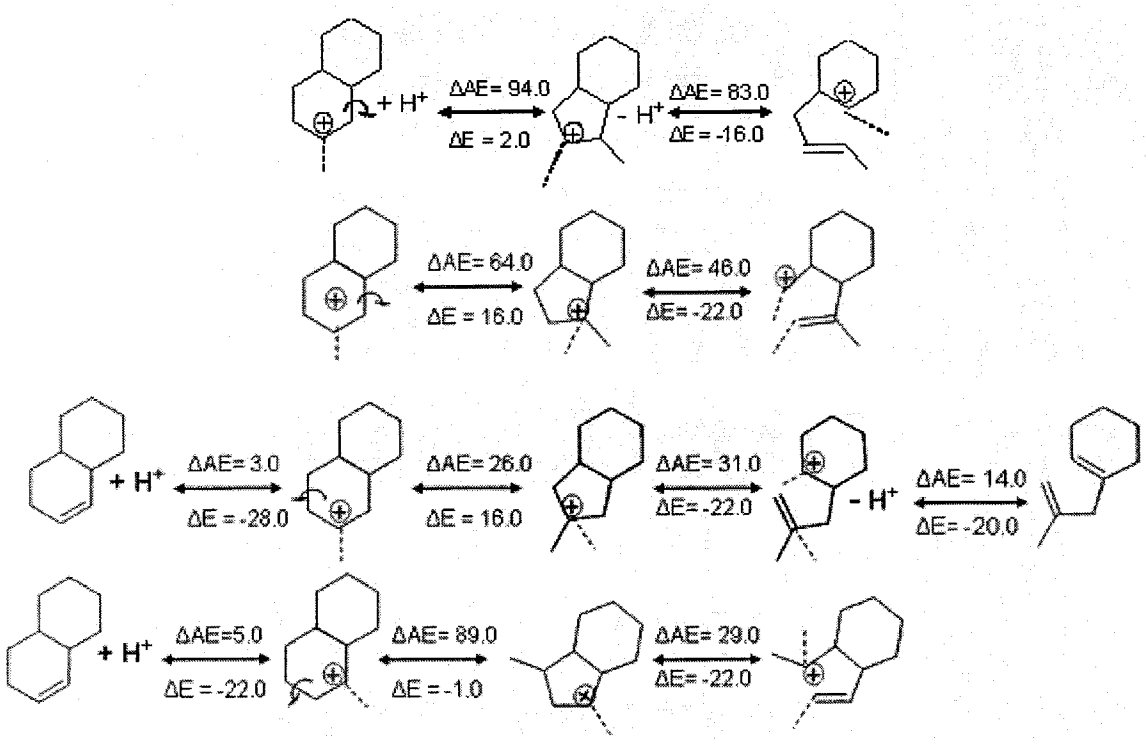

Fig. 4.18 Energetics of ring opening of decalin on ZrO_2 (111)

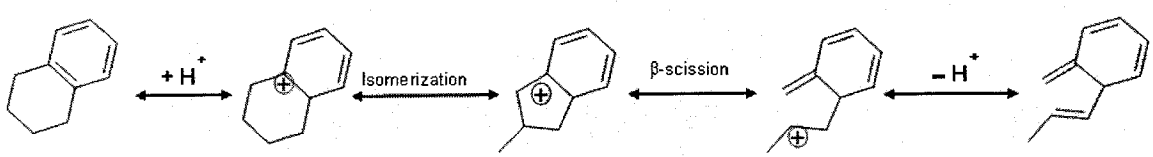

Fig. 4.19 Proposed classical bifunctional mechanism for the ring opening of tetralin

The Eley-Rideal mechanism for protonation was first studied. Several simulations with different possibilities were made, but all the simulations converged with negative activation energy. This prompted towards studying a Langmuir-Hinshelwood mechanism. This simulation was successful; the reaction had activation energy of 26.0 kcal mol^{-1} and an energy difference of -4.0 kcal mol^{-1}.

Different possible mechanisms for the isomerization of the protonated tetralin to protonated methyl indane were attempted. Different pathways varied with respect to the C-C bond breaking in the secondary ring and also with respect to the carbon atom forming the methyl group. The carbon atom in the secondary ring next to the positively charges carbon atom is labeled α-carbon atom. The isomerization of tetralin to protonated methyl indane where the α-β carbon to carbon bond is broken and β-carbon atom form the methyl group was simulated successfully (Fig.4.20). This reaction had an activation energy of 85.0 kcal mol^{-1} and an energy difference of 2.0 kcal mol^{-1} . The β-scission of this was simulated for two routes; one in which the bond between the δ-carbon atom and the primary ring was cleaved and another in which the bond between the α-carbon atom and γ-carbon atom was cleaved. The first case had an activation energy of 43.0 kcal mol^{-1} and an energy difference of -24.0 kcal mol^{-1} . The second case had an activation energy of 49.0 kcal mol^{-1} and an energy difference of -7.0 kcal mol^{-1}. The isomerization of tetralin to protonated methyl indane where the δ-carbon atom formed the methyl group was also simulated successfully. This reaction had an activation energy of 38.0 kcal mol^{-1} and an energy difference of 6.0 kcal mol^{-1}. The β-scission of this where bond between the γ-carbon atom and the primary ring was cleaved had an activation energy of 27.0 kcal mol^{-1} and an energy difference of -17.0 kcal mol^{-1}. Deprotonation of this product was successfully accomplished. Deprotonation had an activation energy of 29.0 kcal mol^{-1} and an energy difference of 5.0 kcal mol^{-1}. The isomerization of tetralin to protonated methyl indane where the β-γ carbon to carbon bond is broken and β-carbon atom form the methyl group was also simulated successfully. This reaction had an activation energy of 52.0 kcal mol^{-1} and an energy difference of 6.0 kcal mol^{-1}. The β-scission of this where bond between the δ-carbon atom and the primary ring was cleaved had an activation energy of 36.0 kcal mol^{-1} and an energy difference of -17.0 kcal mol^{-1}.

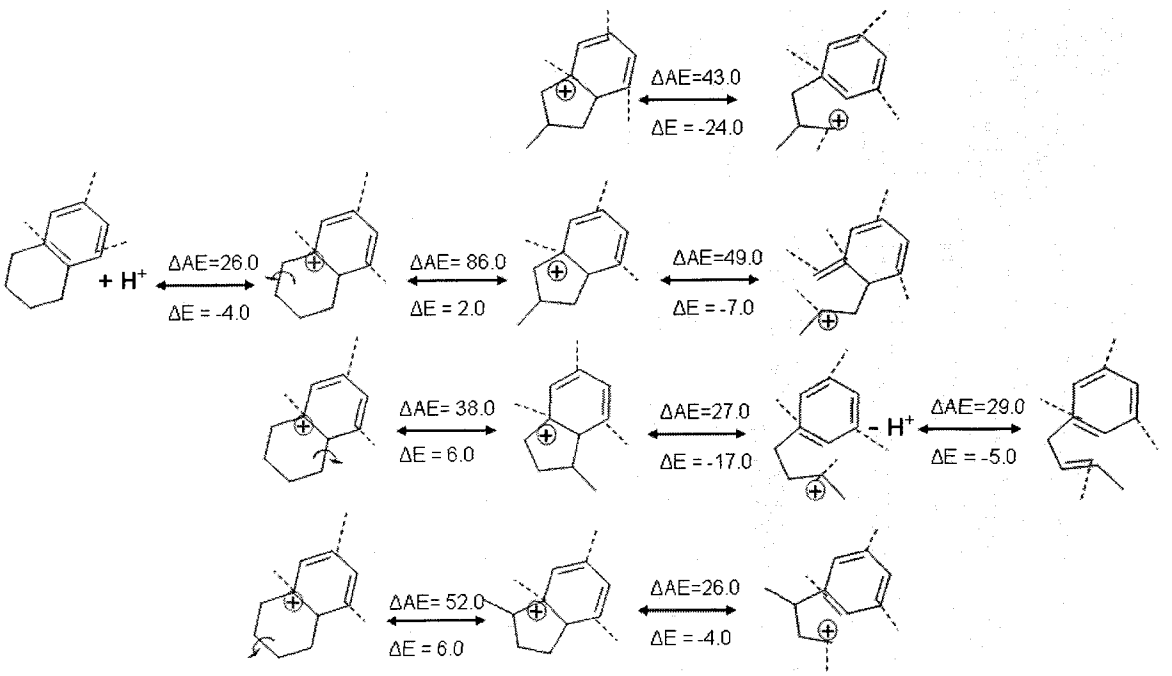

Fig. 4.20 Energetics of ring opening of tetralin on ZrO_2 (111)

4.3.6 Haag-Dessau Methylcyclohexane Ring Opening on ZrO_2 (111)

MCH ring opening through Haag-Dessau mechanism was simulated on ZrO_2 (111). The Haag-Dessau mechanism as described by Weitkamp et al. [3] is shown in Fig.4.21. According to the mechanism, the reactant MCP is directly protonated. During the protonation step, MCP is shown to go through a transition state where a nonclassical carbonium ion with a three-center, two-electron bond is formed in the transition state. The proton attaches to β- carbon atom there by leaving a positive charge on the α-carbon atom (substituted carbon atom). The product of protonation undergoes deprotonation to a mono olefinic alkane.

The steps were simulated step by step, and initially an Eley-Rideal mechanism was simulated for the protonation step with the MCH in the gas phase and the proton attached to the surface (Fig. 4.22). In this mechanism, MCH was positioned in such a manner that proton was close to the β-carbon atom than the α-carbon atom. The reaction had an activation energy of 85.0 kcal mol^{-1} and a reaction energy of -9.0 kcal mol^{-1}. Another simulation was performed where the proton of the reactant was closer to the α-carbon atom than the β-carbon atom. This reaction had an activation energy of 133.0 kcal mol^{-1} and a reaction energy of -9.0 kcal mol^{-1}.

Starting with the product of the first step, deprotonation reaction was also simulated successfully (Fig. 4.23). This step had an activation energy of 39.0 kcal mol^{-1} and a reaction energy of -21.0 kcal mol^{-1}. A similar protonation was attempted at γ-δ carbon atom with the proton attaching to the γ –carbon. This reaction had activation energy of 137.0 kcal mol^{-1} and a reaction energy of -2.0 kcal mol^{-1} . These reactions are shown in Fig. 4.24.

4.3.7 MCH Direct Ring Opening ZrO_2(111)

MCH direct ring opening was attempted on ZrO_2(111). In both classical bifunctional mechanism and Haag-Dessau mechanism, ring opening was done with the assistance of proton. In this simulation (Fig. 4.25), no proton was employed. The MCH in the gas phase was ring opened and adsorbed on to the surface. The α-β bond was severed. The reaction had activation energy of 91.0 kcal mol^{-1} and a reaction energy of -12.0 kcal mol^{-1}.

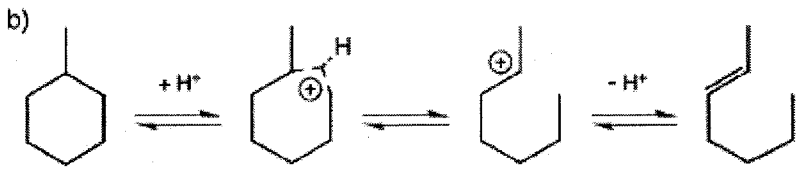

Fig.4.21 Haag-Dessau mechanism as described by Weitkamp et al [3]

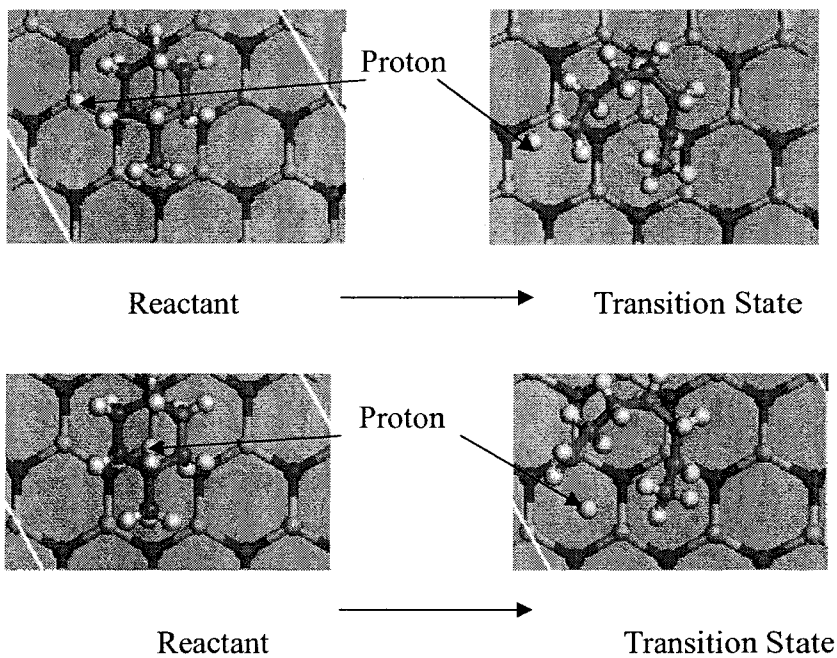

Fig.4.22 Transition state for the protonation reaction in the Haag-Dessau mechanism with proton at different locations on ZrO_2 (111) [11]

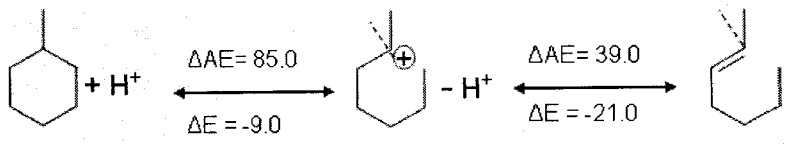

Fig. 4.23 Haag-Dessau mechanism simulated energetics for MCH ring opening on ZrO_2 (111)

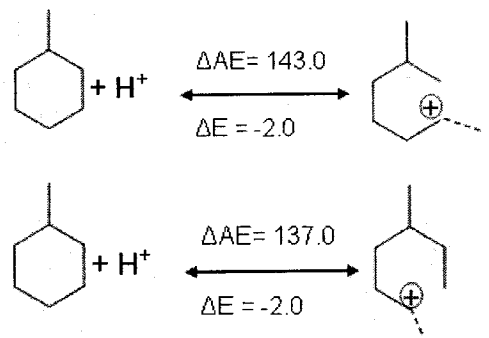

Fig. 4.24 Energetics of MCH protonation on ZrO_2 (111)at different locations of the hexyl ring

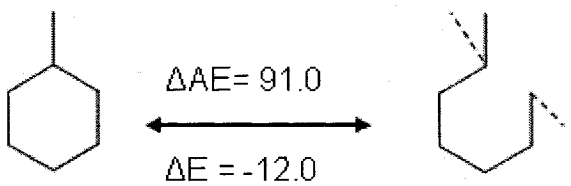

Fig 4.25 Energetics of direct ring opening of MCH on ZrO_2 (111)

4.4 Ring Opening on Al_2O_3 (111)

4.4.1 Structure and Properties of Bohemite

Bohemite (111) was characterized to find its activity in terms of acidity. All the standard parameters were used. It was observed that the simulation failed owing to SCF convergence, so the SCF tolerance was reduced to 0.001. NH_3 adsorption was done as in the case of zirconia. The Lewis acidity was calculated as -37.2 kcal mol^{-1}. The hydroxyl groups had a heat of adsorption of -54.3 kcal mol^{-1}. The Brønsted acidity was calculated as -13.3 kcal mol^{-1}.

4.4.2 Bifunctional Methylcyclohexane Ring Opening on Al_2O_3 (111)

Ring opening reactions were simulated on bohemite (111) surface. The purpose of this was to study the influence acidity has on the energetics of ring opening reaction. Both the classical bifunctional mechanism and the Haag-Dessau mechanisms were simulated. All the standard parameters were chosen except the SCF convergence value. For bohemite surface, convergence could not be reached with the standard SCF value of 0.0001 or 0.0005, therefore, it was increased to 0.001.

The classical bifunctional mechanism was simulated starting with mono olefinic MCH (MCHE-2). Both Langmuir-Hinshelwood and Eley-Rideal mechanism were successful for the protonation of MCHE-2 (Fig. 4.26). The Langmuir-Hinshelwood mechanism had an activation energy of 46.0 kcal mol^{-1} and a reaction energy of 37.0 kcal mol^{-1}. The Eily-Reidel mechanism had activation energy of 37.0 kcal mol^{-1} and a reaction energy of -22.0 kcal mol^{-1}. The isomerization of protonated MCHE-2 to protonated dimethyl cyclopentene was also successful and the reaction had had an activation energy of 144.0 kcal mol^{-1} and a reaction energy of 0.6 kcal mol^{-1}. The β-scission of this to PMHXDE was successfully performed. This reaction had an activation energy of 81.0 kcal mol^{-1} and a reaction energy of 5.0 kcal mol^{-1}. Deprotonation of PMHXDE to MHXDE had an activation energy of 43.0 kcal mol^{-1} and a reaction energy of 9.0 kcal mol^{-1}.

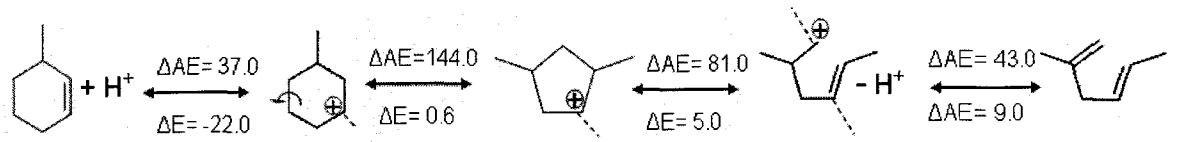

Fig 4.26 Energetics of bifunctional ring opening of MCH on bohemite (111) surface

4.4.3 Haag-Dessau Methylcyclohexane Ring Opening on Al_2O_3 (111)

The Haag-Dessau mechanism was also simulated on bohemite (111) surface starting with MCH. The protonation reaction (Eley-Rideal mechanism) had activation energy of 155.0 kcal $mol^{-1}$and a reaction energy of -9.0 kcal mol^{-1}. The deprotonation reaction proceeded with activation energy of 52.0 kcal $mol^{-1}$and an energy difference of 7.0 kcal mol^{-1}. The entire scheme is shown in Fig. 4.27.

4.5 Ring Opening on Other Surfaces of ZrO_2

Other metal oxide surfaces were attempted for their possible activity for selective ring opening. The surfaces attempted includes pure metal oxide surfaces and modified metal oxide surfaces. Transition state searches were performed on other geometrical planes of zirconia, as well.

4.6 Ring Opening on Modified Zirconia

Ring opening reactions were attempted on zirconia modified with Mo. A zirconia vacuum lab with two layers was modified with Mo on the surface. The Mo concentration was corresponding to 7% on the surface. The bottom layer of the slab was constrained and the top layer was relaxed. The slab was geometrically optimized. As observed before, the Mo atom did not retain all the bond the Zr atom originally had allocation. Once the optimization was completed, the bottom layer of the slab was removed and only the top layer retained. This layer was constrained and further simulations performed.

MCHE was used as the probe molecule. Only the isomerization step of protonated MCHE-2 to protonated DMCP was successful. Both the reactant and the product were bonded to the Mo atom. The reaction had an activation energy of 171.0 kcal mol^{-1} and a reaction energy of -0.2 kcal mol^{-1}. In a similar fashion, the isomerization reaction was tested on Ti modified surface. The reactant and product was bonded to Zr atom next to Ti atom. The reaction had an activation energy of 140.0 kcal mol^{-1} and a reaction energy of -0.3 kcal mol^{-1}.

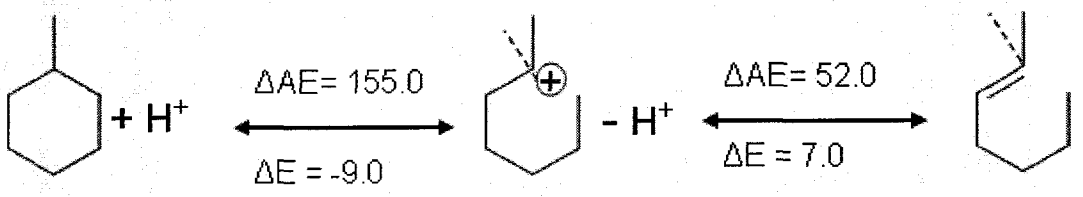

Fig.4.27 Energetics of ring opening of MCH on bohemite (111) for Haag-Dessau mechanism

4.7. Ring Opening on TiO_2 and MoO_3

Ring opening was attempted on the TiO_2 (rutile). However, even geometry optimizations failed on all the three surface panes considered. Ring opening was attempted on (110) surface of MoO_3. This particular geometry was chosen as this surface was more similar to ZrO_2(111) surface. The isomerization reaction was successful, β-scission step failed. The isomerization of protonated MCHE-2 to protonated DMCP had activation energy of 69.0 kcal mol^{-1} and a reaction energy of 1.0 kcal mol^{-1}. The Lewis acidity of this surface was tested with NH_3 adsorption. The calculated acidity was -31.0 kcal mol^{-1}.

4.8 Gas Phase Transition State Search for the Bifunctional Mechanism.

Transition state search was attempted for the ring opening reaction in the gas phase. The model reaction used was the classical bifunctional mechanism and the Haag-Dessau mechanism discussed by Weitkamp et al [3]. The reactants and products were optimized before performing the transition state. As this involves only gas phase, the net charge of the system was +1, whenever a proton was involved.

The first step, the dehydrogenation of methylcyclohexane (MCH) to methylcyclohexene (MCHE) had an activation energy of 29.0 kcal mol^{-1} and a reaction energy of 32.0 kcal mol^{-1} (Fig. 4.28). The second step, the protonation of MCHE showed a negative activation energy despite several attempts. Also, the hydrogen attached to the substituted carbon atom (α-carbon atom) was observed moving to the β-carbon atom. The reaction had a reaction energy of -99.0 kcal mol^{-1}. The third step, isomerization of protonated MCHE to protonated dimethyl cyclopentane (PDMCP) had an activation energy of 54.0 kcal mol^{-1} and a reaction energy of –0.6 kcal mol^{-1}. The β-scission of PDMCHE to protonated methyl hexadiene had an activation energy of 27.0 kcal mol^{-1} and a reaction energy of 40.0 kcal mol^{-1}. The deprotonation of this to methyl hexadiene had an activation energy of 86.0 kcal mol^{-1} and a reaction energy of 76.0 kcal mol^{-1}. The hydrogenation of this to methyl hexene had an activation energy of 2.0 kcal mol^{-1} and a reaction energy of -34.0 kcal mol^{-1}.

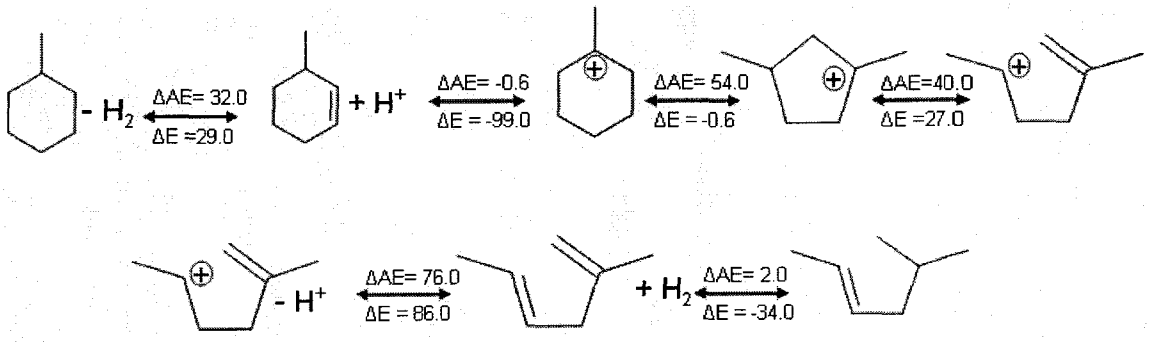

Fig. 4.28 Energetics of the the gas phase classical ring opening reaction of MCH

4.9 Simulation Results Using Different Parameters in Simulation

Transition state searches were performed to compare the influence of choosing between different parameters. Reactants and products were geometrically optimized using standard parameters except the one for which the study is made. Isomerization reaction of protonated MCHE to protonated dimethyl cyclopentene was used as the model reaction. The results are discussed below and finally summarized in Table 4.6.

The influence of the set point of energy cutoff was studied using 2 transition state searches one in which the cutoff energy was set as 4.5 Å and another in which the value was 5.5 Å. For the first case, the reaction had an activation energy barrier of 51.9 kcal mol^{-1} and a reaction energy of 2.1 kcal mol^{-1}. For the second case, the reaction had a reaction energy of 2.0 kcal mol^{-1} and an activation energy barrier of 50.7 kcal mol^{-1}. Different functionals available were studied for their influence on the energy.

Three simulations were performed using 3 different functionals, namely PW91, BLYP and PBE. For the simulation using PW91 functional, the reaction had an activation energy barrier of 51.9 kcal mol^{-1} and a reaction energy of 2.1 kcal mol^{-1}. For the simulation using BLYP functional, the reaction had an activation energy barrier of 19.3 kcal mol^{-1} and a reaction energy of 2.6 kcal mol^{-1}. For the simulation using PBE functional, the reaction had an activation energy barrier of 43.4 kcal mol^{-1} and a reaction energy of 1.7 kcal mol^{-1}. Simulations were performed to find out the difference in results between using the options of 'effective core potentials' and all 'electron relativistc'. For the choice of 'effective core potential' the reaction had an activation energy barrier of 51.9 kcal mol^{-1} and a reaction energy of 2.1 kcal mol^{-1}. For the 'all electron relativistic' the reaction had an activation energy barrier of 47.6 kcal mol^{-1} and a reaction energy of 2.0 kcal mol^{-1}. The difference between using k-point sets with k point separation of 0.07/Å (coarse) and 0.05Å (medium) were studied. For the 'coarse' k-point set, the reaction had an activation energy barrier of 51.9 kcal mol^{-1} and a reaction energy of 2.1 kcal mol^{-1}. For the 'medium' option, the reaction had an activation energy barrier of 48.7 kcal mol^{-1} and a reaction energy of 2.1 kcal mol^{-1}. Simulations were performed to find out the influence of the settings of integration accuracy on the simulation results. The available options are coarse, medium and fine. The medium option corresponds to 1000

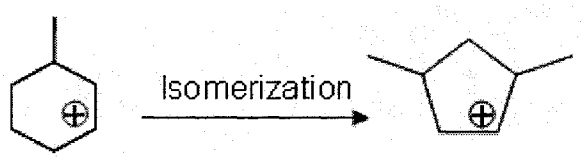

Energy	Cutoff, Å		Core Potential		Functionals		
	4.5	5.5	ECP	All Electron	PW91	BLYP	PBE
Δ E	2.1	2.0	2.1	2.0	2.1	2.6	1.7
A.E	51.9	50.7	51.9	47.6	51.9	19.3	43.4

Energy	k-point set		Integration accuracy	
	Coarse	Medium	Coarse	Medium
Δ E	2.1	2.1	2.1	1.5
A.E	51.9	48.7	51.9	46.0

Table 4.6 Comparison of the results of simulation between different options

grid points for each atom. For the setting with the 'coarse' option, the reaction had an activation energy barrier of 51.9 kcal mol^{-1} and a reaction energy of 2.1 kcal mol^{-1}. For the setting with the 'medium' option, the reaction had an activation energy barrier of 46.0 kcal mol^{-1} and a reaction energy of 1.5 kcal mol^{-1}

Chapter 5 Discussion

5.1 Structure and Properties of Zirconia and Modified Zirconia

The following discussion regarding the structure and properties of zirconia and modified zirconia, follows from the DFT calculations presented in Chapter 4.

5.1.1 Bulk Zirconia and Modified Zirconia

The simulations of the total energy of bulk zirconia indicate that monoclinic zirconia has lower total energy than cubic zirconia. Thus, at ambient conditions zirconia prefers to be in the monoclinic phase compared to the cubic polymorph. This is in agreement with experimental observations, where it has been observed that at ambient conditions zirconia exists in its monoclinic phase [10]. The energetic results obtained from molybdenum incorporation shows that the stability of the cell is not lost with the incorporation of Mo in the bulk zirconia structure. This is true for both monoclinic and cubic polymorphs. From the energetics, it can also be noted that there is no preferred location for molybdenum to replace the zirconium in the original lattice structure, and consequently the replacement is equally likely at any zirconium atom. This observation is also in agreement with experimental results that indicate Mo^{6+} stabilizes zirconia [5].

5.1.2 Surface Structures of Cubic Zirconia

The stabilized cubic structure of zirconia has been shown to have significantly higher catalytic activity for several industrially significant reactions. In order to understand the fundamental significance of these experimental observations as they pertain to ring opening reactions, all calculations were performed using cubic zirconia.

Based on the calculated surface energies, the most probable geometrical plane in a cubic zirconia system is the (110) orientation, followed with equal probability for the (100) and (111) surface orientations. One related study found in the literature were the DFT calculations performed by Christensen et al. [1] for surface energies of different forms of zirconia using the LDA functional. However, they did not calculate the surface energies for the relaxed cubic phase, rather they limited their calculations to the monoclinic and tetragonal phase. According to their calculations for both monoclinic and tetragonal structures, the (111) surface orientation has the lowest energy and is therefore

most probable. The observations are directly not comparable to the present study as they are for different zirconia system (i.e tetragonal and monoclinic compared to cubic). Additionally, the functional used for their DFT calculations was different, which would yield different surface energies. Moreover, LDA is known to over predict total energies, and be a poor quality functional for solid-state calculations. In a DFT study Hasse et al. [3] on pure tetragonal zirconia, they concluded the (101) surface orientation is the most stable surface in terms of the surface energy. If we consider the fact that tetragonal zirconia is very close to the cubic phase in terms of the lattice parameters, then a (101) surface can be considered identical to a (110) surface and is agreement with our results. Furthermore, the (111) surface was found experimentally to be the most abundant in termination in sintered tetragonal ZrO_2 powders [2].

5.1.3 Acidity of Different Surface Orientations of Zirconia

The three lower indices planes (100), (110) and (111) were studied to determine Brønsted and Lewis surface acidity. It can be concluded the most acidic of all the surface orientations studied is the (100) surface followed by the (111) surface (Table 4.1). The (100) surface exhibits the maximum acidity for both Lewis and Brønsted type acidities. However, it can be seen that (111) surface has the maximum binding energy for surface –OH groups. In other words, –OH groups, the origin of Brønsted acidity, are more stable on the (111) surface than any other surface orientation. Additionally, the (110) surface exhibited positive heat of adsorption for surface –OH groups, indicating that –OH groups are unlikely to be adsorbed on a (110) surface. On the (111) surface, a tetragonal coordination of the oxygen atom of the –OH group with surface zirconium atoms is energetically preferred over coordination over a single zirconium atom. These observations are consistent with experimental results. Hydroxyl groups have been experimentally observed on monoclinic zirconia surfaces [4], and also on sintered tetragonal zirconia (modified with yitria) surfaces [4].

The objective of these studies was to elucidate the energetics and features of the various low index surface planes. The results indicate that different crystallographic surface orientations of cubic zirconia show moderate to strong acidity. However, based on the above discussion, a definitive conclusion cannot be reached as to which surface

orientation is the most prominent or the most catalytically active, but the (110) and (111) surface orientations are clearly the most probable. To ensure a comprehensive study of ring opening reactions was performed, all three orientations were subsequently studied to determine the most active orientation for ring opening reactions.

5.1.4 Modifier Incorporation at the Surface

From the literature survey, it is clear that acidity plays an important role in ring opening reactions. Thus, modifier elements were incorporated at the surface to understand the effect of elemental substitution on the acidity and stability of the surface (Tables 4.2-4.5). Modifier element incorporation was attempted at all the three low index planes, (100), (110) and (111) surface orientations. However, the (100) plane was not stable following the incorporation of any modifier elements, and thus the results are not reported. Modifier element incorporation in the (110) and (111) orientations also showed a relative degree of instability. Following incorporation and geometry optimization, most modifier elements did not retain the bond the zirconium atom had with the neighboring atoms, thus leading to a total distortion of the surface. In other words, the modifiers are less likely to stay at the surface due to the structural instability. The stability of a catalyst is an important factor and an unstable catalyst cannot be employed even if it has superior initial catalytic activity.

From the results, it can be seen that the response of the (110) surface is almost 'passive' to modifier incorporation. The Lewis acidity does not vary appreciably with respect to different locations or even between the modifier element and the neighboring zirconium atom. As far as Brønsted acidity is concerned, the heat of adsorption of surface –OH groups is positive for Zr, Al and Ti atoms and negative for Mo, Si and W atoms. This means that the formation of –OH group is not favored over Zr, Ti and Al. However, it can be seen that the heat of adsorption for –OH groups is monotonically changing (increasing or decreasing) for all the cases and it can be assumed that it will reach an asymptotic value over zirconium geometrically located far from the modifier element. The Brønsted acidity (approx. -4.0 kcal mol^{-1}) itself is not strong over the (110) surface orientation. The observation that Si doping increases the acidity of zirconia is well in agreement with experimental observation [13].

The (111) surface behaves markedly different from the (110) surface. As far as Lewis acidity is concerned, there is a marked difference between different atoms, but the change is not monotonic. Titanium modified zirconia exhibited the highest Lewis acidity (- 36.5 kcal mol^{-1}) and Mo exhibited the lowest Lewis acidity (-21.9 kcal mol^{-1}). With regards to Brønsted acidity, the (111) surface facilitates adsorption of –OH groups for all modifier elements examined. The highest heat of adsorption for –OH groups is exhibited by zirconium (-191.0 kcal mol^{-1}) and the lowest one by Mo (-23.0 kcal mol-^{1}). It should also be noted the values for Brønsted acidity on the (111) surface are higher than that of the (110) surface.

Thus, ZrO_2(111) is much more active than the (110) surface, and the (100) surface cannot be stabilized with any of the modifier elements examined. Both Lewis as well as Brønsted acidity of the surface can clearly influenced by the incorporation of modifier elements. However, unlike incorporation at bulk, the modified surface is less stable compared to the pure zirconia composition. While these are important findings, the stability of surface modifier element incorporation requires additional verification through experimental observations.

5.2 Ring Opening Energetics and Mechanisms

5.2.1 Bifunctional Methylcyclohexane (MCH) Ring Opening

The initial bifunctional ring opening mechanism studied was the mechanism proposed by Weitkamp et al. [6]. The failure of the isomerization and deprotonation step indicated this mechanism required additional consideration, specifically with regards to modifying the steps and/or starting with other isomers of MCHE (Fig. 4.8). The energies of different isomers of MCHE are not very different and this shows that thermodynamically all are equally probable (Fig. 4.9).

The energetics of the first step, i.e. protonation, shows that this is a facile step, both kinetically and thermodynamically, and an Eley-Rideal mechanism is found to be more favorable than Langmuir-Hinshelwood mechanism. These two mechanisms are compared in the form of an energy surface in Fig. 5.1. For all the three isomers of

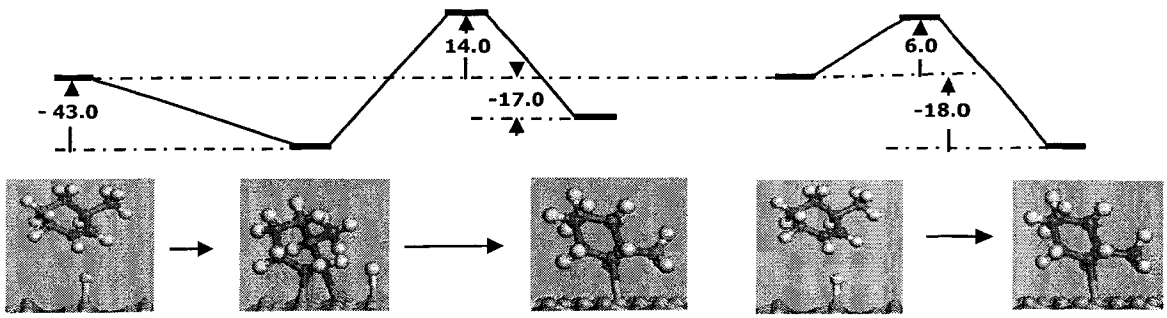

Langmuir-Hinshelwood Mechanism for the protonation reaction over $ZrO_2(111)$

Eley-Rideal Mechanism for the protonation reaction over $ZrO_2(111)$

Fig.5.1 Comparison between Langmuir-Hinshelwood and Eley-Rideal mechanism for the protonation of MCHE For both the schemes, same reactant and product configuration were considered [15].

MCHE, the lowest activation energy barrier for this step through the Eley-Rideal mechanism is remarkably small (6.0 kcal mol^{-1}). The heat of adsorption of protonated MCHE varies between -10.0 to -20.0 kcal mol^{-1}. This shows that the protonation reaction can be easily achieved, provided there are hydrogen atoms on the surface available for protonation.

A closer inspection of the second step (Fig. 4.8) shows that the bonding of the carbon atom with the surface has to shift to the neighboring carbon atom, and hydrogen 'scrambling' is required to achieve the configuration of the isomerized product. This could be the reason for the failure of this step. The repeated failure of the deprotonation step was also analyzed. It was seen that hydrogen was being abstracted from the substituted carbon atom with the methyl group when this carbon atom was attempting to bond with the zirconia surface. This carbon atom was bonded to the neighboring carbon atom through a double bond. It is postulated that the bond between the carbon atom and the zirconium atom is insufficient to break the C=C bond, resulting in the breaking of the C-H bond to satisfy the valency of the carbon atom. This definitively shows that the C-Zr bond is stronger than the C-H bond in this particular configuration. However, in other simulations it has been noted that if the carbon atom is not a substituted, this situation does not arise.

The failure of the isomerization and deprotonation steps supported revisiting the mechanisms and energetics of these steps. It was observed that moving the charge to the carbon atom next to the substituted carbon atom would help in achieving the transition for the isomerization step. With this insight, all the possible reaction routes starting with all three isomers of MCHE were attempted (Fig. 4.10 through 4.15). With the new location for the charge, it was possible to successfully simulate the entire reaction mechanism, including the deprotonation step. From the energetics, it can be seen that like the initial protonation, deprotonation is also an easy step.

Fig. 5.2 presents the summary of the most favored (kinetically and thermodynamically) ring opening pathways in the form of an energy diagram for the ring opening for all the three isomers of the MCHE. From Fig. 5.2, it can be seen that the ring opening can take place starting with all the three isomers of MCHE. It is worth

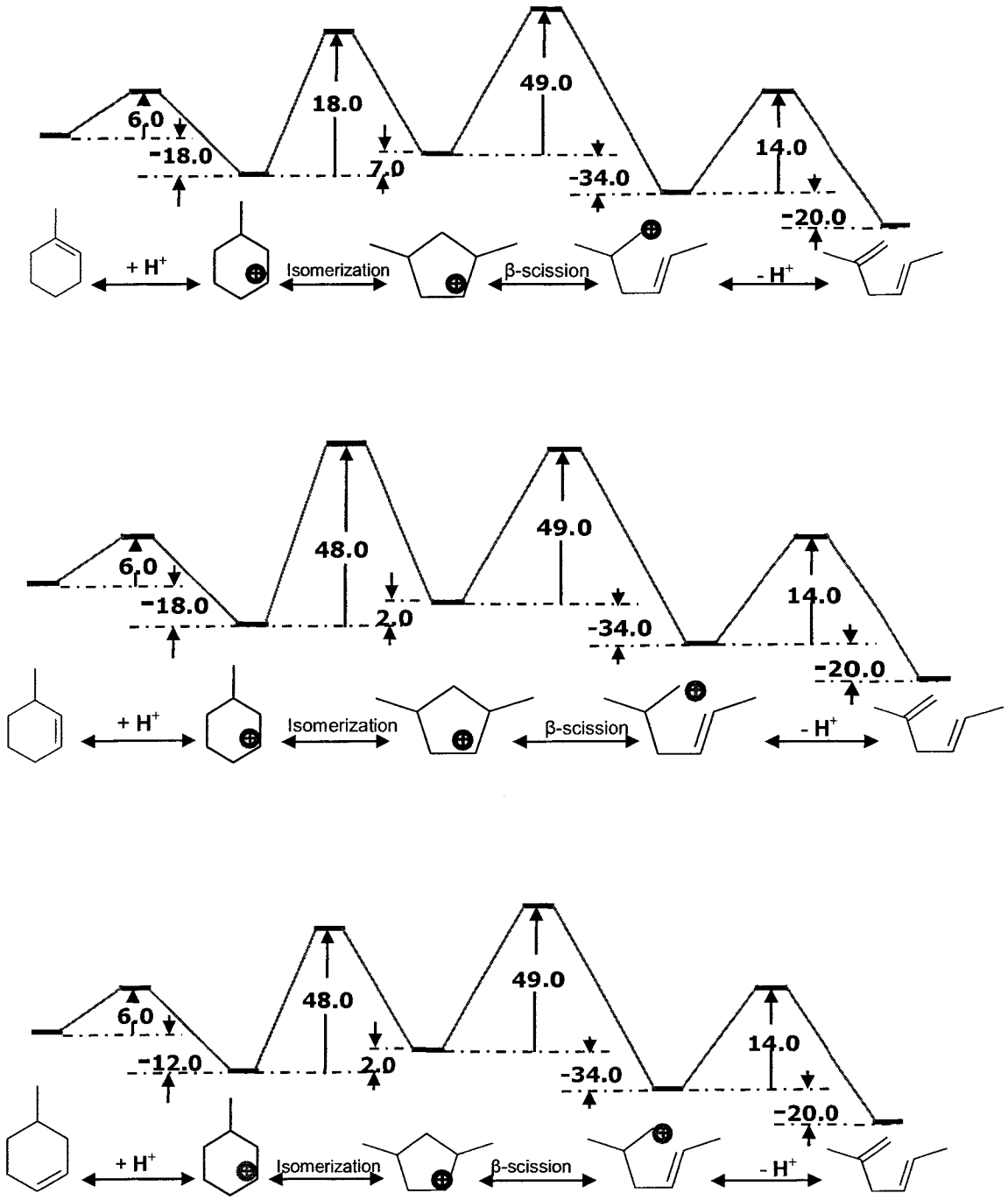

Fig. 5.2 The potential energy diagram for the most energetically favorable ring opening pathways for 3 different isomers of MCHE over $ZrO_2(111)$. For each step, several simulations were performed before concluding on the most favorable one.

repeating here that all the three isomers of MCHE were found to be equally energetically probable. As stated previously, both protonation and deprotonation are energetically favorable steps. In all three reactions, it should also be noted that ring contraction is the least thermodynamically favorable step and ring opening is the least kinetically favorable step. This means that these are the rate limiting steps for the selective ring opening of MCHE, and thus, more attention should be directed towards making these steps more favorable. With the above insight, the original mechanism proposed by Weitkamp et al. [6] is modified as shown in Fig. 5.3. In this new mechanism, the position of the charge moves from the substituted carbon atom in the MCHE ring.

The literature review clearly shows that acidity plays an important role in the ring contraction step. The reaction on other metal oxide surfaces and modified surfaces provides some insight into the influence of acidity on ring opening reactions. The best comparison for reactions on the zirconia (111) surface is reactions on the other planes of zirconia. However, the calculations on the (100) and (110) indicated failures at various steps in the reaction mechanism, and thus were not able to successfully describe the energetics of ring opening reactions. This is not surprising if the zirconium concentration per unit surface area for three orientations is considered. As the steps in the ring opening reaction involve bonding to more than one zirconium atom at the surface, it is plausible that the surface with the highest number of zirconium atoms per unit surface area should directionally facilitate the reaction. The (111) surface has the highest number of zirconium atoms per unit surface area, and the (110) surface has the least (Fig. 5.4). Also, on the (111) surface, the zirconium atoms are not oriented linearly, and this would cause molecules to 'stretch' in order to form a stable bond with the surface. In fact during simulation of ring opening reactions on the (110) and (100) surface, it has been seen that such stretching would break the skeleton of the adsorbate. A further inspection shows that of all the steps, the isomerization reaction is the least influenced by the surface structure as this involves bonding only to one atom. MCHE isomerization on the (100) surface had an activation energy of 69.0 kcal mol^{-1} and a reaction energy of 2.0 kcal mol^{-1}. On the (110) surface, this reaction could not be successfully simulated. Thus, over the (100) surface the activation barrier of the isomerization step is higher than

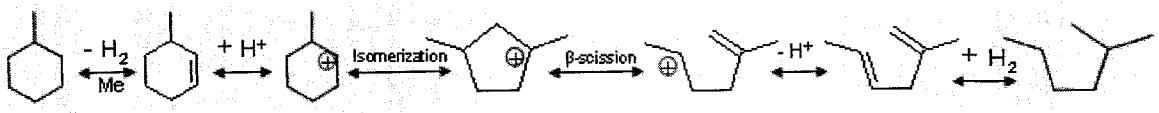

Fig. 5.3(a) Classical bifunctional mechanism described by Weitkamp et al.[1]

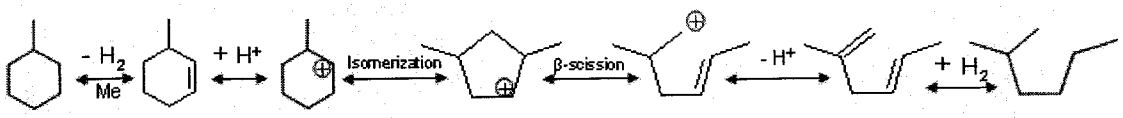

Fig. 5.3(b) The bifunctional mechanism modified after simulation over $ZrO_2(111)$. Note that the change begins with the position of charge on the PDMCPE. In both the cases, reactant and product are the same.

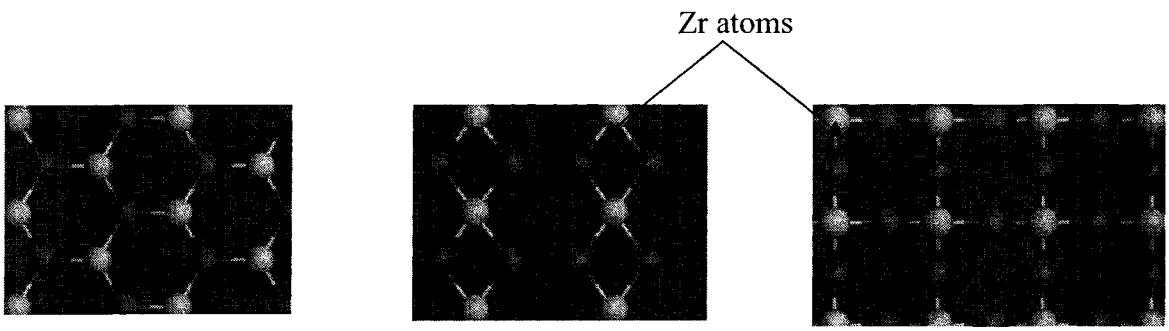

Fig.5.4 Different geometrical planes of ZrO_2. The (111) surface has the maximum number of Zr atoms per unit area and is also the Zr atoms are favorably staggered to facilitate bonding from surface species [15].

that of (111) surface. It should also be noted that the (100) surface exhibited the maximum Lewis acidity.Though several other metal oxide surfaces were studied, only bohemite favored the entire ring opening reaction. The (111) surface of pure TiO_2 (rutile) could not even successfully simulate the adsorption of protonated MCHE. On pure MoO_3, only the isomerization step could be successfully simulated on (111) surface. This step had an activation energy of 69.0 kcal mol^{-1} and a reaction energy 1.0 kcal mol^{-1}. This surface is also slightly more acidic than the zirconia (111) surface (-31.0 k.cal mol^{-1} vs. -29.0 kcal mol^{-1}). On Mo modified zirconia (111), the isomerization reaction with MCHE bonded to the Mo atom had activation energy of 171.0 kcal mol^{-1} and a reaction energy of -0.2 kcal mol^{-1}. The Lewis acidity at this location is appreciably lower than that of pure zirconia (-22.0 kcal mol^{-1} vs. -29.0 kcal mol^{-1}). The potential energy diagram for the bifunctional mechanism on bohemite (111) is shown in Fig. 5.5. The Lewis acidity of bohemite was calculated as -37.0 kcal mol^{-1} which is higher than that of pure zirconia. It can be seen that all the values of activation energy and reaction energy (except for the energy change in the isomerization step) are higher than that in the case of pure zirconia.

The above discussion clearly indicates that acidity has a marked influence on the energetics of the reaction. If Lewis acidity of pure zirconia is examined as the base case, it can be seen that the energetics of the ring opening reaction are significantly affected at higher or lower surface acidities. Thus, it is apparent the ZrO_2(111) surface possesses an optimum acidity to maximize ring opening activity, and this optimum is not a universal constant, but a system dependant value. McVicker et al. [12] emphasized the need to control the acidity and metal/acid for a more favorable yield and rate of ring opening reactions. This observation is also in agreement with the known fact that for the optimum catalytic activity, the reacting species should not be too weakly or too strongly bound to the catalyst surface. It is well known that at very highe acidities, cracking reactions are favored, which is the reason why highly acidic zeolite catalysts are used in FCC [11]. One of the ways of modifying the property of the catalyst is to modify the structure of the catalyst by incorporation of modifier elements. A literature review shows that this modification is possible [5,7], and the present simulation results also show that modification of bulk zirconia with molybdenum creates a stable structure. This research also indicated that both Lewis and Bronsted acidity can be controlled by incorporating

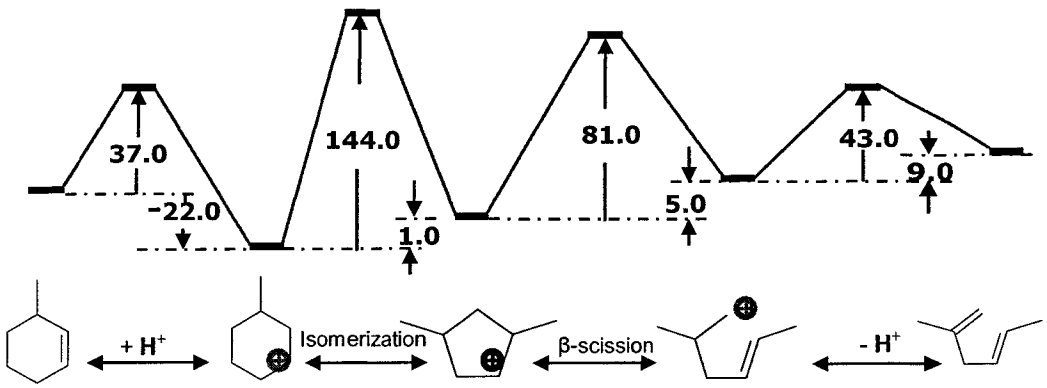

Fig. 5.5 The energy diagram for the ring opening of MCH on bohemite (111) surface. Except for the protonation step, all the energy changes are positive and all the activation barriers are higher than that of the reaction on ZrO_2 (111) surface

modifier elements at the surface of zirconia, but the stability of the resulting structure is a concern. It would be worthwhile confirming the simulations with direct experimental observations.

5.2.2 Haag-Dessau Methylcyclohexane (MCH) Ring Opening

The energetics of MCH ring opening on zirconia (111) as well as bohemite (111) by the Haag-Dessau mechanism is shown in Fig.s 5.6 and 5.7, respectively. It is quiet obvious that the energetics are much more favorable for the bifunctional mechanism compared with the Haag-Dessau mechanism. Considering that the bifunctional mechanism is distinctly more energetically favorable than the Haag-Dessau mechanism for two entirely different catalyst surfaces (i.e. zirconia and bohemite) it can be confirmed that the bifunctional mechanism is generally preferred compared to the Haag-Dessau mechanism. Furthermore, Weitkamp et al. [6] noted that in the Haag-Dessau mechanism, MCH directly protonates forming a non-classical carbonium ion with a three centre, two electron bond in the transition state. However, the simulation of such a transition state was not observable.

5.2.3 Gas Phase Methylcyclohexane (MCH) Ring Opening

The objective of the gas phase transition state search was to compare the energetics of the ring opening reactions with and without catalysts (Fig. 5.8). A detailed discussion of each step is not justified as these reactions are presented only for comparison and are not energetically possible. From the values of energy changes, it can be clearly seen that many of the reactions in the series would be impossible without involving a catalyst. This emphasizes the role played by the catalyst in bringing about the reaction by an alternate mechanism.

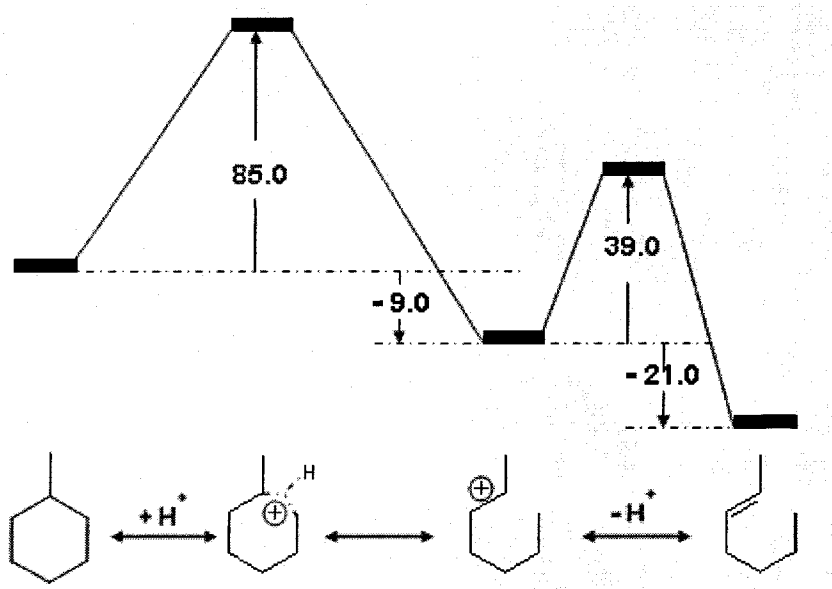

Fig. 5.6 The energy diagram for the ring opening of MCH on ZrO_2 (111) surface by Haag-Dessau mechanism.

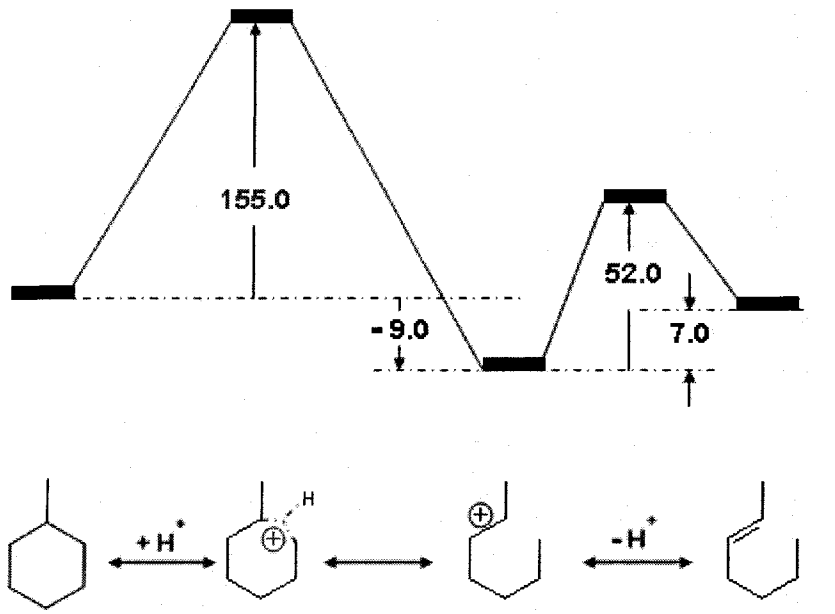

Fig. 5.7 The energy diagram for the ring opening of MCH on bohemite (111) surface by Haag-Dessau mechanism. Energetics is clearly in favor of ZrO_2.

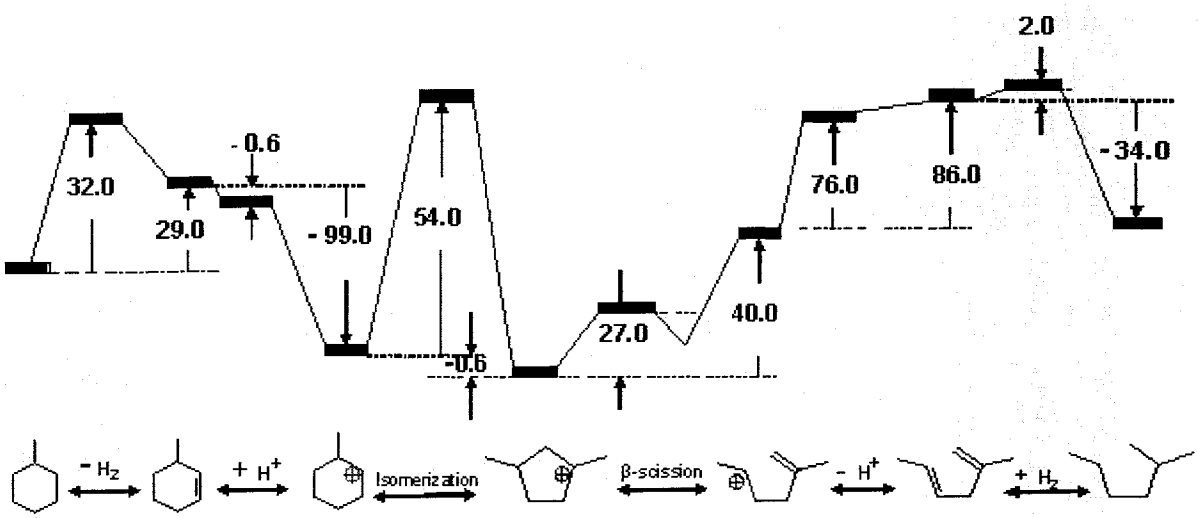

Fig. 5.8 Potential energy surface of gas phase transition state search of MCH over ZrO_2 (111). The values clearly show that these reactions are practically not possible without involving a catalyst.

5.3 Multiring Aromatic Ring Opening

Tetralin and decalin were used as probe molecules to study the ring opening reactions of multiring aromatic structures. These probe compounds were included in the study since diesel predominantly contains C10 + hydrocarbons [8]. Only the bifunctional mechanism was attempted as the Haag-Dessau mechanism was previously found to be unfavorable for MCH ring opening.

5.3.1 Decalin Ring Opening

Fig. 5.9 summarizes the most favorable energetics of decalin ring opening on zirconia (111). The successful simulation shows that ring opening of decalin is possible on zirconia. As before, the protonation and deprotonation steps were found to be energetically favored steps. Despite several attempts with different geometry optimizations, protonation through an Eley-Rideal mechanism successfully completed but with a negative activation energy. Normally negative activation energy indicates that the reactant is not at its energy minimum, but here it does not appear to be the case. Thus, protonation was modeled with a Langmuir-Hinshelwood mechanism.

From Fig. 4.18, it is clear that for the isomerization step, a product resulting with bonding of the substituted carbon atom to the catalyst surface is clearly thermodynamically not favored. It is also interesting to note that the activation energy required for the ring opening step itself is lower compared to that of the activation energy for the isomerization of PDMCPE. This is in agreement with the general belief that it is easier to open secondary rings than the primary rings. In this case, it can also be seen that the non branching ring opening, or opening of the secondary ring as a straight chain, is kinetically more demanding than the branched ring opening.

5.3.2 Tetralin Ring Opening

Fig. 5.10 summarizes the most favorable energetics of tetralin ring opening on zirconia (111). As in the case of decalin, the protonation step via an Eley-Rideal mechanism successfully completed but with negative activation energy, and thus the protonation was modeled with a Langmuir-Hinshelwood mechanism. Protonation and

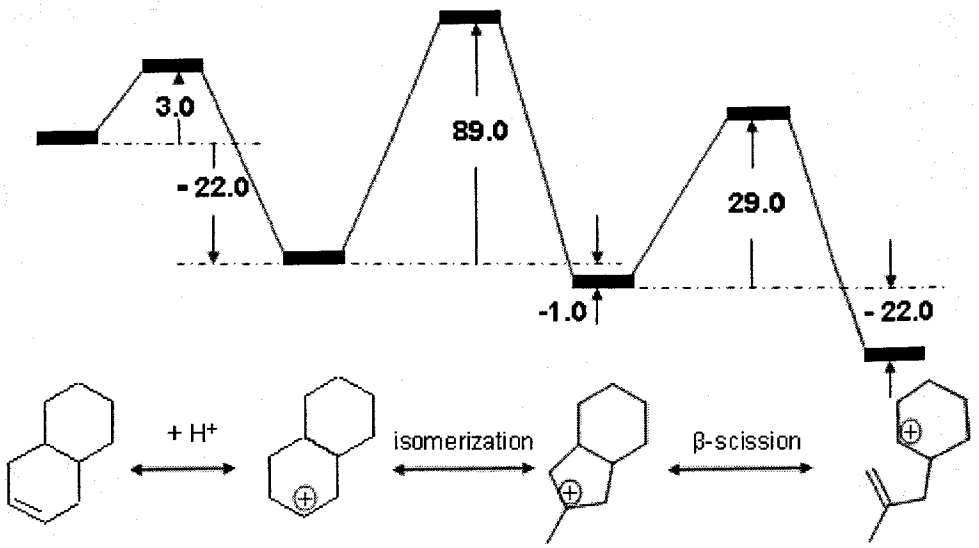

Fig. 5.9 The most energetically favorable ring opening pathways for decalin ring opening over ZrO_2 (111) by classical bifunctional mechanism. Several simulations were performed to find out the most favorable step.

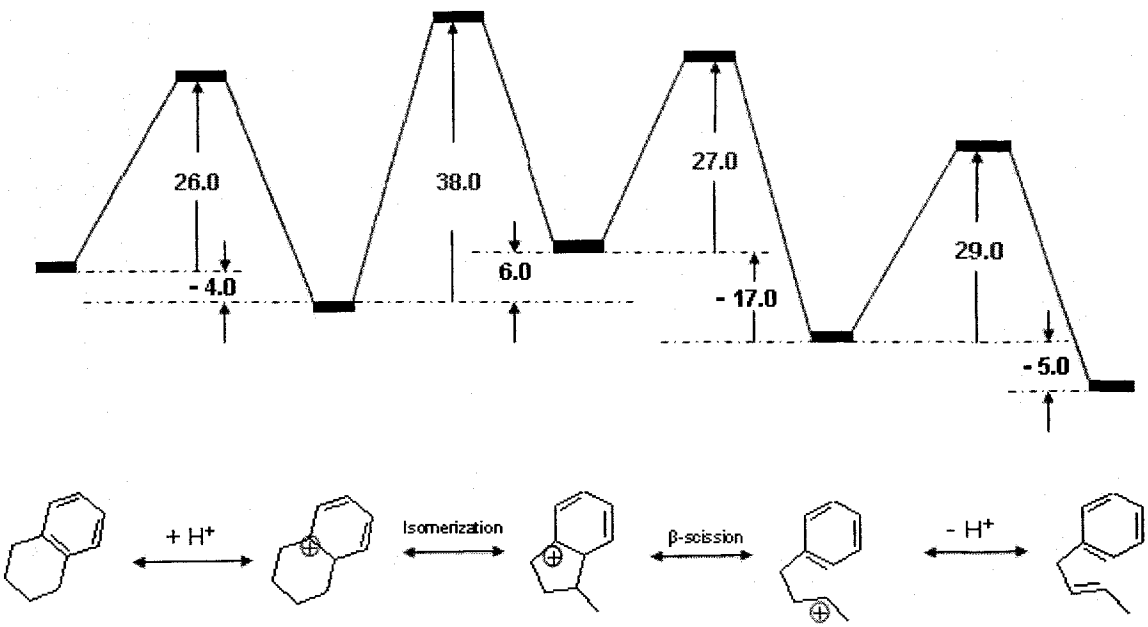

Fig.5.10 The most energetically favorable ring opening pathways for tetralin ring opening over ZrO_2 (111) by classical bifunctional mechanism. Several simulations were performed to find out the most favorable step. Like in the case of decalin, the barrier for ring opening is more favorable than in the case of PDMCHE

deprotonation steps are relatively easy but compared to decalin, the activation energies are higher. Unlike decalin, where during the protonation, only one double bond was attacked, tetralin was attacked through one of the double bonds of the stable benzene structure. This could be the reason for the higher activation energy. Also, the energetics of the ring opening step is more favorable than that for a primary ring. In this case, it can be seen that non branching ring opening is possible with favorable energetics.

5.4 Protonation from Brønsted Acidity

The previous studies were performed assuming a proton from the catalyst surface is present from the dissociation of H_2 by the metal function. A further attempt was made to determine if protonation is possible from the hydroxyl groups present in the surface. Prior to these studies, zirconia (111) was studied to determine if the surface facilitated water dissociation and stable formation of hydroxyl groups. The potential energy diagram for this process is presented in Fig. 5.11. The calculations show that hydroxyl groups are formed on the surface through a 3 step mechanism. Firstly, the water molecule adsorbs on the surface with a negative activation energy indicating the process is non-activated. Then the water molecule dissociates in to a hydroxyl group and a hydrogen atom. The hydroxyl group itself then achieves a more stable state by co-coordinating with three neighboring zirconium atoms. The energetics clearly shows that zirconia (111) favors dissociation of water on the surface with very low activation energies.

An attempt was also made to determine whether zirconia (111) can facilitate the dissociation of H_2 without a metal function. The potential energy diagram for this process is located in Fig. 5.12 .The simulation shows that H_2 dissociation on the surface is very much feasible and it is a two step mechanism. Initially, molecular H_2 dissociatively adsorbs on the surface and then one of the surface hydrogen atoms migrates to the zirconium atom to achieve a lower energy state. Although thermodynamics shows the feasibility of this migration, the activation energy barrier for this transition could not be determined owing to the failure of the transition state search. From the energetics it is clear that the zirconia (111) surface favors H_2 dissociation with a lower activation energy. The heterolytic splitting of hydrogen in to a proton (H^+) and a hydride ion (H^-) is known to occur in the hydrogenation of olefins, carbon monoxide and aromatic carboxylic acids

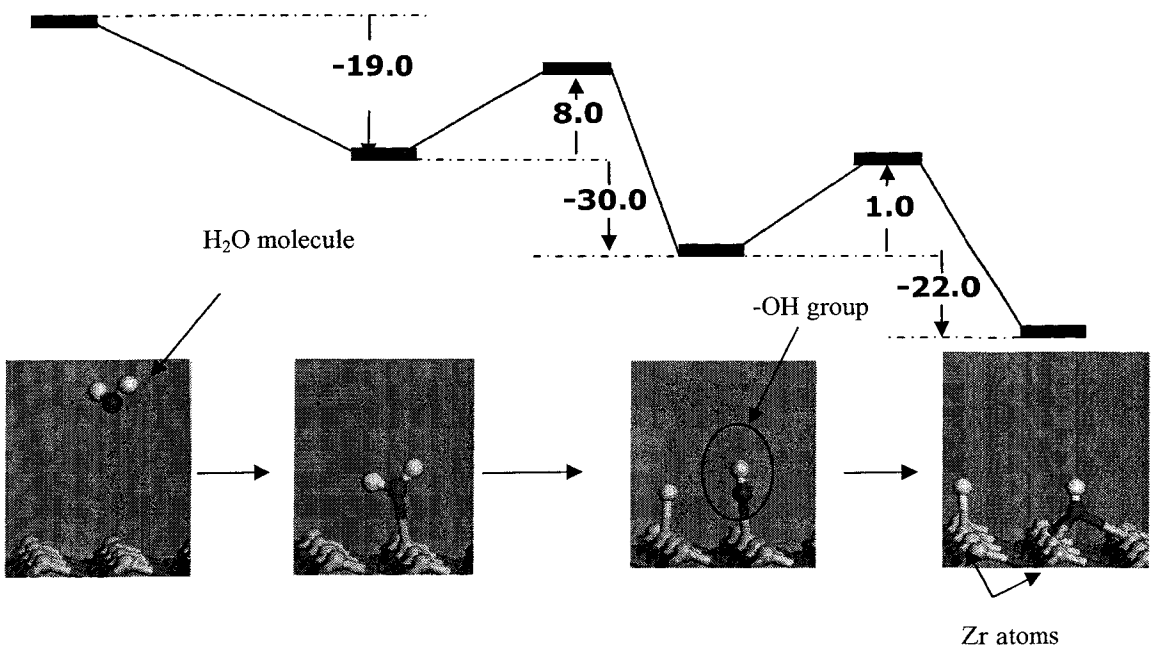

Fig. 5.11 Energetics of water dissociation on ZrO_2 (111). The result shows that ZrO_2 (111) surface favors water dissociation and it is a 3 step process [15].

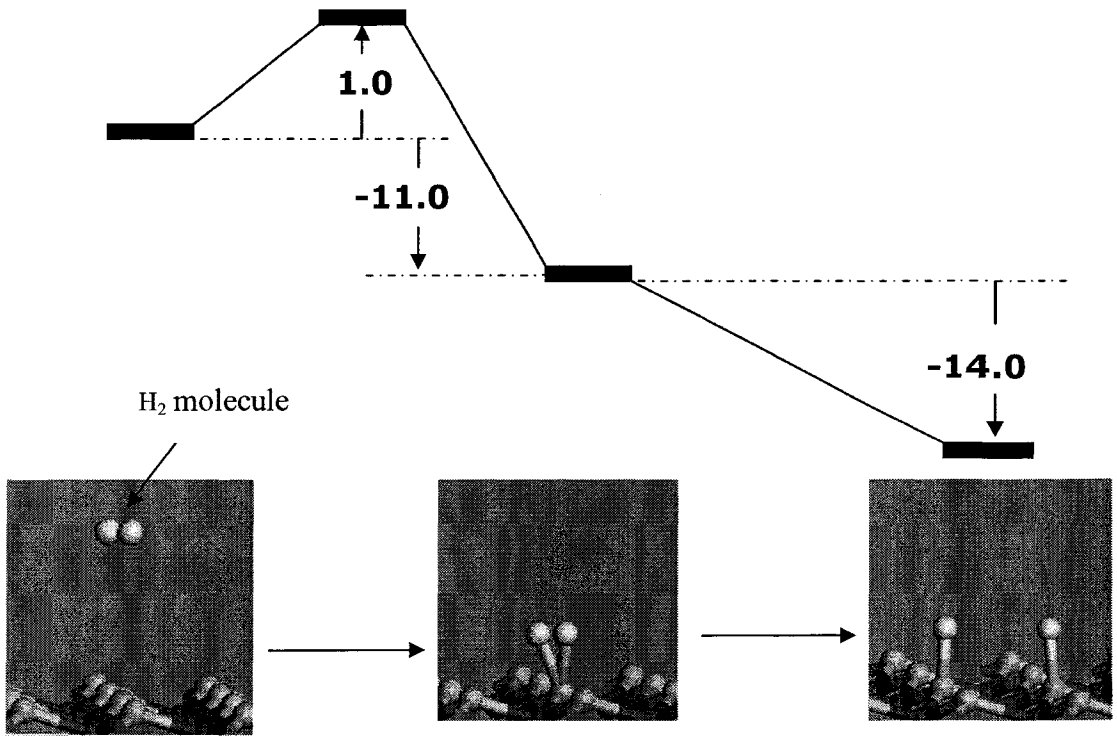

Fig. 5.12 Energetics of H_2 dissociation on ZrO_2 (111). It is clear that H_2 is dissociated easily on ZrO_2 (111) surface [15].

over zirconia catalysts[14]. The result of the protonation (Fig. 4.16) shows that although hydroxyl groups can release protons and protonate the molecule, the mechanism would prefer to replenish the lost H^+ with an H^+ from the surface. Protonation by hydroxyl group with H^+ scrambling is energetically much more favorable than protonation with just the release of H^+ from the hydroxyl group.

However, it is interesting to note that the energetics of protonation from hydroxyl group with H^+ scrambling are almost the same as protonation with H^+ from the surface (i.e. a reaction energy of approx. -20.0 kcal mol^{-1} and an activation energy of 8.0 kcal mol^{-1}). Thus, if atomic hydrogen and hydroxyl groups are present on the surface, the protonation reaction is equally probable from both sources. The study also shows that oxygen would not exist on the surface as atomic oxygen, rather exist on the surface as a hydroxyl group. The presence of surface hydroxyl groups over zirconia surface is consistent with experimental findings [9]. All the above observations clearly favor the use of zirconia as a catalyst for the ring opening reactions.

5.5 Comparison of Simulation Results Using Different Parameters in Simulation

An attempt was made to compare the influence of different simulation parameters on the accuracy of the simulation results. Isomerisation of PMCHE was selected as the model reaction to evaluate the effect of calculation parameters, as this step was identified as a critical step in ring opening. The parameters investigated include the cutoff length, core potential, exchange-correlation functional, k-point set, and integration accuracy. Because the LDA functional was not deemed appropriate for these type of systems, only options available under GGA were considered.

In general, it was noted that the selection of an appropriate functional has the most significant influence on the outcome of the simulation. It can also be seen that the absolute value of activation energy is affected by changing simulation parameters, and this effect is mpre pronounced when the BLYP functional was used. From the literature, it has been seen that BLYP underestimates the bond dissociation energies (hence activation energies) in metals [16]; therefore, this is not an appropriate functional for this study. It was also observed that the absolute values of energies change dramatically using different functionals; however, the difference in energies, which is the primary interest of

the present study, remains approximately constant. The cutoff distances chosen do not seem to affect the energies, and this could be attributed to the fact that the cutoff distance chosen was well above the bond lengths involved, and hence interactions beyond these distances are not expected to add any significant contributions to the energy values. The activation energy values for finer k-point sets and integration accuracy provided slightly different results, although not significant. Therefore, it can be concluded that one has to be careful in chosing the appropriate parameters, especially functionals. For this simulation study, the most appropriate parameters were chosen for the reasons discussed in Chapter 3. As the study involved comparing energy differences, and not absolute values of energies themselves, the differences of using different parameters are mitigated.

Chapter 6 Conclusion

6.1 Conclusion

The total energy values of bulk zirconia indicate that monoclinic zirconia has lower total energy and is thus more probable at ambient conditions. This is in agreement with the experimental observation that zirconia exists in its monoclinic phase up to 1440 K. The observation that zirconia can be stabilized by incorporation of Mo at bulk is in agreement with the experimental observation that MoO_3 stabilizes zirconia.

The $ZrO_2(110)$ surface was found to be the most stable in terms of surface energies, but was found to be less active compared to the (111) surface. This was not surprising as thermodynamically a more stable (probable) plane will be least active as its surface energy is low compared to other surfaces. In terms of acidity (Lewis and Brønsted) calculations, the (100) surface was the most active; however in terms of ring opening reactions, it was seen that the (111) surface was the most active. This is attributed to the 'optimum' activity the (111) surface has and also to the higher Zr surface density and favorably staggered positions of Zr atoms on the (111) surface. The simulations also proved the fact that different crystallographic surface orientations of the same species could have significantly different activities for catalysis.

Modifier element incorporation was studied to determine the effect on surface acidity. The results indicate that this could be one of the methods to tailor the surface acidity to optimize catalytic activity. The result obtained with Si is in agreement with experimental observation. However, it was observed that modifier incorporation on the surface may affect the stability of the surface and this need to be verified experimentally.

ZrO_2 was observed to promote ring opening of methylcyclohexane very favorably. However, it was seen that the classical bifunctional mechanism previously proposed does not hold strictly and so it was modified. The isomerization and β-scission were found to be the most difficult steps. The classical bifunctional mechanism clearly out performed the Haag-Dessau mechanism in terms of energetics. These mechanisms were simulated on bohemite as well, and zirconia was found to be a better catalyst than bohemite for both the cases. In all the cases, Eley-Rideal mechanism was more energetically favorable than Langmuir-Hinshelwood for the protonation reaction. Ring opening studies on different planes of pure zirconia, surface modified zirconia and

bohemite showed that there exists an optimum value for the surface acidity (Lewis) for favorable energetics of ring opening reactions.

The ring opening studies with decalin and tetralin over zirconia surface showed a very promising result. Both molecules could be ring opened with favorable energetics. As expected, the ring opening of the secondary ring turned out to be easier than that of the primary ring. In the case of tetralin, it was observed that non branching ring opening was possible with favorable energetics.

The dissociation of hydrogen and water molecules showed that these are very easily accomplished over zirconia surface. This is clearly in favor of using zirconia as a ring opening catalyst. It was also observed that protonation could be done with hydrogen from hydroxyl group (Brønsted acidity) with the same ease as it could be done from protons from surface.

Gas phase transition state search simulation of the bifunctional mechanism showed that without a catalyst, these reactions are not possible.

6.2 Future work

It was observed that ZrO_2 offers excellent promise as a catalyst for ring opening. More work should be done to fine tune the acidity of the catalyst to optimize the rate and yield of desired ring opening products. The simulations showed that incorporation of surface modifiers is one of the ways to accomplish this. The long term feasibility (stability) of this should be investigated.

The metal function of the bifunctional mechanism was not included in this study for the stated reasons. The *Literature Review* shows that Ir selectively promotes ring opening, and thus, both theoretical and experimental work should be done to find the factors affecting the activity and selectivity of the Ir/ZrO_2 system. Other promoters like Ni and Co should also be considered. Additionally, real hydrocarbon gas oil feeds should be tested against these catalytic systems.

References

Chapter 1

1. Ulf Nylen, Juana Frontela Delgado, Sven Jaras and Magali Boutonnet, "*Low and high pressure ring opening of indan over 2 wt. % Pt,Ir and bi-metallic Pt25Ir75/bohemite catalysts prepared from micro emulsion system*", Applied Catalysis A: General 262 (2004) 189-200.
2. Official Journal of European Communities (No.L350) (1998) 58; Official Journal of the European Communities (No.L 287) (2000) 46.
3. Gy.Onyestyak, G.Pal-Borbely and H.K.Beyer, "*Cyclohexane conversion over H-zeolite supported platinum*", Applied Catalysis A: General 229 (2002) 65-74.
4. Communication from the commission to the council and the European parliament, Brussels, 9.12.2002, COM (2002) 693 final.
5. P.Greening, "*European Vehicle Emission Legislation—Present and Future*", Topics in Catalysis 16-17 (2001) 5-13.
6. A. Corma, V.Gonz´alez-Alfaroy, A.V.Orchill´esy, *"Decalin and tetralin as probe molecules for cracking and hydrotreating the light cycle oil"*, Journal of Catalysis 200 (2001) 34–44.
7. Melanie Jacquin, Deborah J Jones et al. and the references within, "*Cetane improvement of diesel with a novel bimetallic catalyst*", Journal of Catalysis 228 (2004) 447-459.
8. G. B. McVicker, M. Daage, M. S. Touvelle, C.W. Hudson, D. P. Klein, W. C. Baird, Jr., B. R. Cook, J. G. Chen, S. Hantzer,D. E.W. Vaughan, E. S. Ellis, and O. C. Feeley, *"Selective ring opening of naphthenic molecules"*, Journal of Catalysis 210 (2002)137-148.
9. Andreas Raichle, Yvonne Traa, Franz Fuder, Martin Rupp and Jens Weitkamp, "*Haag-Dessau catalysts for ring opening of cycloalkanes*", Angewandte Chemie International Edition 40 (2001) 1243-1246.
10. S.K.Maity, M.S.Rana, B.N Srinivas, S.K.Bej, G.Muralidhar and T.S.R.Prasada Rao, "*Characterization and evaluation of ZrO_2 supported hydro treating catalysts*", Journal of Molecular Catalysis A: Chemical 153 (2000) 121-127.

11. Thallada Bhaskar, Kondakindi Rajender Reddy, Chinthala Praveen Kumar, Mamidanna R.V.S Murthy,Komandur V.R. Chary and the reference within, "*Characterization and reactivity of MoO_3 catalysts supported on zirconia*", Applied Catalysts A :General 211 (2001) 189-201.
12. E.V.Stefanovich and A.L Shluger, *"Theoritical studies of the stabilization of cubic phase ZrO2 by impurities"*, Physical Review B 49 (1994) 11560-11570.
13. Carolyn Kenney, "*Thermochemical characterization of a monofunctional ZrO_2-MoO_3 catalysts for selective ring opening of aromatics and cycloalkanes*", M.Sc. thesis, University of Alberta, 2004.

Chapter 2

1. Walter E. Alvarez and Daniel E. Resascoy, "*Methylcyclopentane ring opening as a reaction test for pt catalysts supported on non-acidic materials*", Journal of Catalysis 164, (1996) 467–476.
2. G. B. McVicker,, M. Daage, M. S. Touvelle, C.W. Hudson, D. P. Klein, W. C. Baird, Jr., B. R. Cook, J. G. Chen, S. Hantzer,D. E.W. Vaughan, E. S. Ellis, and O. C. Feeley, *"Selective ring opening of naphthenic molecules"* Journal of Catalysis 210 (2002) 137-148.
3. Andreas Raichle, Yvonne Traa, Franz Fuder, Martin Rupp, and Jens Weitkamp, "*Haag-Dessau catalysts for ring opening of cycloalkanes*", Angewandte Chemie International Edition 40(2001) 1243-1246.
4. Ulf-Nylén, Juana Frontela Delgado1, Sven Järås and Magali Boutonnet, "*Low and high- pressure ring opening of indan over 2 wt. % Pt, Ir and bi-metallic Pt25Ir75/boehmite catalysts prepared from microemulsion systems*", Applied Catalysis A: General 262 (2004) 189–200.
5. Francesco Arenaa, Roberto Dariob and Adolfo Parmalianaa, "*A characterization study of the surface acidity of solid catalysts by temperature programmed methods", Applied Catalysis A: General 170 (1998) 127-137.*
6. Avelino Corma, "*Solid acid catalysts*", Current Opinion in Solid State and Materials Science, 2 (1997) 63-75.

7. Francois Figueras, Bernard Coq, Christian Walter and Jean-Yves Carriaty, "*Hydroconversion of methylcyclohexane on bifunctional sulfated zirconia-supported platinum catalysts*", Journal of Catalysis 169 (1997) 103–113.
8. Christine Berger, Andreas Raichle, R A. Rakoczy, Yvonne Traa and Jens Weitkamp, "*Hydroconversion of methylcyclohexane on TEOS-modified H-ZSM-5 zeolite catalysts: production of a high-quality synthetic steamcracker feedstock*", Microporous and Mesoporous Materials 59 (2003) 1-12.
9. Gy. Onyestyák, G. Pál-Borbély and H.K. Beyer, "*Cyclohexane Conversion over H-Zeolite supported Platinum*", Applied Catalysis A: General 229 (2002) 65-74.
10. Fransisco Zaera, "*Surface Chemistry of hydrocarbon fragments on transition metals owards understanding catalytic processes*", Catalysis Letters 91 (2003) 1-10.
11. M.A Arribas, F. Marquez and A. Martinez, "*Activity, selectivity and sulfur resistance of Pt/WOx-ZrO2 and Pt/beta catalysts for the simulataneous hydroisomerization of n-heptane and hydrogenation of benzene*", Journal of Catalysis 190 (2000) 309-319.
12. A.Góra, E. Brocławik, "*Theoretical estimation of acid–base properties of Lewis and brønsted centres at the V-W-O catalyst surface: water molecule as the probe in DFT calculations*", Journal of Molecular Catalysis A: Chemical 215 (2004) 187–193.
13. V.R Chary, Rajender Reddy, Gurram Kishan, J.W Niemanstsverdriet and Gerhard Mestl, "*Structure and catalytic properties of molybdenum oxide catalysts supported on zirconia*" , Journal of Catalysis 226 (2004) 283-291.
14. Christian G. Walter, Bernard Coq, Franqois Figueras Marc Boulet, "*Competitive reaction of methylcyclohexane and n-hexane over alumina-supported platinum, iridium and ruthenium catalysts*", Applied Catalysis A: General 133 (1995) 95-102.
15. Matt Steljns, Gilbert Froment, Peter Jacobs, Jan Yytterhoeven and Jens Weitkamp, "*Hydroisomerization and hydrocracking*", Industrial and Engineering Chemistry Process Design and Development 20 (1981) 654-660.

16. Enrique Rodr'ıguez-Castellón , Josefa Mérida-Robles , Lourdes D'ıaz , Pedro aireles-Torres , Deborah J. Jones , Jacques Rozière and Antonio Jiménez-López, "*Hydrogenation and ring opening of tetralin on noble metal supported on zirconium doped mesoporous silica catalysts*", Applied Catalysis A: General 260 (2004) 9-18.

17. M.A Arribas, A. Corma, M.J. Dı'az-Caban˜as, A. Martı'nez, "*Hydrogenation and ring pening of Tetralin over bifunctional catalysts based on the new ITQ-21 zeolite*", Applied Catalysis A: General 273 (2004) 277-286.

18. Roberto Galiasso, Juan Ravigli, Samuel Quenza and Norma Valencia, "*Catalyst for ultra-low sulfur and aromatic diesel*", Applied Catalysis A: General 282 (2005) 227-235.

19. F.Garin, P.Girard, G. Maire, G.Lu, and L.Guczi, "*Isomerization of 2-methyl pentane and ring opening of methyl cyclopentane over Pt-Co/NaY catalysts*", Applied Catalysis A: General 152(1997) 237-247.

20. Yiping Zhuang and Alfred Frennet, "*Kinetic studies of methylcyclopentane ring opening on EuroPt-1 (Pt/SiO2)*", Applied Catalysis A: General 177 (1999) 205-217.

21. Dominique Martin and Daniel Duprez, "*Evaluation of the acid-base surface properties of several oxides and supported metal catalysts by means of model reactions*", Journal of Molecular Catalysis A: Chemical 118 (1997) 113-128.

22. Mar'ıaA. Arribas, Patricia Concepción and Agust'ın Mart'ınez, "*The role of metal sites uring the coupled hydrogenation and ring opening of tetralin on bifunctional Pt(Ir)/USY catalysts*", Applied Catalysis A: General 267 (2004) 111-119.

23. Bhaskar Reddy, Praveen Kumar, Murthy and V.R Charry, "*Characterization and valuation of Molybdenum Oxide Catalysts Supported on Zirconia*", Applied catalysis A: General 211(2001) 189-201.

24. E.V Stefanovich and A.L Shluger "*Theoritical Studies of the stabilization of cubic phase ZrO_2 by impurities*", Physical Review B 49 (1994)11560-11570.

25. J.K Dewhurst and J.E Lowther, "*Relative Stability, structure and elastic properties of several phases of pure zirconia*", Physical Review B, 57 (1998) 741-746.

26. F.G Gault, *"Mechanism of skeletal isomerisation of Hydrocarbons on metals"*, Advances in Catalysis, Vol 30, Academic Press, 1981.

27. J.H Sinfelt, "*Catalytic Hydrogenolysis on Metals*", Catalysis Letters, 9 (1991) 159-172.

28. Corma A., V. Gonz′ alez-Alfaroy and A. V. Orchill ′esy, *"Decalin and tetralin as probe molecules for cracking and hydrotreating the light cycle oil"*, Journal of Catalysis 200, (2001) 34–44.

29. Ming Chow and Gray B. McVicker, "*Conversion of methyl cyclopentanes and acyclic hexanes over supported platinum catalysts*", Journal of Catalysis 112 (1988) 292-302.

30. G. Maire, G.Plouidy, J.C Prudhomme and F.G Gault, "*The mechanism of hydrogenolysis and isomerization of hydrocarbons on metals*" Journal of Catalysis 4 (1965) 556-569.

31. Mélanie Jacquin, Deborah J. Jones, Jacques Rozière, Simone Albertazzi,Angelo Vaccari, Maurizio Lenarda, Loretta Storaro and Renzo Ganzerla, "*Novel supported Rh, Pt, Ir and Ru mesoporous aluminosilicates as catalysts for the hydrogenation of naphthalene*", Applied Catalysis A: General 251 (2003) 131–141.

32. J.G Van Senden and coworkers, *"Selectivity of Ir catalysts in reactions of C_6 hydrocarbons; the role of surface carbonaceous layers and metal particle size"* Journal of Catalysis 87 (1984) 468-477.

33. D. Teschner, K. Matusek, and Z. Pa′ al, "*Ring opening of methylcyclopentane on alumina-supported Rh catalysts of different metal loadings"*, Journal of Catalysis 192 (2000) 335–343.

34. Rossener, U.Mroczek and A.Hagen, Studies in Surface Science and Catalysis 77 (1993) 151.

35. T. J. McCarthy, G.-D. Lei, and W. M. H. Sachtler, "*Methylcyclopentane conversion catalysis over zeolite-Y encaged rhodium: a test for the metal–proton adduct model"*, Journal of Catalysis 159 (1996) 90–98.

36. Vagif M.Akhmedov, Soliman H. Al-Khowaiter, "*Hydroconversion of hydrocarbons over Ru-containing supported catalysts prepared by metal vapor method"*, Applied Catalysis A: General 197 (2000) 201–212.

37. K. Iijima, S. Shimiza, T.Farukawa, N.Yoshida, Bulletin of Japanese Petroleum Institute 5 (1963) 1.

38. R. L. Smith, P. A. Naro and A. J. Silvestri, *"Reaction paths for decyclization of methylcyclopentane over Pt/Al2O3 catalyst"*, Journal of Catalysis 20 (1971) 359.

39. Sachtler, Park and Chow, Applied Catalysis 19 (1985) 349.

40. V.Ponek, M.H.B Bol and M.J Dees, Applied Catalysis 64 (1990) 279.

41. Communication from the commission to the council and the European parliament, Brussels, 9.12.2002, COM (2002) 693 final.

42. Angus P. Wilkinson, Georgia Institute of Technology, *"zeolitic materials: ion exchange and shape selective catalysis"* from http://web.chemistry.gatech.edu/~wilkinson/Class_notes/CHEM_3111_6170/Introduction_to_zeolites.pdf, visited 10th April, 2005.

43. J.H Sinfelt and Y.L.lam, Journal of Catalysis 42 (1976) 319.

44. Andreas Raichle, Yvonne Traa and Jens Weitkamp, *"Preparation of a high-quality synthetic steam cracker feedstock from methylcyclohexane on acidic zeolite H-ZSM-5: influence of the hydrogen partial pressure"*, Applied Catalysis B: Environmental 41 (2003) 193–205.

45. Carolyn Kenney, *"Thermochemical characterization of a monofunctional ZrO_2-MoO_3 catalysts for selective ring opening of aromatics and cycloalkanes"*, M.Sc. thesis, University of Alberta, 2004.

46. http://www.chevron.com/prodserv/fuels/bulletin/diesel/L2_4_6_rf.htm, visited on 10th April, 2004.

47. US patent # 6,241,876, *"Process for selectively opening naphthenic rings"*.

48. Guido Busca, *"Spectroscopic characterization of the acid properties of metal oxide catalysts"*, Catalysis Today 41(1998) 191-206.

49. L.B Galperin, J.C Bricker, J.R Holmgren, *"Effect of support acid–basic properties on activity and selectivity of Pt catalysts in reaction of methylcyclopentane ring opening"*, Applied Catalysis A: General 239 (2003) 297–304.

50. www.zeolyst.com visited on 20th April, 2005.

51. J. Weitkamp and S. Ernst, *'Large pore molecular sieves: Chapter 5 Catalytic test reactions for probing the pore width of large and super-large pore molecular sieves'*, Catalysis Today 19 (1994) 107-149.

52. Clark J. Egan, G.E Langlois and R.J White, *"Selective hydrocracking of C_9 - C_{12} alkylcyclohexanes on acidic catalysts. Evidence for the paring reaction"*, Journal of American Chemical Society 84 (1962) 1204.

53. V. Haensel, Chemistry of Petroleum Hydrocarbons 2 (1955) 189.

54. Gault, F.G, Barron, Y., Cornet, D., Maire, G., *"The mechanism of isomerization of hexanes on platinum catalysts"*, Journal of Catalysis 2 (1963)152.

55. Thallada Bhaskar, Kondakindi Rajender Reddy, Chinthala Praveen Kumar, Mamidanna R.V.S Murthy and Komandur V.R. Chary, *"Characterization and reactivity of MoO_3 catalysts supported on zirconia"*, Applied Catalysts A :General 211 (2001) 189-201.

56. Yasuo Miki, Shoko Yamadaya and Masaaki Oba, *"The selectivity in ring opening of cyclohexane and methylcyclopentane over a nickel-alumina catalyst"*, Journal of Catalysis 49 (1977) 278-284.

57. Z.Paal, P.Tetenyi, *"A new classification of metal catalysts in skeletal reactions of hydrocarbons"*, Nature (London.) 267 (1977) 234-236.

58. D. Teschner,, Z. Paál and D. Duprez, *"The effects of hydrogen pressure and temperature on the methylcyclopentane conversion on Rh catalysts"*, Catalysis Today 65 (2001) 185-190.

59. F. Hoffmeister and J.B. Butt, *"Selectivities in methylcyclopentane and n-hexane conversion on some metal-loaded SAPO-11 catalysts"*, Applied Catalysis A: 82 (1992) 169-184.

60. B. A. Lerner, B. T. Carvill and W. M. H. Sachtler, *"Microgeometry of Pt/mordenite and stereoselectivity of methylcyclopentane ring-opening catalysis"*, Journal of Molecular Catalysis 77 (1992) 99-108.

61. J.A. Oliver and C. Kemball, Journal of Chemical Research Synopses, 6 (1982) 168.

62. Vaarkamp M., Dijkstra P., Vangrondelle J., Miller J. T., Modica F. S., Koningsberger D. C. and Vansanten R. A., *"The effect of hydrogen partial-pressure on methylcyclopentane ring-opening"*, Journal of Catalysis 151 (1995) 330- 337.
63. Gabriela Diaz, Francois Garin, Gilbert Maire, Saaed Alerasool and Richard D. Gonzalez, *"Hydrogenolysis of methylcyclopentane and isomerization of 2-methylpentane over well characterized silica-supported platinum-ruthenium catalysts"*, Applied Catalysis A: General 124 (1995) 33-46.
64. T. J. McCarthy, G. D. Lei and W. M. H. Sachtler, *"Methylcyclopentane conversion catalysis over zeolite-y encagedrhodium: a test for the metal–proton adduct model"*, Journal of Catalysis 159 (1996) 90-98.
65. A.B.Gaspar and L.C. Dieguez, *"Dispersion stability and methylcyclopentane hydrogenolysis in Pd/Al_2O_3 catalysts"*, Applied Catalysis A: General 201 (2000) 241-251.
66. R.J. Fengolio, G.M. Nunez and D.E. Resasco, Applied Catalysis 63 (1990) 319

Chapter 3

1. Klaus Capelle at department de F′ısica e Inform′atica, Universidade de S˜ao Paulo, Brazil, *"A Bird's-Eye View of Density-Functional Theory"* available at http://arxiv.org/abs/cond-mat/0211443 (visited on 1st April, 2005).
2. Keller and Gasquez. Springer-Verlag 1983, *"Lecture notes in Physics -187, Density Functional Theory"*.
3. http://newton.ex.ac.uk/research/qsystems/people/jenkins/mbody/mbody3.html (visited on 30th March, 2005).
4. www.accelrys.com/technology/qm/erich/dft.htm(visited on 5th April, 2005).
5. Help topic associated with the $DMol^3$ in the Materials Studio® version 2.2.
6. http://en.wikipedia.org/wiki/Density_functional_theory (visited on 3rd April, 2005) .
7. http://encyclopedia.laborlawtalk.com/Density_functional_theory (visited on 20th April 2005.

8. http://hyperphysics.phy-astr.gsu.edu/hbase/quantum/schr.html#c1 (visited on 21st April, 2005).
9. http://www.ccl.net/cca/documents/DFT/dft-overview/previous-version/dft_hamil.html (visited on 21st April, 2005).
10. http://www.cmm.upenn.edu/~ensing/thesis/node11.html (visited on 21st April 2005).
11. *"Transition State Modeling for Catalysis"*, ACS symposium series 721, American Chemical Society, P.247.
12. http://www.public.asu.edu/~dmatyus/teaching/chm341/lecture_notes/chapter27 visited 17th April, 2005.
13. http://mutuslab.cs.uwindsor.ca/vacratsis/lecture3a%20ppt.pdf, visited 17th April, 2005.
14. *"Transition State Modeling for Catalysis"*, ACS symposium series 721, American Chemical Society, P.5.
15. Help topic associated with the $DMol^3$ in the Materials Studio® version 2.2.

Chapter 4

1. Mingyong Sun , Alan E. Nelson , John Adjaye, "*Adsorption and hydrogenation of pyridine and pyrrole on NiMoS: an ab initio density-functional theory study*", Journal of Catalysis 231 (2005) 223–231
2. Help topics associated with $DMol^3$ from Accelrys® (version 2.2)
3. Andreas Raichle, Yvonne Traa, Franz Fuder, Martin Rupp, and Jens Weitkamp, "*Haag-Dessau catalysts for ring opening of cycloalkanes*", Angewandte Chemie International Edition 40(2001) 1243-1246.
4. E.V.Stefanovich and A.L Shluger, *"Theoritical Studies of the stabilization of cubic phase ZrO2 by impurities"*, Physical Review B 49 (1994) 11560-11571.
5. Carolyn Kenney, "*Thermochemical characterization of a monofunctional ZrO_2-MoO_3 catalysts for selective ring opening of aromatics and cycloalkanes*", M.Sc. thesis, University of Alberta, 2004.

6. A. Gora and E. Broclawik, "*Theoretical estimation of acid –base properties of Lewis and Brønsted centres at the V-W-O catalysts surface: water molecule as the probe in DFT calculations*". Journal of Molecular Catalysis A: Chemical 215 (2004) 187–193.
7. Xiaobo Zheng, Paul Blowers, "*An ab initio study of ethane conversion reactions on zeolites using the complete basis set composite energy method*", Journal of Molecular Catalysis A: Chemical 229 (2005) 77–85.
8. http://www.cat.hokudai.ac.jp/ichikawa/e_reserch.htm, visited on 28th April, 2005.
9. http://www.britannica.com/nobel/micro/283_94.html, visited on 28th April, 2005.
10. F.G Gault, Y. Barron, D. Cornet, G. Maire, Journal of Catalysis 2 (1963)152.
11. Library and/or simulation files from DMol^3 from Accelrys® (version 2.2).

Chapter 5

1. A.Christensen and Emily A. Carter, "*First-principles study of the surfaces of zirconia*", Physical Review B 58 (1998) 8050-8065.
2. C.Morterra, G. Cerrato and L. Ferroni, "*Surface characterization of tetragonal zirconia*", Applied Surface Science 65/66 (1993) 257-264.
3. Frank Haase and Joachim Sauer, "*The surface structure of sulfated zirconia*: periodic *ab initio study of sulfuric acid adsorbed on ZrO2 (101) and ZrO2 (001)*", Journal of American Chemical Society 120(1998) 13503- 13512.
4. C.Morterra, G. Cerrato and L. Ferroni, "*Surface characterization of yttria-stabilized tetragonal ZrO2 Part 1. Structural, morphological, and surface hydration features*", Materials Chemistry and Physics", 37 (1994) 243-251.
5. Carolyn Kenney, "*Thermochemical Characterization of Monofunctional ZrO2-MoO3 cartalysts for the Selective Ring Opening of Aromatics and Cycloalkanes*", M.Sc Theisis, University of Alberta, 2004.
6. Andreas Raichle, Yvonne Traa, Franz Fuder, Martin Rupp and Jens Weitkamp "*Haag-Dessau catalysts for ring opening of cycloalkanes*" Angewandte Chemie International Edition 40(2001) 1243-1246.

7. V.Stephanovich, A.L Shluger and C.R.A.Catlow and the references within *"Theoretical study of the stabilization of cubic-phase ZrO_2 by impurities"*, Physical Review B, 49 (1994)11560-11571.
8. *www.chevron.com* visited on 15th July, 2005
9. S.K. Maity, M.S. rana, B.N. Srinivas, S.K.Bej, G.Muralidhar and T.S.R Prasada Rao, *"Chracterization and evaluation of ZrO2 supported hydrotreatong catalysts"*, Journal of Molecular Catalysis A: Chemical 153 (2000) 121-127.
10. Henri J.F.Jansen, *"Electronic structure of cubic and tetragonal zirconia"*. Physical Review B 43 (1991) 7267-7278.
11. *www.zeolyst.com,* visited on 15th June, 2005.
12. G.B. McVicker, M.Daage and co-workers, *"Selective ring opening of napthenic molecules"*, Journal of Catalysis 210 (2002) 137-148.
13. Ruth Franklin, Peter Goulding, Jean Haviland, Richard W. Joyner, Ian McAlpine, Peter Moles, Colin Norman and Trevor Norwell, *"Stabilization and catalytic properties of high surface area zirconia"*, Catalysis Today 10 (1991) 405-407.
14. K. Tanabe and T.Yamaguchi, *"Acid-base bifunctional catalysys by ZrO2 and its mixed metal oxides"*, Catalysis Today 20 (1994)185-197.
15. Library and/or simulation files from $DMol^3$ from Accelrys® (version 2.2).
16. Sam P. de Visser, Yuval Alpert, David Danovich, and Sason Shaik, *"No-Pair Bonding" in High-Spin Lithium Clusters"* Journal of Physical Chemistry A 104 (2000)11223-11231.